

NASA CONTRACTOR REPORT 177340

STUDY FOR PREDICTION OF ROTOR/  
WAKE/FUSELAGE INTERFERENCE  
PART I: TECHNICAL REPORT

(NASA-CR-177340-Vol-1) STUDY FOR PREDICTION  
OF ROTOR/WAKE/FUSELAGE INTERFERENCE, PART I  
Final Report, 1 Jun. 1980 - 1 Nov. 1983  
(Analytical Methods, Inc., Redmond, Wash.)  
92 p HC A05/MF A01

N85-22346

Unclas  
20169

CSCI 01A G3/V1

D. R. Clark  
B. Maskew

CONTRACT NAS2-10620  
March 1985

**NASA**



**NASA CONTRACTOR REPORT 177340**

**STUDY FOR PREDICTION OF ROTOR/WAKE/  
FUSELAGE INTERFERENCE  
PART I: TECHNICAL REPORT**

**D. R. Clark  
B. Maskew**

**Analytical Methods, Inc.  
2047 - 152nd Avenue, N.E.  
Redmond, WA 98052**

**Prepared for  
Ames Research Center  
under Contract NAS2-10620**

**NASA**

**National Aeronautics and  
Space Administration**

**Ames Research Center  
Moffett Field, California 94035**

ABSTRACT

A method has been developed which allows the fully coupled calculation of fuselage and rotor airloads for typical helicopter configurations in forward flight. To do this, an iterative solution is carried out based on a conventional panel representation of the fuselage and a blade element representation of the rotor where fuselage and rotor singularity strengths are determined simultaneously at each step and the rotor wake is allowed to relax (deform) in response to changes in rotor wake loading and fuselage presence. On completion of the iteration, rotor loading and inflow, fuselage singularity strength (and, hence, pressure and velocity distributions) and rotor wake are all consistent.

The results of a fully coupled calculation of the flow around representative helicopter configurations are presented. The effect of fuselage components on the rotor flow field and the overall wake structure is detailed and the aerodynamic interference between the different parts of the aircraft is discussed. In particular, the flow field developed by the rotor head is followed and the effect of a rotor head cap and pylon modifications in redirecting the rotor head flow are illustrated. Good correlation between measured and calculated fuselage airloads in low-speed flight is achieved and correspondence with observed flow field behavior is demonstrated.

(4)

TABLE OF CONTENTS

<u>Section</u>	<u>Page No.</u>
ABSTRACT . . . . .	i
LIST OF FIGURES . . . . .	iii
LIST OF SYMBOLS . . . . .	vi
1.0 INTRODUCTION . . . . .	1
2.0 ANALYSIS	
2.1 Background to the Analysis . . . . .	6
2.2 Body Aerodynamics . . . . .	12
2.3 Wake Cutting Procedure . . . . .	13
2.4 Rotor Blade Aerodynamics . . . . .	18
2.5 Rotor Disc Panel Model . . . . .	21
3.0 THE COMPUTER PROGRAM . . . . .	24
4.0 DISCUSSION OF RESULTS	
4.1 Application of the Analysis to a Simple Body/ Rotor Example . . . . .	25
4.2 Basic Body/Rotor Results for a Representative Configuration . . . . .	25
4.3 The Effect of Configuration Elements on the Rotor/Fuselage Flow Field . . . . .	39
4.4 The Potential to Study Full Configurations . .	48
5.0 CONCLUSIONS AND RECOMMENDATIONS . . . . .	50
6.0 REFERENCES . . . . .	51
APPENDIX A: Wake Shape and Model Surface Pressure Correlation Results	

LIST OF FIGURES

<u>Fig. No.</u>	<u>Title</u>	<u>Page No.</u>
1	Typical Output from Vortex Filament Wake Model	7
2	Typical panel Representation for Helicopter Analytical Model . . . . .	7
3	Body/Rotor/Wake Influence Block Matrix . . . . .	8
4	Panel Model with Vortex-Lattice Singularities--Implicit Velocity Component . . . . .	8
5(a)	Comparison of Off-Body Streamlines Calculated using VSAERO with Exact Solution Result . . . . .	10
(b)	With Pressure Distribution . . . . .	10
6	General Program Schematic . . . . .	11
7	Schematic of Wake Cutting Model . . . . .	14
8(a)	Wake Cutting Study--Side View . . . . .	15
8(b)	Wake Cutting Study--Top View . . . . .	15
9	Wake Cutting Study--Spanwise Doublet Distribution (0.25 Chord) . . . . .	16
10	Wake Cutting Study--Spanwise Velocity (0.25 Chord) . . . . .	17
11	Body/Rotor Interference Calculation Schematic	22
12	Blade Model/Panel Model/Wake Schematic . . . . .	22
13(a)	Body Rotor Interference Study--Starting Condition . . . . .	26
13(b)	Body Rotor Interference Study--Starting Condition . . . . .	26
14(a)	Body Interference Study, Relaxed Wake . . . . .	27
14(b)	Body Interference Study, Relaxed Wake . . . . .	27
14(c)	Body Interference Study, Relaxed Wake . . . . .	28
15	Isolated Rotor, Relaxed Wake . . . . .	28
16	Outline of Freeman-Mineck Model used in Analysis (Scaled to 20 ft. Rotor Radius) . . . . .	30

LIST OF FIGURES (Continued)

<u>Fig. No.</u>	<u>Title</u>	<u>Page No.</u>
17	Basic Panel Model for Body/Rotor Studies . .	30
18(a)	Aft Fuselage--Typical Correlation with Test Data; 0.05 Advance Ratio, Run/Point 22/139, Station 17.6 (0.88) . . . . .	31
18(b)	0.15 Advance Ratio, Run/Point 25/148, Station 17.6 (0.88) . . . . .	31
19(a)	Front Fuselage--Typical Correlation with Test Data--0.05 Advance Ratio, Run/Point 22/139, Station 1.80 (0.09) . . . . .	32
19(b)	0.15 Advance Ratio, Run/Point 25/148, Station 1.00 (0.05) . . . . .	32
20	Calculated Distorted Wake--Low Advance Ratio .	33
21	Cross Section through Typical Low Advance Ratio Wake (Station 30.0) . . . . .	33
22	Typical Effect of Rotor Wake/Pylon Intersec- tion--Body and Rotor Alone	
(a)	Calculated Pylon Doublet Distribution--Low Advance Ratio (Waterline 3.00) . . . . .	35
(b)	Calculated Pylon Horizontal Velocity Ratio, $V_x/V_\infty$ --Low Advance Ratio (Waterline 3.00). .	35
23	Calculated Vertical Velocity Ratio $V_z/V_\infty$ ; Waterline 0.0; Body and Rotor Alone	
(a)	Advance Ratio 0.05 . . . . .	36
(b)	Advance Ratio 0.15 . . . . .	36
24	Calculated Effect of Body on Rotor Angle of Attack--0.05 Advance Ratio . . . . .	37
25	Calculated Effect of Body on Rotor Angle of Attack--0.30 Advance Ratio . . . . .	37
26	Calculated Contours of Upwash Velocity in Rotor Plane; Body and Rotor Alone; 0.30 Advance Ratio	38
27	Body-Rotor Panel Model with Tail Assembly . .	38

LIST OF FIGURES (Concluded)

Fig. No.	Title	Page No.
28	Pressure Distribution on Lifting-Surface Model	40
29	Effect of Tail Surfaces on Calculated Blade Angle of Attack; 0.15 Advance Ratio . . . . .	40
30	Basic Body Model with Nacelles and Tail Surfaces Added . . . . .	41
31	Effect of Nacelles on Calculated Blade Angle of Attack--0.15 Advance Ratio . . . . .	41
32	Calculated Rotor Head Model Wake Development--0.15 Advance Ratio . . . . .	42
33	Rotor Head Wake Cross Sections--0.15 Advance Ratio . . . . .	42
34	Effect of Rotor Head and Wake on Calculated Blade Angle of Attack--0.15 Advance Ratio . . . . .	44
35(a)	Calculated Rotor Head Cap Wake Development--0.15 Advance Ratio . . . . .	44
35(b)	Calculated Rotor Head Wake Development with Modified Pylon--0.15 Advance Ratio . . . . .	45
36(a)	Calculated Wake Cross Section with Rotor Head Cap Wake--0.15 Advance Ratio . . . . .	45
36(b)	Calculated Wake Cross Section with Modified Pylon--0.15 Advance Ratio . . . . .	46
37(a)	Effect of Rotor Head Cap on Calculated Blade Angle of Attack--0.15 Advance Ratio . . . . .	47
37(b)	Effect of Pylon Modification on Calculated Blade Angle of Attack--0.15 Advance Ratio . . . . .	47
38	Mock-up of Full Configuration with Rotor Head Cap (Actual Run Exceeds Present Program Panel Capacity) . . . . .	49
39	Effect of Tail Rotor on Vertical Stabiliser Loads at WL 5.75 (Main Rotor Present--0.15 Advance Ratio) . . . . .	49

## LIST OF SYMBOLS

Note: In this report two different analyses which have (separately) well defined sets of conventional symbols are brought together. The conventions have been retained and, as a result, some symbols have double definition. Their meaning, however, remains clear when they are considered in the context of their applications. The symbols involved are  $\sigma$  and  $\mu$ . In the panel model convention these represent the doublet and source singularity strengths, while in the rotor model convention, they represent rotor solidity and advance ratio. The uses are sufficiently separate that confusion should not occur.

$\Delta A$	Rotor panel model panel area
$b$	Number of blades
$c$	Blade chord
$\bar{c}$	Mean blade chord
$\Delta C_p$	Rotor panel model differential pressure coefficient
	$(C_{P_{UPPER}} - C_{P_{LOWER}}) = \frac{\Delta \bar{L}}{\frac{1}{2} \rho V_{\infty}^2 \Delta A}$
$C_T$	Rotor thrust coefficient = $\frac{T}{\rho \pi R^2 (\Omega R)^2}$
$e$	Blade flapping hinge offset
$L$	Rotor lift in wind axis system
$\Delta L$	Blade model segment load
$\Delta \bar{L}$	Panel model time-averaged load = $\frac{L}{\Delta r} \cdot \Delta r \cdot \frac{b}{NC}$
$M$	Mach number
$NC$	Number of azimuthal increments into which disc is broken for panel model
$P$	Rotor propulsive force in wind axis system
$r$	Radial location on blade
$R$	Blade tip radius
$\Delta l$	Blade segment length
$T$	Rotor thrust
$U$	Velocity components in blade section axis system
$V$	Velocity components in wind (global) axis system
$v'$	Rotor local resultant velocity
$X, Y, Z$	Global coordinate system
$\alpha$	Rotor control axis orientation
$\alpha$	Body pitch attitude
$\beta$	Blade flapping angle
$\dot{\beta}$	Blade flapping rate ( $\partial \beta / \partial t$ )
$\gamma$	Blade local yaw angle

## LIST OF SYMBOLS (Concluded)

$\psi$	Blade azimuth angle
$\Omega$	Blade rotation rate ( $\partial\psi/\partial t$ )
$\sigma$	Rotor panel model, doubled strength
	$= \frac{1}{4\pi} \int_0^r \frac{\Delta C_P}{2(V'/V_\infty)} dr$
$\sigma$	Rotor solidity = $\frac{b\bar{c}}{\pi R}$
$\rho$	Air density
$\mu$	Panel model source strength
$\mu$	Rotor model advance ratio, $V_\infty/\Omega R$

### Subscripts

$x, y, z$	Components of local velocity in global coordinate system
$c$	Climb
$i, p, r$	Components of local velocity in blade section system; I = inplane, P = perpendicular, R = radial
$\infty$	Free stream conditions. $V_\infty$ is defined along global system x-axis

## 1.0 INTRODUCTION

As helicopter designers work towards the development of a vehicle which can compete with fixed-wing aircraft, if not in terms of speed, at least in terms of passenger acceptance in the areas of ride quality, vibration, and noise, they are being forced more and more to acknowledge the complex interaction that takes place between the rotor and the airframe. Body/rotor interference manifests itself throughout the operational range of the helicopter; it is as significant at low speed in the form of rotor induced fuselage downloads as it is at high speed where the most important effects are the irregularities in rotor loads induced by the passage of the blades through the fuselage flow field. Added to these effects is the controlling role of the main rotor wake in the handling qualities, passing as it does over and around the horizontal and vertical tail surfaces and the tail rotor as speed and flight conditions change. The term "interactional aerodynamics", coined by Sheriden and Smith,<sup>1</sup> aptly describes the very involved process which controls helicopter loads, dynamics, handling qualities and performance.

Throughout the first three decades of the helicopters existence as a practical machine, the profound effect that the presence of the fuselage can have on rotor behavior was hardly acknowledged. This was largely due to the fact that there was not a strong, driving requirement to understand the interaction and rotors were designed, analysed and tested in isolation. The fact that when installed they behaved differently, trimmed at different cyclic pitch settings and had considerably different aeroelastic response and dynamic characteristics was correctly attributed, in most cases, to the presence of the fuselage. However, no serious attempt was made to understand the phenomenon and since the modest performance and dynamics goals of the period were being met, there was no incentive to refine the design methods.

The situation changed dramatically in the early seventies as a result of the competition to provide the U.S. Army with new utility transport and attack helicopters. A prime requirement in both programs was that the designs must all be airtransportable within certain very clearly defined limits and this resulted in designs in which the rotor was placed, initially, very close to the fuselage in an attempt to reduce the overall height of the vehicle. All of the vehicles tested in this configuration exhibited undesirable dynamic characteristics where were attributed to fuselage induced rotor inflow variations.

The phenomenon was first explored analytically by Landgrebe et al.,<sup>2</sup> in a paper which examined the mathematical tools available for the design of the new generation of rotor craft. In this work the flow field induced by the fuselage in the region of the rotor was calculated by an early potential flow configuration modelling program. For this early study there was no direct coupling of rotor and fuselage effects, and the velocities

calculated in the rotor plane by the fuselage analysis. The rotor is simply fed as inflow into the rotor analysis. Because of the size of the individual programs and the limitations of the computing facilities available at the time, no coupling of the rotor on fuselage effects was attempted beyond very simple source plane or vortex tube rotor models. Despite these limitations the analysis was used with some success to explore alternative rotor locations. The study showed how, when operating close to the fuselage, the rotor is exposed to an azimuthally varying inflow, predominantly up over the nose and down aft of the shaft but containing higher harmonics, which significantly degrade the aircraft vibration environment. Also, it was realized that the upwash over the front fuselage was severe enough, causing very large increases in angle of attack as the blade passed through the forward portion, to precipitate stall as far out as mid-span. Inclusion of the fuselage induced flow field in the dynamic analysis dramatically improved correlation with measured data.

Fuselage/rotor interference has been explored from both experimental and analytical sides. Noteworthy from the experimental point of view has been the work of the group at NASA Langley. Following the early work of Wilson and Mineck,<sup>3</sup> directed mainly at handling qualities and low speed fuselage loads, the work of Freeman with Mineck,<sup>4</sup> and later with Wilson<sup>5</sup> explored systematically the influence of body shape and relative rotor/body position on fuselage and rotor airloads. They showed how with increased fuselage width and reduced body/rotor spacing the performance of both systems is degraded. The work of Sheridan and Smith,<sup>1</sup> concentrating on a particular configuration also explored the effects of body/rotor placement. More recently, Betzina and Shinoda<sup>6</sup> working with a scale model of a wind tunnel test module (from the NASA Ames 40 x 80 wind tunnel) have examined coupled rotor/body integrated performance. Formerly a rarity, test of rotor/fuselage combinations are now standard procedure as designers try to define more closely the differences between analysis and actuality and between model and full-scale test results. Reference 6 presents a fairly typical outline of the gaps that still exist in the understanding of the coupled flow field.

In parallel with the expansion of the experimental data base, work has continued on the development of analytical tools to explore rotor/body phenomena. Several different approaches to modelling the flow field have been employed ranging from involved combinations of vortex filament wake models and full fuselage panel models to simple stacked vortex ring arrays. In all cases, however, inclusion of the effect of the presence of the fuselage in the description of the rotor inflow improves the prediction of unsteady effects.

At a rotor wake workshop held by the U.S. Army Research Office (AROD), Smith<sup>8</sup> presented a method where the fuselage was represented by a single source element in a uniform flow and the rotor by a series of constant strength vortex rings, displaced

upwards as they passed through the sphere of influence of the body source. Despite the relative crudity of the model, the predicted rotor loading shape was good. The same basic model was used by Young.<sup>9</sup> With a more refined fuselage model and considering both vertical and horizontal displacement of vortex rings, he was able to show some improvements in correlation with test data. Incorporation of cyclically varying circulation around the rings further enhanced the correlation.

A more detailed analysis which more accurately represents the fuselage with a complex panel model and the rotor with a wake filament model was used by Landgrebe et al.<sup>2</sup> The method was used in the work discussed in References 7 and 10. Here, the flow around the panel model is first calculated and the velocity field in the plane of the rotor determined. This is used as input to a rotor performance calculation which can include as much detail as desired, up to and including a full filament wake distortion calculation. It is not clear from the published work whether any higher-order coupling is involved. Certainly, in the schematics presented in Reference 7, the arrows connecting fuselage and rotor aerodynamics modules only go one way, from fuselage to rotor, implying no higher-order coupling than a simple rotor onset flow modification. However, comparison between results predicted using the method and test data show good agreement.

A similar approach is taken by Huber and Polz.<sup>11</sup> Using a detailed panel model they calculate the flow in the plane of the rotor for input to a rotor analysis. Again, no higher-order coupling is used. This is reflected in the fuselage induced upwash profiles presented in Reference 11, which are symmetric about the center plane. If coupling had been present, the upwash contours would have been asymmetric, reflecting the differences in loading between the advancing and retreating inboard blade sections. Despite this, they show very graphically the large impact of the fuselage on the rotor loads, especially in the region of the fourth and fifth harmonic.

Huber and Polz<sup>11</sup> also present results from earlier studies where, for the first time, attempts have been made to calculate the effect of regions of separated flow on downstream components. The earlier work<sup>12</sup> presents the method in detail. Following the by now conventional technique (See References 13 and 14), the authors, using a panel method and streamline procedures, calculate the extent of regions of separated flow; then, with a novel volumetric vorticity singularity model, are able to determine the velocity field inside the separation zone downstream. They do not, however, present any calculation on the effect of these flows and, in fact, their sample cases are unnaturally truncated. This is done since the type of singularity model used in the analysis cannot handle a direct vortex/surface intersection.

Another theoretical approach to the body/rotor problem is that taken by Freeman.<sup>15</sup> Again, using a basic panel model for the fuselage and a vortex tube model of the rotor wake, following Heyson,<sup>16</sup> he is able to show quite impressive correlation between the results of his analysis and body/rotor test data. However, there was no coupling present between rotor and fuselage flows, the rotor model being simply used to perturb the fuselage model onset flow, and no fuselage induced wake distortion was introduced into the rotor calculation.

None of the rotor/fuselage analyses examined couples fully the flow fields of the two components to the extent that terms of higher than first order; that is, fuselage on rotor<sup>2,7,9</sup> or rotor on fuselage<sup>15</sup> are included, and none have been able to calculate the deformation of the rotor wake in the presence of the fuselage or handle the direct vortex wake/fuselage cutting situations. The reasons for this were outlined by the present author at the U.S. Army Conference on Wake Modelling in 1979,<sup>17</sup> and in detail in Reference 18. The lack of an adequate coupling analysis results partly from the limited capacity of the computing machines then in use (the fuselage panel codes and vortex wake codes on their own consuming most of the machine capacity--precluding directly coupled calculation), but mostly from the inability of the potential flow models to handle the close approach of strong singularities in the external flow and direct vortex/surface encounters.

The goal of the present study was a full description of the highly interactive helicopter flow field including powerplant exhaust, horizontal and vertical stabilisers, tail or other auxiliary rotors and separated wakes from upstream components such as bluff rotor heads. This was made possible by the coupling of a rotor module to an advanced potential flow modelling code. The program, designated VSAERO (Vortex Separation AERODynamics),<sup>19,20</sup> uses combinations of doublet and source singularities, together with changes in the way in which the boundary conditions are applied, to solve for the local, scalar doublet strength. This is differentiated to define the local velocity field. Techniques have been developed to handle not only close vortex approach but also direct wake cutting. The rotor wake (wakes if more than one rotor is present) is represented by time-averaged vortex sheaths which are allowed to deform in the presence of the fuselage flow field. The rotor/fuselage coupling is made through a blade element model for the rotor supplied with inflows from the fuselage/wake calculation and feeding back circulation strengths to the wake.

The model has been used with some success to look at basic body/rotor performance over an advance ratio range from 0.05 to 0.3. Correlation of fuselage loads inside the wake interference zone is generally good. The test data used for the correlation was that of Freeman and Mineck.<sup>4</sup> The same basic configuration was used as a starting point for a study of the effects of adding configuration components and a full buildup was carried out. The

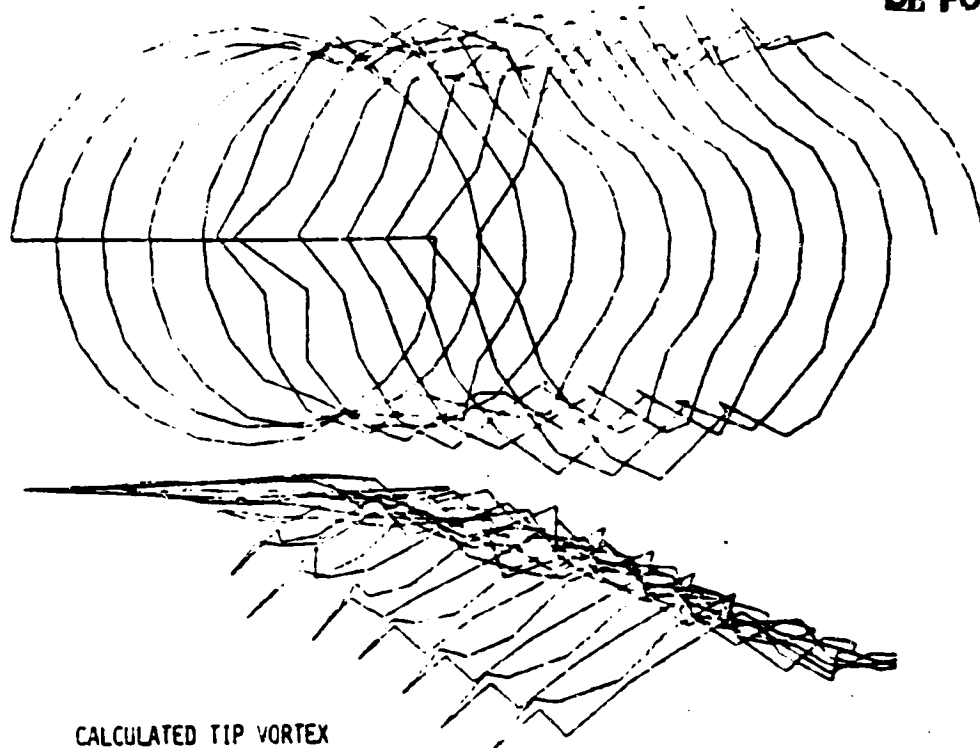
effects of adding horizontal and vertical stabiliser, tail rotor, engine nacelles and exhaust plumes, a rotor head representation, and finally, a rotor head fairing were explored. The role of the rotor head "beanie" and pylon modifications in deflecting the center portion of the rotor wake downwards was demonstrated.

## 2.0 ANALYSIS

### 2.1 Background to the Analysis

Earlier approaches to the analysis of body on rotor or rotor on body interference has generally been limited to first-order effects. That is, the presence of the fuselage has been included in the rotor calculation by means of some perturbation of the rotor inflow field or the presence of the rotor is considered in a calculation of the fuselage aerodynamics through the inclusion of an actuator disc or vortex tube model which alters the fuselage onset flow. No attempt is made, however, to introduce any coupling by, say, including the presence of the fuselage in the calculation of the rotor downwash field passing over the fuselage. One reason for this is the complexity of the models required to adequately represent (alone) the rotor and fuselage flow fields.

Figure 1 represents a fairly typical vortex filament model of a helicopter rotor wake in forward flight. This illustration, taken from the work of Landgrebe,<sup>21</sup> presents the rotor wake as a series of straight line vortex elements. Every one of these vortex segments induces a velocity on every other and on the rotor blade; determination of the equilibrium position of the wake, and, hence, the rotor inflow, loading and performance involves the solution of the wake circulation matrix at each instant in time, with the wake being progressively generated until some equilibrium shape is reached. This is a procedure which demands most of the resources of even today's advanced computing machines. Similarly, in the calculation of the fuselage aerodynamics, the airframe is discretized and represented as a collection of flat panels, Figure 2, each modelled by singularities whose strengths are determined by position of the panel on the body and the onset flow. The strengths of the singularities, the unknowns in the solution, are conventionally determined by the inversion of a matrix equation involving the influence of each panel on every other panel and the boundary conditions. In the more advanced analyses of this type, Ref. 20 is typical, viscous and separated flow regions can be modelled. Again, as with the vortex filament models of the rotor wake, an analysis of this type demands most of the capability of today's computing machines. Coupling these two already involved analytic tools immediately, therefore, presents a problem of computing machine capacity. Figure 3 pictures an influence block diagram where the blocks on the diagonal represent the influence of the fuselage on the fuselage and the rotor and its wake on themselves. The off-diagonal blocks are the coupling terms, rotor on fuselage and fuselage on rotor, which must be included for a second- or higher-order solution to be achieved and, as was noted above, since the solution of each of the major blocks on their own, that is, fuselage on fuselage or rotor/wake on rotor/wake, absorb most of the machine capacity, some way must be found to simplify the model if a full solution is to be achieved. This is made even more complex by the fact that although the body/body block is



CALCULATED TIP VORTEX  
TRAJECTORIES IN FORWARD FLIGHT  
(AFTER LANDGREBE)

Figure 1. Typical Output from Vortex Filament Wake Model.

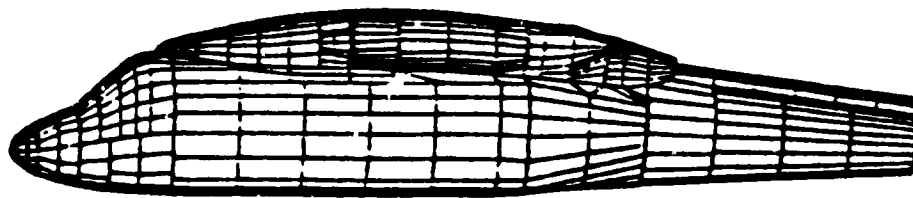


Figure 2. Typical Panel Representation for Helicopter  
Analytical Model.

	ROTOR	WAKE	FUSELAGE
ROTOR	RR <i>(diagonal hatching)</i>	RW	RF
WAKE	WR	WW <i>(diagonal hatching)</i>	WF
FUSELAGE	FR	FW	FF <i>(diagonal hatching)</i>

Figure 3. Body/Rotor/Wake Influence Block Matrix.

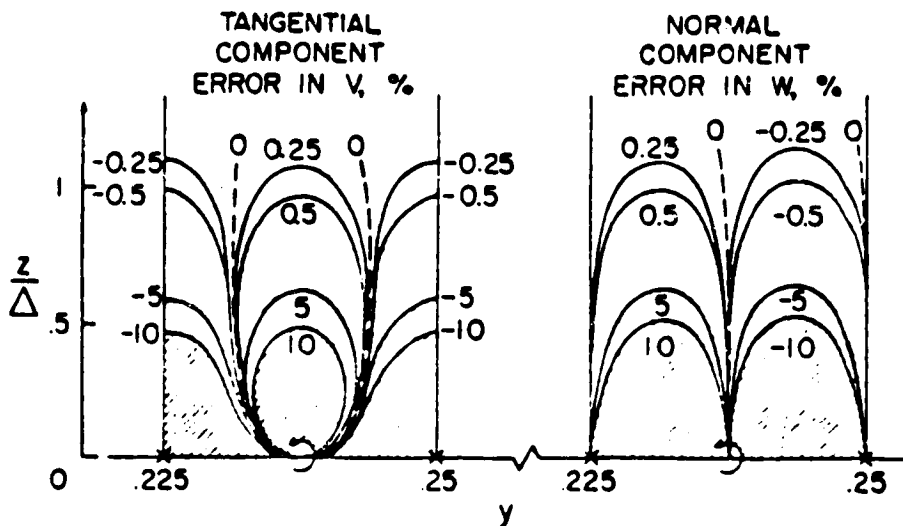


Figure 4. Panel Model with Vortex-Lattice Singularities--  
Implicit Velocity Component Errors.

steady, all the other blocks are time dependent when considered in the body axis system.

In the present analysis this is overcome by working with a time averaged vortex sheath rather than the time varying vortex filament model that is more conventionally used. The vortex sheath is attached around the edge of the rotor disc and represents the envelope within which the rotor wake will be transported downstream. This type of wake model may be distorted (relaxed) in the same way as the filament models and will provide all the inflow distributional effects in the rotor disc plane in that a rotor blade moving through the inflow field will experience the same low harmonics that would be felt in a filament model. This is felt to be adequate for performance prediction. The higher harmonics of inflow needed for rotor loads work may be simulated, but this is beyond the scope of the present study.

Another technical problem which must be overcome before coupled fuselage and rotor wake calculations could be achieved arises from the nature of the fuselage model itself. In the conventional panel model representation, the flow solution is strictly only correct at the panel control point. Away from this location substantial errors can exist and Figure 4, taken from Reference 18, shows how these can vary in a typical case. For the body/rotor flow field calculation, streamlines close to the body have to be defined if fuselage induced rotor wake deformation is to be calculated and some way must be found to avoid the errors pictured in Figure 4 if this is to be achieved.

A solution to this problem is provided by a new method developed by Maskew and described in detail in Reference 20. In this approach the surface is modelled using doublet singularities. The use of doublets together with an appropriate choice of boundary conditions and an interpolation technique which determines local doublet gradients, and through them surface and off-body velocities, gives a continuous definition of the local flow field. With the earlier source singularities models this would have been impossible, especially when the strong vortex elements from the leading edge of the rotor passed close to the fuselage panels. Figure 5(a), again taken from Reference 20, illustrates the ability of the doublet code to handle this type of close passage problem. Here, the streamlines around a strong vortex positioned above an airfoil leading edge are shown. As can be seen in Figure 5(b), the calculated pressure distribution is smooth and the derived off-body streamlines are well defined.

Together the vortex sheath model of the rotor wake and the doublet analysis provide the tools with which to represent the flow around helicopter fuselage/rotor combinations. What is needed now is some means of coupling the wake and fuselage models. This is provided by a rotor blade element model embedded within the potential flow solution. The solution proceeds iteratively and is represented by the block diagrams given in Figure 6.

ORIGINAL PAGE IS  
OF POOR QUALITY

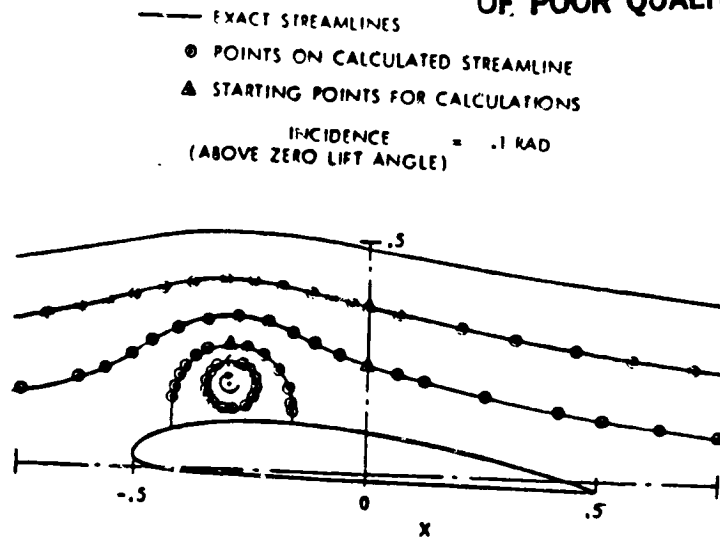


Figure 5(a). Comparison of Off-Body Streamlines Calculated using VSAERO with Exact Solution Result.

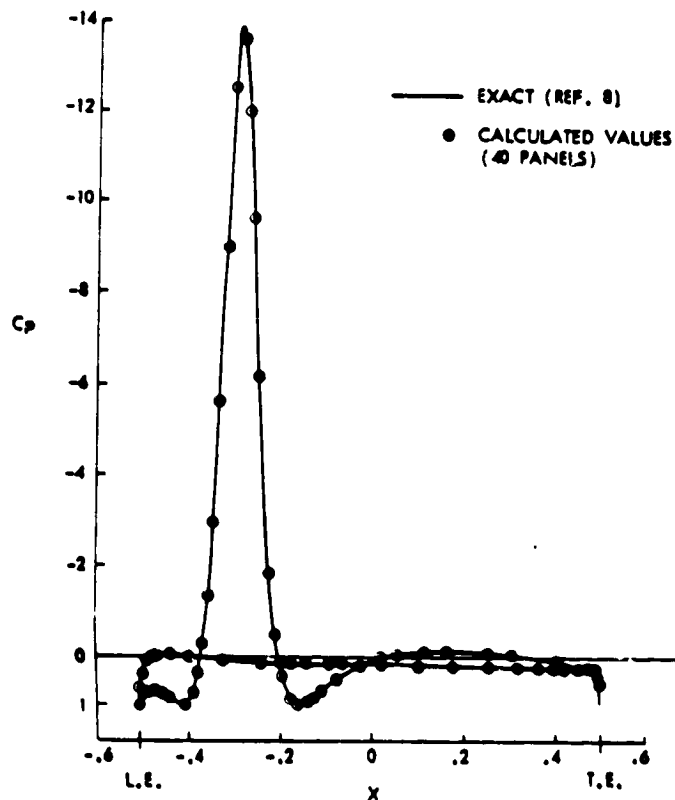


Figure 5(b). Comparison of Pressure Distribution Calculated with Program VSAERO and Exact Solution.

ORIGINAL PAGE IS  
OF POOR QUALITY

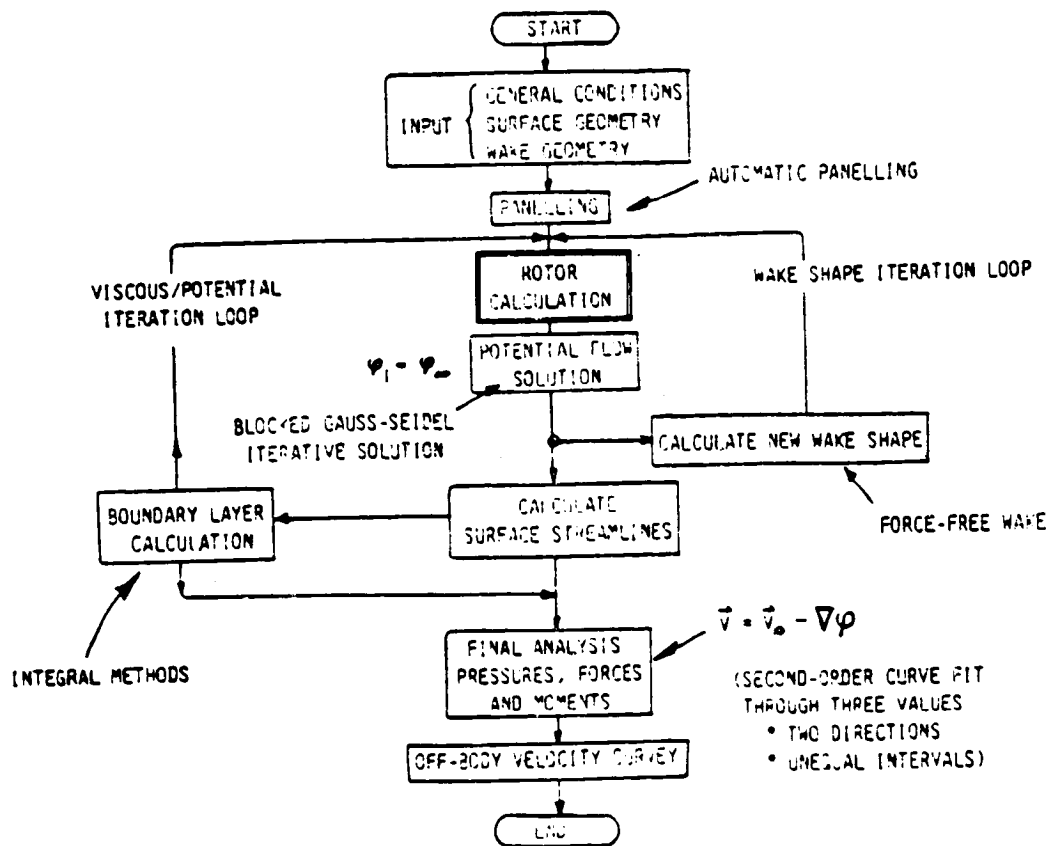


Figure 6. General Program Schematic.

The approach, first outlined in Reference 17, is built around a panel model of the fuselage and a vortex sheath model of the rotor wake attached around the edge of a panel model of the rotor disc. The whole assembly is driven by a blade element model of the rotor. Having panelled the fuselage and the rotor disc and set up the rotor wake in some initial position, the rotor blade element calculation is used to define the variation of blade loading around the azimuth. Assuming some initial inflow, the blade element calculation provides the loading distribution which becomes the boundary conditions that are enforced on the rotor disc panel model. This loading is fed into the rotor wake sheet and is included in the solution for the strength of singularities used in the fuselage model. With fuselage singularities then known and the rotor loading defined it is possible to calculate the flow field velocities around the rotor wake and to relax (deform) the wake as dictated by the local flow. Following the wake relaxation the rotor inflow field is re-evaluated based on the new wake position and the blade element calculation re-run to update the now radially and azimuthally varying time-averaged, disc loading distribution. The whole procedure may then be repeated as often as is required to arrive at a converged rotor loading, wake position and fuselage airloads solution. When this is complete, the loadings represent fully the effect of rotor on fuselage and fuselage on rotor, including the second and higher-order effects.

The blade element model used in the present calculation is the conventional, rigid blade, flapping analysis. Airfoil section data is included in the standard manner. Since the procedure is modularized, it would be very easy at a later date to replace the performance routine with a more elegant model.

## 2.2 Body Aerodynamics

The aerodynamics of the body and wake components are calculated using program VSAERO. Program VSAERO (Vortex Separation AEROdynamics analysis) is a refined surface singularity analysis which removes the limitations of the earlier generations of codes (Reference 22 is typical) and provides a much more rigorous aerodynamic model without sacrificing the simple, flat panel model of the aircraft shape. The program development was funded by NASA and the U.S. Navy and has been documented most fully in Reference 23. Using a combination of source and doublet singularities and modifying the way in which the boundary conditions are applied, the program solves for the local doublet strength. This is then differentiated to obtain the local velocities. The method of solution has been extended to handle strong external vortex/surface interactions and is no longer constrained as were the earlier codes to align external flow vortices along panel edges. This permits relaxation of the wake (iteration to a force-free location) without the repanning between iterations that was implicit in the earlier programs.

The program used in the present study was the potential flow model for general configurations with multiple components. The program capacity is for 1,000 panels on each side of the plane of symmetry with an additional 1,000 panels of separated wake. The wakes may be shed by all the components along any edge (say the wing tip edge) and any or all wake(s) may be relaxed. Engine inlet and exhaust flow may be modelled and high energy jets simulated. The program can also be used to survey the velocity field off the body, and to carry out iterative calculations of the viscous/potential flow on the body surface. Also available in other versions of the program are on- and off-body streamline capability, coupled viscous/potential flow iterations with extensive separation modelling and time-stepping and harmonic wake analysis, respectively, for large and small amplitude unsteady body motions.

The principal problem working against the application of the old panel codes to the rotor and other highly interactive flows is their inability to handle wake/surface cutting. In a conventional source or vortex-lattice method, impact of a vortex element on the surface anywhere other than along a panel joint will cause a divergent solution. In VSAERO, because of the nature of the solution, it simply causes a jump in the doublet distribution along the line of the cut. Provided that this jump is accommodated in the surface differentiation used to determine the velocity field, the resulting solution can be continuous through the cut. To demonstrate the procedure on a configuration somewhat simpler than the typical helicopter, a simple test case was set up.

### 2.3 The Wake Cutting Procedure

In order to explore whether the potential jump associated with wake cutting would violate the basic formulation or at least cause a numerical problem in the solution, a test case was set up with a vertical surface ahead of a wing, Figure 7. The vertical surface is modelled with a 3 x 12 panel array on a zero thickness lifting surface. The tips of this surface have a 5 degrees backward rake. The vertical surface is set at 20 degrees to the x-axis; i.e., to carry a side force directed to the plane of symmetry. The horizontal wing has a rectangular planform with an aspect ratio 4 and a NACA 0012 section: it is modelled with a 24 x 20 array of panels on the main surface and a 3 x 12 array on the half-round tip. The spanwise panelling is arranged with concentrations near the tip and just outboard of the spanwise station of the vertical surface trailing edge (i.e., where the maximum vortex wake interaction is expected to occur). The onset flow was set at 10 degrees.

Figure 8 shows two views of the calculated wake geometry after three wake shape iterations. The side view, Figure 8(a), demonstrates a very nice behavior of the basic vortex roll-up calculation on the vertical wake. The top view of the wake

ORIGINAL PAGE IS  
OF POOR QUALITY

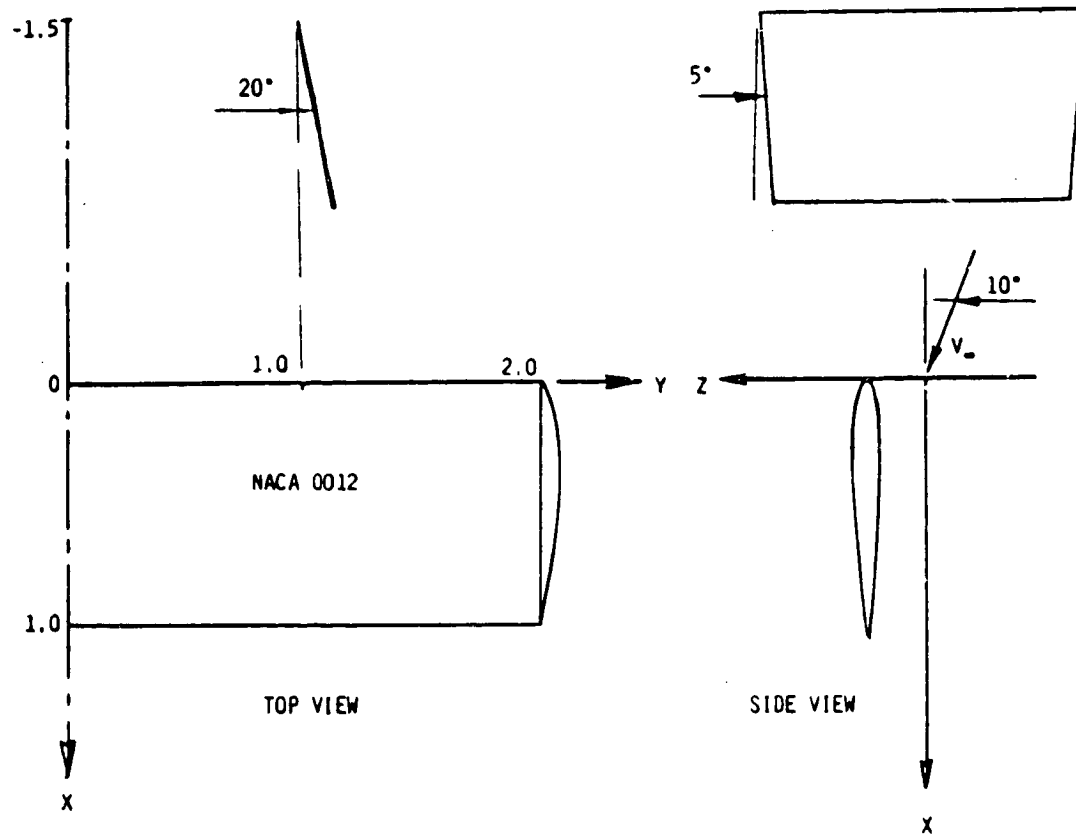


Figure 7. Schematic of Wake Cutting Model.

ORIGINAL PAGE IS  
OF POOR QUALITY

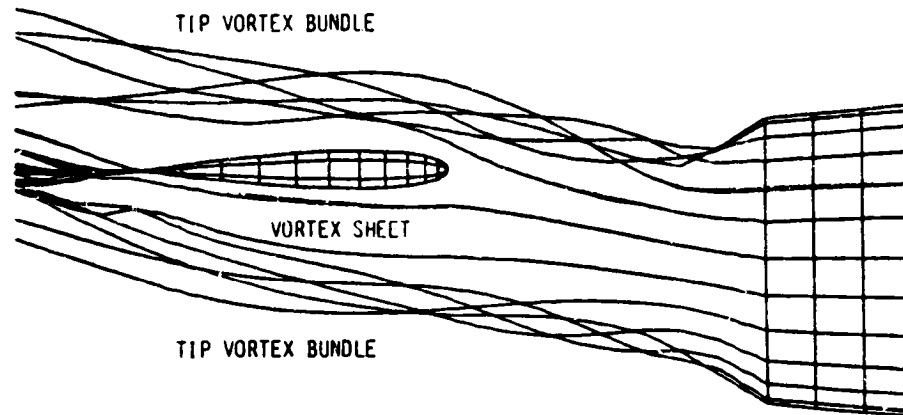


Figure 8(a). Wake Cutting Study--Side View.

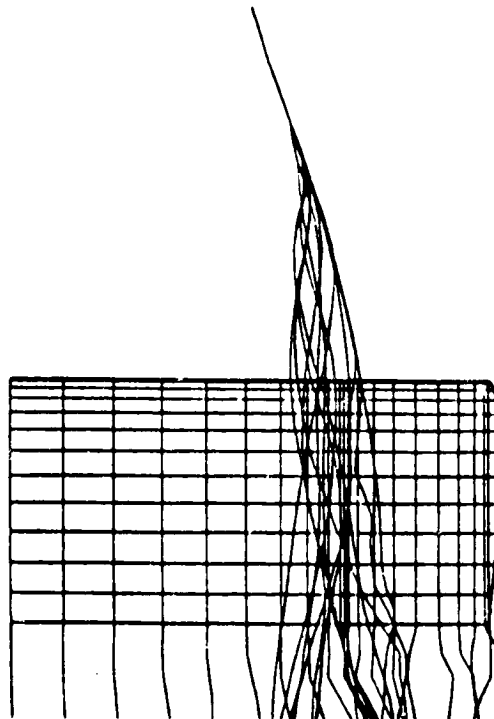


Figure 8(b). Wake Cutting Study--Top View.

ORIGINAL PAGE IS  
OF POOR QUALITY

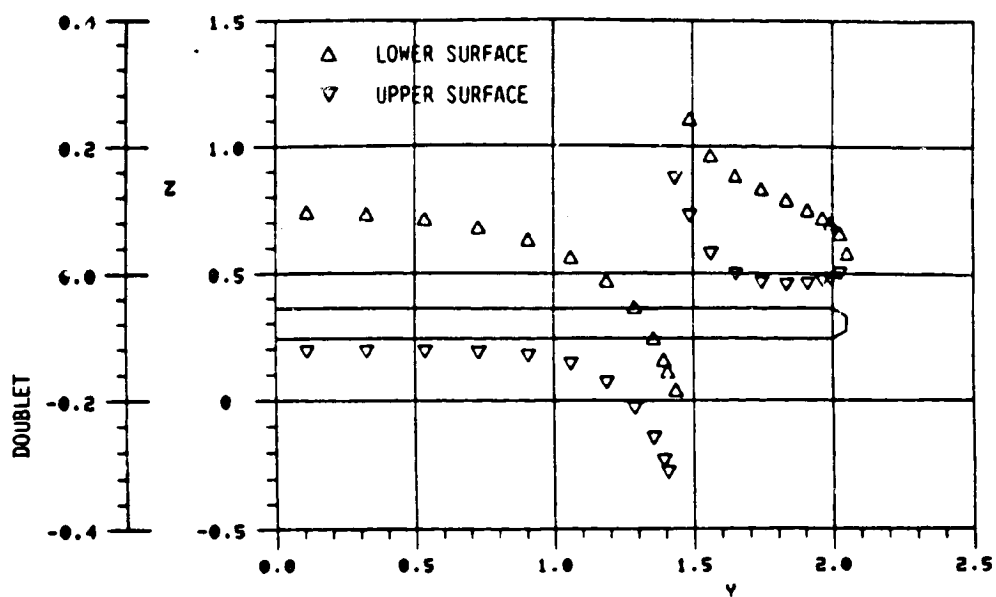


Figure 9. Wake Cutting Study--Spanwise Doublet Distribution (0.25 Chord).

ORIGINAL PAGE IS  
OF POOR QUALITY

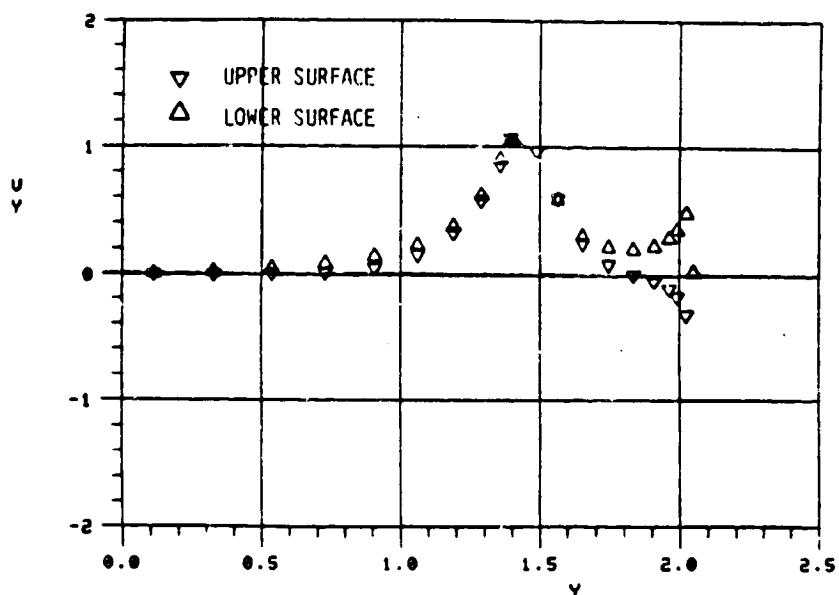


Figure 10. Wake Cutting Study--Spanwise Velocity  
(0.25 Chord).

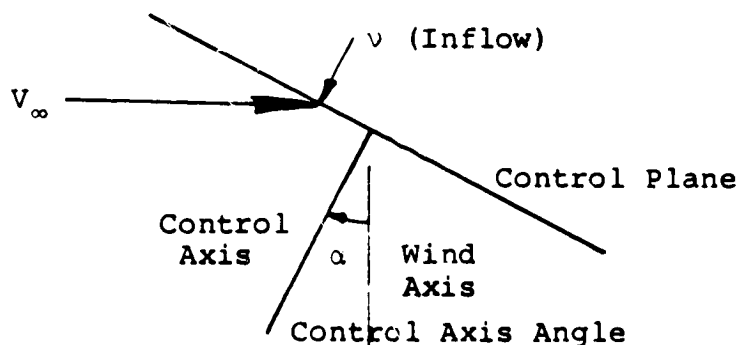
geometry (Figure 8(b)) shows reasonably good behavior except that beyond the wing trailing edge the effect of widening the spacing of the grid planes used in the wake calculation, for reasons of economy, can be seen.

A spanwise cut through the doublet distribution, Figure 9, shows the expected jump in doublet value (i.e., jump in surface perturbation potential) due to the vertical wake intersection. The jump occurs at slightly different spanwise locations on the upper and lower surfaces due to the local tilt of the wake panels at this station ( $x/c = .25$ ). It is easily verified that the spanwise doublet gradient (i.e.,  $V_y$ ), plotted in Figure 10, is essentially continuous as we pass through the wake--only the doublet value is discontinuous. During the analysis phase of the calculation, where the doublet distribution is differentiated to obtain the velocities, the program senses the wake cut induced jump and selects the appropriate differencing scheme. Similar good behavior was also noted in the other velocity components and in the surface pressure distributions. The vortex pair from the vertical surface clearly dominates the spanwise flow on the wing. The otherwise inboard flow (negative  $V_y$ ) on the wing upper surface has been totally reversed by the vortices except in the very tip region where there is clearly still some flow moving around from the lower to the upper side.

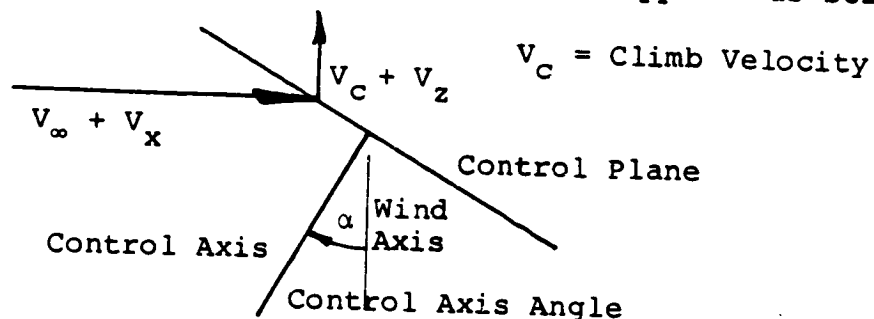
#### 3.4 Rotor Blade Aerodynamics

Rotor blade aerodynamics is calculated using a simple blade element theory model. Inflow velocity, after the first iteration during which the inflow is assumed constant at the momentum value, is calculated in the body/wake portions of the program and passed over to the rotor internally. This includes all three components of velocity and contains, in addition to the contribution of the fuselage, the wake induced terms. These velocity components coming over from program VSAERO are in the body coordinate system. As a result they must be transformed into the rotor control axis system to be considered as elements of the inflow velocity.

In the conventional rotor calculation the velocity components at the rotor disc control plane are commonly represented as below:



In the present case the situation has been generalized by introducing three components of induced velocity which contain the influence of the fuselage and the rotor self induced (through the wake) effects. The more general case appears as below:



and includes an out of plane lateral component,  $V_y$ .

Following convention these are resolved into and perpendicular to the control axis system and become

Inplane  $(V_\infty + V_x) \cos \alpha - (V_C + V_z) \sin \alpha$

Normal  $(V_C + V_z) \cos \alpha + (V_\infty + V_x) \sin \alpha$

Transverse  $V_y$

Still following normal rotor conventions these are then resolved into the blade axis system where they take on the form:

Perpendicular to the Blade

$$U_p = - (r - e) \dot{\beta} + \left[ (V_\infty + V_x) \sin \alpha + (V_C + V_z) \cos \alpha \right] \cos \beta$$

$$- \left[ (V_\infty + V_x) \cos \alpha - (V_C + V_z) \sin \alpha \right] \cos \psi + V_y \sin \psi \sin \beta$$

Inplane

$$U_I = \Omega r + \left[ (V_\infty + V_x) \cos \alpha - (V_C + V_z) \sin \alpha \right] \sin \psi - V_y \cos \psi$$

Radial

$$U_R = \left[ (V_\infty + V_x) \cos \alpha - (V_C + V_z) \sin \alpha \right] \cos \psi + V_y \sin \psi \cos \beta$$

$$+ \left[ (V_\infty + V_x) \sin \alpha + (V_C + V_z) \cos \alpha \right] \sin \beta$$

The induced velocity components are updated as the rotor body iteration proceeds. As an example, on the first pass through the rotor analysis, the vertical induced velocity,  $V_z$ , will contain only the prescribed momentum inflow velocity. On the second pass, it will contain the first-order body induced upwash (the isolated body effect) and the induced velocity from the skewed vortex sheath model of the rotor wake. The strength of the rotor wake is set by the rotor loading calculated in the first iteration. On the third pass, the  $V_z$  term contains the body effect, this time including second-order rotor and wake-induced components, and the inflow from a now distorted sheath wake. Subsequent iterations add higher-order corrections. Experience has shown that for low-speed flight, 0.05 advance ratio, two wake relaxations are required (3 passes through the rotor code). At high speed, advance ratios of greater than 0.15, two have been found to be adequate.

Convergence was based on several parameters, chief among them being the behavior of the rotor wake. This was followed from one iteration to the next and was observed to stabilize very quickly as the interactions were included in the wake relaxation. Other criteria included rotor total and blade section parameters, and perhaps most sensitive, the local velocity at rotor panel centers passed back to the blade element calculation by the fuselage/rotor wake segments of the program.

No small angle assumptions have been made to permit extension of the analysis to propeller, tilt rotor cases at some future date.

With the blade section onset flow determined, the local angle of attack is known and the section and blade loads can be calculated in the conventional manner with radial and then azimuthal integrations. Only rigid blade flapping is permitted. No aeroelastic effects are considered. The rotor module has deliberately been isolated from the rest of the calculation so that, if required at a later time, a more involved rotor algorithm may be substituted. The present module may be operated at prescribed collective and cyclic pitch settings or may be allowed to iterate to requested gross weight and rolling and pitching moment targets.

## 2.5 Rotor Disc Panel Model

Coupling of the body and rotor aerodynamic phases of the calculation are carried out through the panel model of the rotor disc, Figure 11. This happens in two ways. The first is the straightforward model of the incremental velocity added to the flow by an actuator disc (or more correctly, mosaic) where the velocity on individual "tile" or panel is the impulse produced by the time averaged loading on a disc segment bounded by pre-identified radial and azimuthal boundaries. The second is the way in which the radial distribution of loading is integrated to provide a local doublet strength and ultimately provide the strength of the vorticity passed over into the wake attached along the disc inner and outer edges. This is illustrated in the schematic in Figure 12.

One of the features available in program VSAERO, 23 is the "type 4" patch. This type of patch allows actuator disc panel models of propellers and rotors to be constructed and requires that both the source and doublet parts of the singularity be specified.

For a type 4 patch, the doublet strength is given by:

$$\sigma = \frac{1}{4\pi} \int_0^r \frac{\Delta C_p}{2(V'/V_\infty)} dr$$

$\Delta C_p$  is the panel differential pressure coefficient (upper-lower),  $V'$  is the resultant local velocity at the panel and  $V_\infty$  is the onset flow velocity. The incremental loading for the panel model may be easily determined from the blade element calculation.

$$\Delta C_p = \frac{\Delta \bar{L}}{\frac{1}{2} \rho V_\infty^2 \Delta A}$$

where  $\Delta \bar{L}$  is the time averaged segment load and  $\Delta A$  the segment area and  $\Delta \bar{L}$  is given simply for a particular azimuth and radial location by

$$\Delta \bar{L} = \frac{\Delta L}{\Delta r} \cdot \Delta r \cdot \frac{b}{NC}$$

In this expression,  $\Delta L/\Delta r$  is the blade lift per unit span,  $\Delta R$  is the segment spanwise extent,  $b$  is the number of blades and  $NC$  is the number of azimuth increments into which the disc circumference is broken.

ORIGINAL PAGE IS  
OF POOR QUALITY

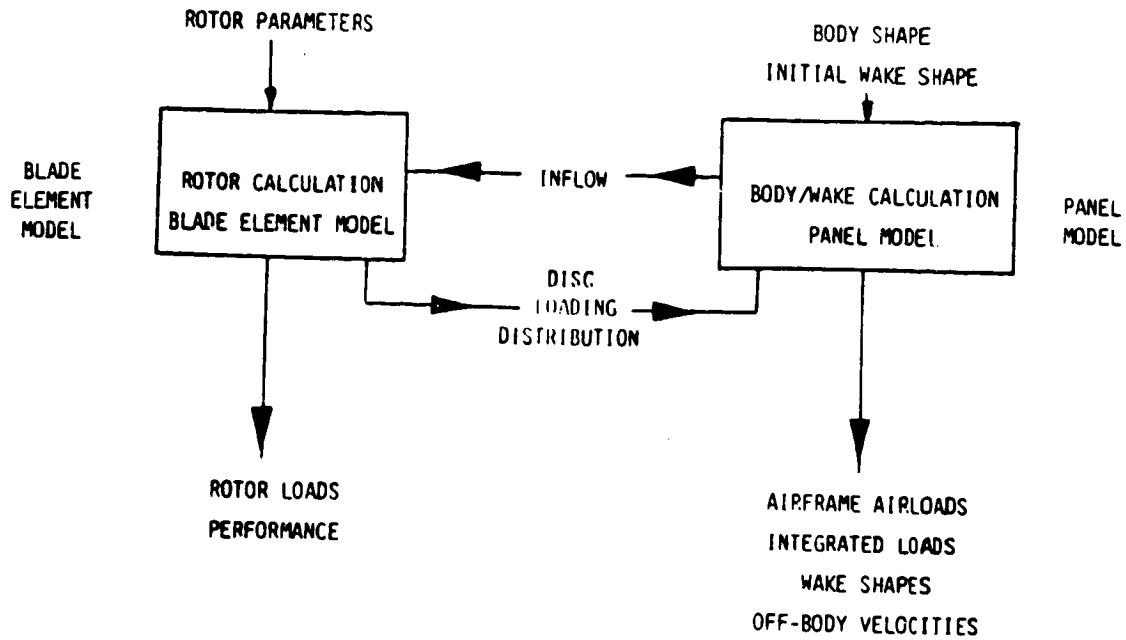


Figure 11. Body/Rotor Interference Calculation Schematic.

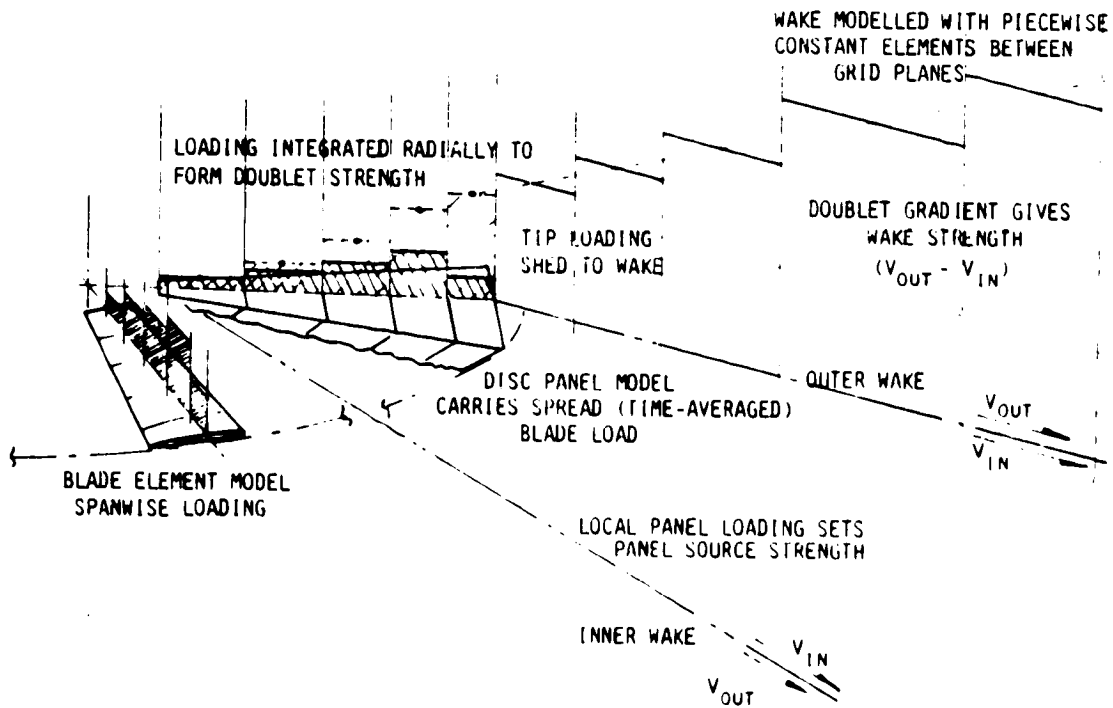


Figure 12. Blade Model/Panel Model/Wake Schematic.

Definition of the source term in the singularity expression requires the normal velocity on the disc panels and this also can be determined from the blade element calculation output and simple momentum theory. The doublet strength and the normal velocity for each panel are passed over from the rotor code to the body solution internally and require no user input.

The rotor wake is automatically fed by the doublet strength determined for those panel fringing the disc model using the basic VSAERO capability. With the wake sheath being fed by the tip doublet strength, the sum of the spanwise integration of loading, the inflow calculation has the same order of fidelity as a filament model of the wake in which only the tip vortex is modelled.

### 3.0 THE COMPUTER PROGRAM

The Body-Rotor analysis program (BodRot) is an extension of the basic program VSAERO.23 The rotor program is a self contained subroutine called by the main program whenever a type 4 patch, a rotor or propeller disc, is loaded. The code is available as an update deck to the basic program. The analysis has been loaded and executed on Control Data Cyber 176 and 7600 machines and has recently been demonstrated on CRAY. The only additional data required beyond the general configuration description is the rotor details and the blade section airfoil data.

Part 2 of this technical report contains the program user's guide, sample input and output listing and a listing of the rotor subroutine source code.

## 4.0 DISCUSSION OF RESULTS

### 4.1 Application of the Analysis to a Simple Body/Rotor Example

To evaluate the combined body/rotor analysis program, a simple test case was set up with the fuselage sized to exaggerate the body/rotor interference effects. Figure 13(a) and (b) shows, respectively, an oblique view and a side view of this test configuration. The panelling on both body and rotor is deliberately less dense than in a practical case in an attempt to preserve some clarity in the illustration. The rotor panelling is set to coincide with the azimuthal stations at which the blade element calculation is performed, while the panel centroids are coincident with the blade element control point locations. Also shown in this figure is the initially prescribed wake location with only the streamwise legs of the wake panels shown for clarity. Note that the wake has been "draped" over the fuselage. At this stage in the development of the analysis, the calculation is limited to cases where the wake passes either completely above the body or totally immerses the body.

In Figure 14(a) and (b) the rotor wake is shown from the same view points as above after two iteration cycles. For this case, which represents a rotor at a low advance ratio and a thrust coefficient solidity ratio ( $C_T/\sigma$ ) of roughly 0.08, the very pronounced wake roll-up that would be expected is clearly seen. The rotor wake behaving in its time-averaged form much like the wake of a low aspect ratio wing begins to roll up at the outer edges as it leaves the trailing edge of the disc. The roll-up process begins well ahead of the rotor shaft axis as can be seen by the pronounced divergence of the streamwise wake lines. In the side view, Figure 14(b), the presence of the body is evident in the path followed by the lines from the disc leading edge, much higher than would be expected from the rotor in isolation. Body influence is most marked, however, in the plan view, Figure 14(c), where the wake roll-up is taking place at a spanwise (lateral) location further outboard than in the isolated rotor case. The plan view for the equivalent isolated rotor case is shown in Figure 15. With the capability to calculate the wake trajectories and coupled behavior demonstrated with the simple model, the study was broadened to examine more representative shapes.

### 4.2 Basic Body/Rotor Results for a Representative Configuration

The model chosen for the study was that tested by Freeman and Mineck<sup>4</sup> scaled to a rotor radius of 20 feet. This size was chosen to give a full scale machine typical of helicopters in the small to medium size range. A target vehicle weight of 7,000 lb. gave a rotor thrust coefficient of 0.00554. Calculations were made at three advance ratios: these were 0.05, 0.15 and 0.3.

ORIGINAL PAGE IS  
OF POOR QUALITY

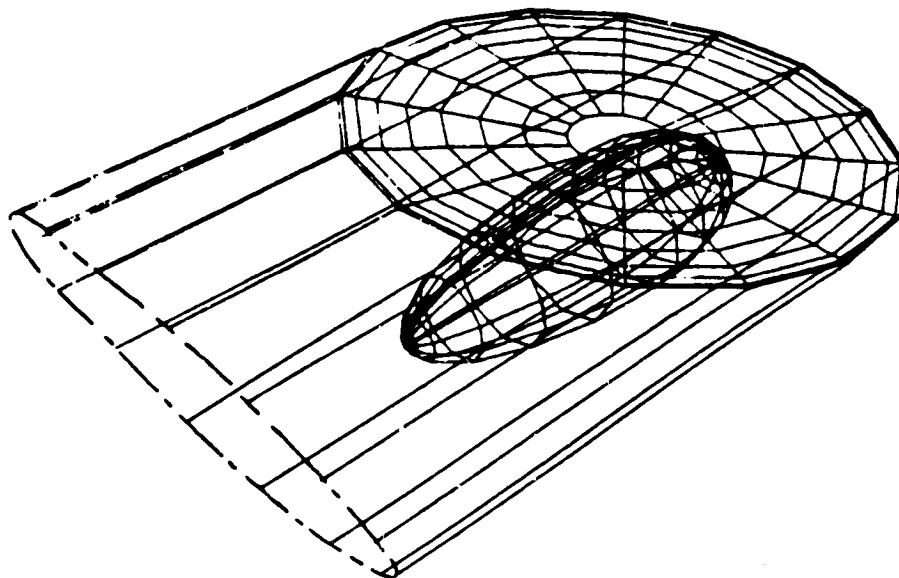


Figure 13(a). Body Rotor Interference Study--  
Starting Condition.

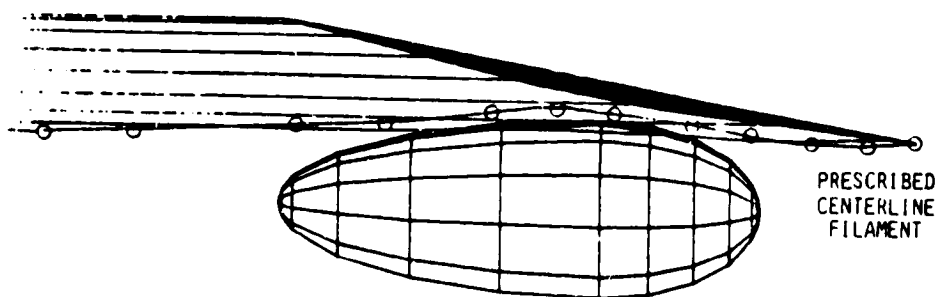


Figure 13(b). Body Rotor Interference Study--  
Starting Condition.

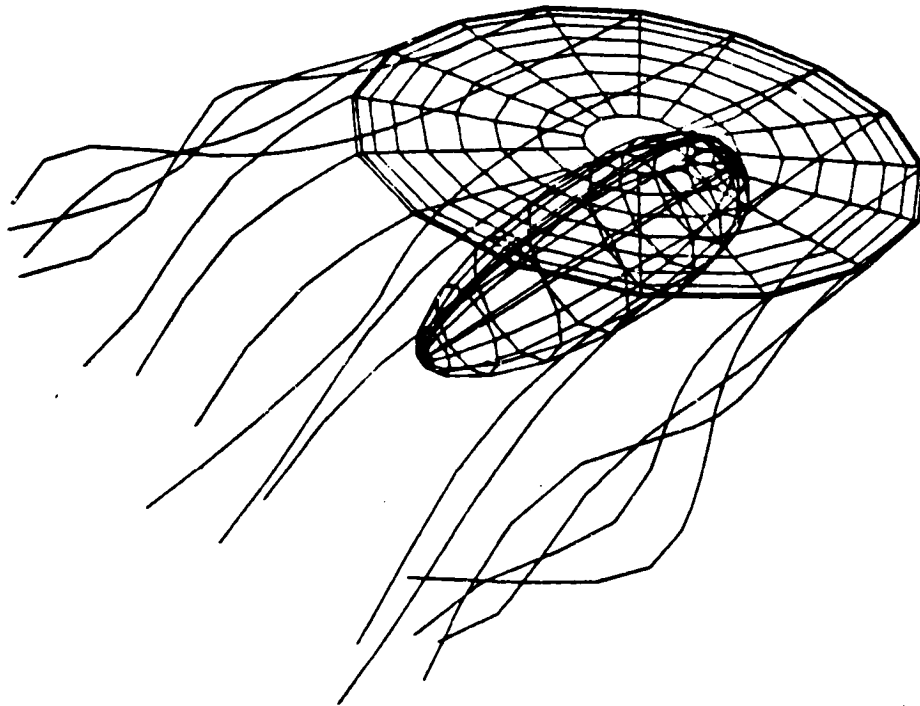


Figure 14(a). Body Interference Study, Relaxed Wake.

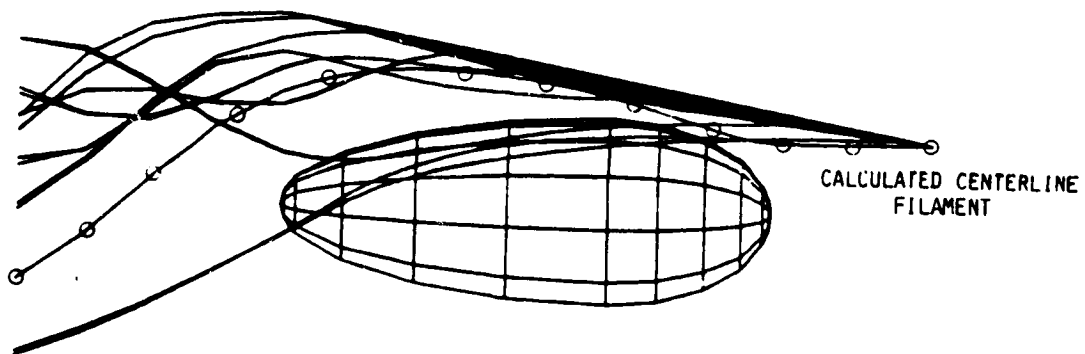


Figure 14(b). Body Interference Study, Relaxed Wake.

ORIGINAL PAGE IS  
OF POOR QUALITY.

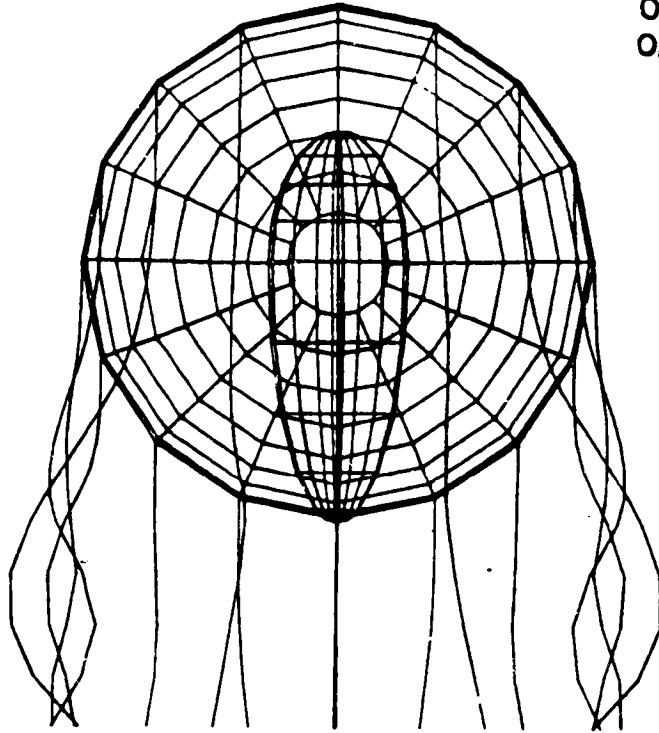


Figure 14(c). Body Inter-  
ference Study--Relaxed  
Wake

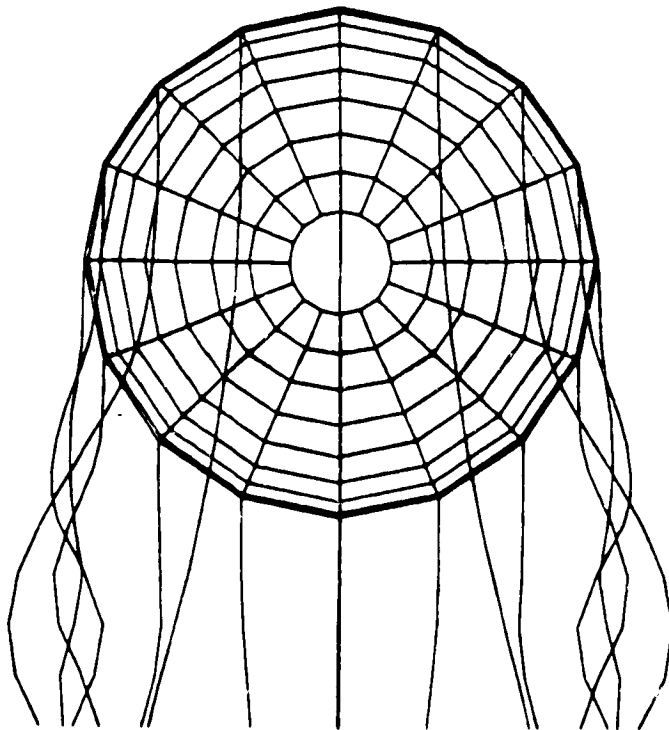


Figure 15. Isolated Rotor,  
Relaxed Wake.

The two low values were chosen to provide an overlap with the Freeman data, the high value to give a more realistic case for studying body rotor interference close to the cruise condition. The body is shown in outline in Figure 16 comparing the original model and calculation scales.

Figure 17 shows an oblique view of the basic panel model of the fuselage and rotor. Correlation with measured surface pressure data is generally acceptable. Certainly on those regions most influenced by the rotor wake, the fuselage aft of the rotor center, agreement is good. Figure 18 shows comparisons at station 17.6 for two advance ratios. The comparison is presented at the same data scales as in the original report,<sup>4</sup> at advance ratios of 0.05 and 0.15. Correlation over the front fuselage, Figure 19, is less good. This probably results, to a certain extent, from the relative crudity of the panel model in this region, and from a mismatch in the calculated and actual angles of attack. Wind tunnel corrections had been allowed for the test data. In the analysis, the lower surface was made deliberately sparse to allow for increased panel density on the upper and aft sections. Sections within the rotor influence should be less sensitive to model rigging angle/analysis angle mismatch than would be those sections on the nose. For comparison purposes the isolated body results are superimposed on the open scale ( $\mu = 0.15$ ) plots. The full correlation set for all the stations at which data were measured in the original test are shown in Appendix A of this report for the advance ratios at which analysis and test overlapped.

An oblique view of the low advance ratio case, Figure 20, shows the wake draped over the fuselage. This is explored further in Figure 21 where cross sections are taken through the wake as it develops aft and downwards. It is interesting to note the roll-up of the edges of the rotor wake. Since the wake is made up of rectilinear vortex elements, some crossing is to be expected in the model. In practice, however, the wake simply coils around itself. In the model, the wake leaving the leading edge of the disc moves first upwards as it is convected aft. It then passes downward, held up above the isolated rotor position by the flow developing around the fuselage. The wake cuts the pylon, recombining above the tail cone in the region aft of the rotor head. In the absence of detailed experimental data on wake/body cutting, it is difficult to judge how valid the present model is in this region. It does, however, appear to behave as a membrane made of discrete, traverse vortex elements would act on an oblique approach to a surface, first deforming as the surface is sensed and then, at some point, dividing with the torn edges rolling up along the surface. The theoretical wake does not, of course, tear. Here, the streamwise elements defining the edges of the wake panels pass, following the external flow lines, over the body, reacting to their reflections in the surface while the

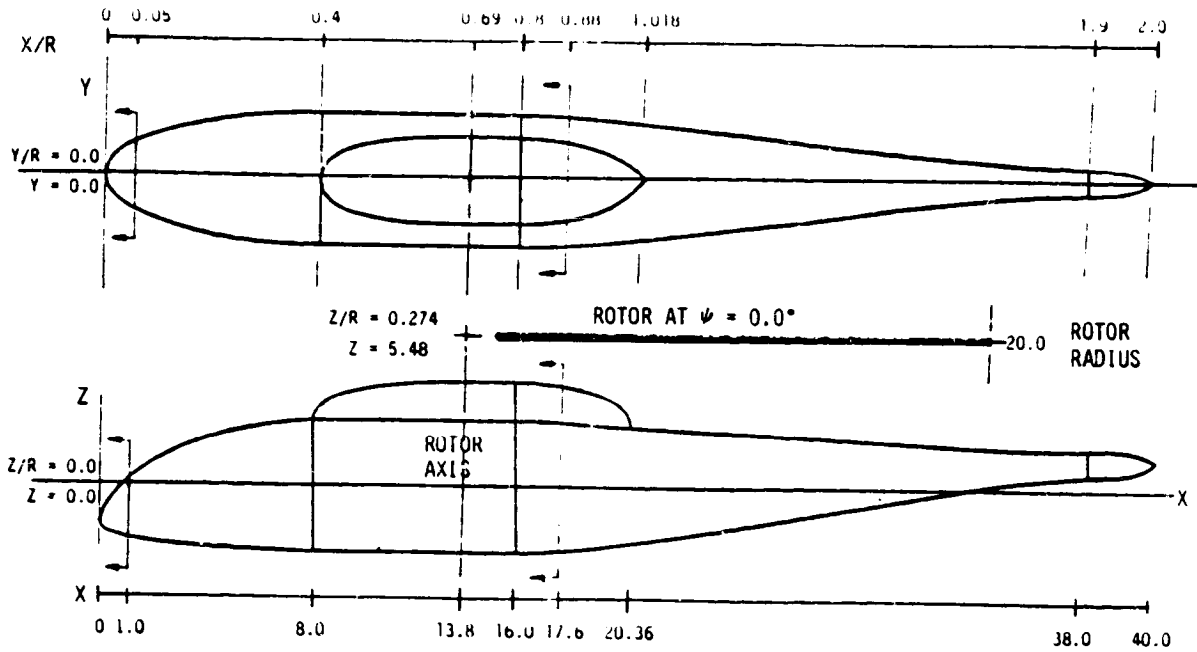


Figure 16. Outline of Freeman-Mineck Model used in Analysis (Scaled to 20 ft. Rotor Radius).

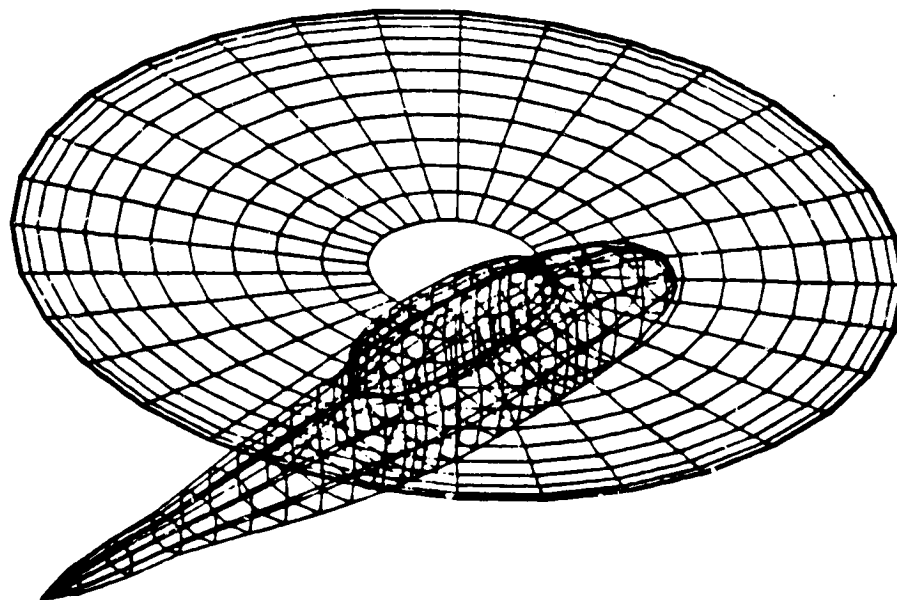


Figure 17. Basic Panel Model for Body/Rotor Studies (After Freeman and Mineck, Ref. 4).

ORIGINAL PAGE IS  
OF POOR QUALITY

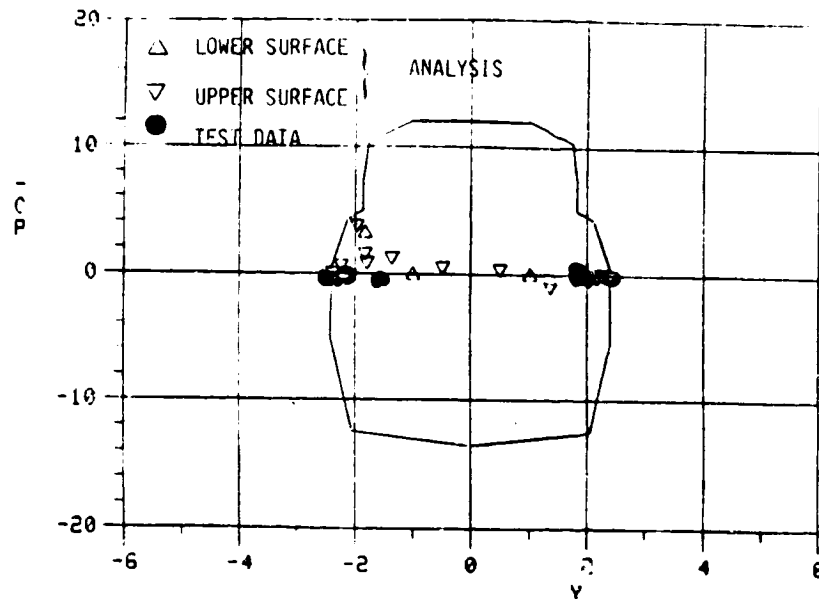


Figure 18(a). Aft Fuselage--Typical Correlation with Test Data; 0.05 Advance Ratio, Run/Point 22/139, Station 17.6 (0.88).

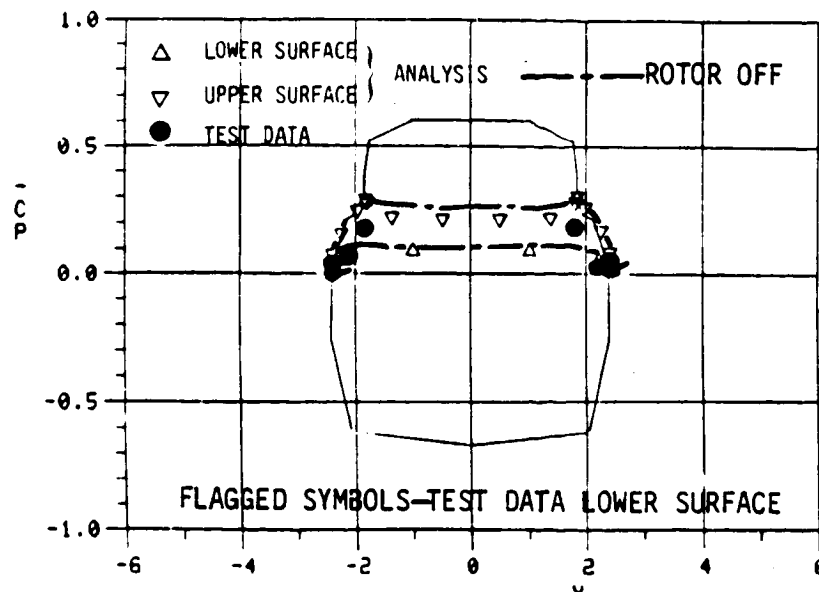


Figure 18(b). 0.15 Advance Ratio, Run/Point 25/148, Station 17.6 (0.88).

ORIGINAL PAGE IS  
OF POOR QUALITY

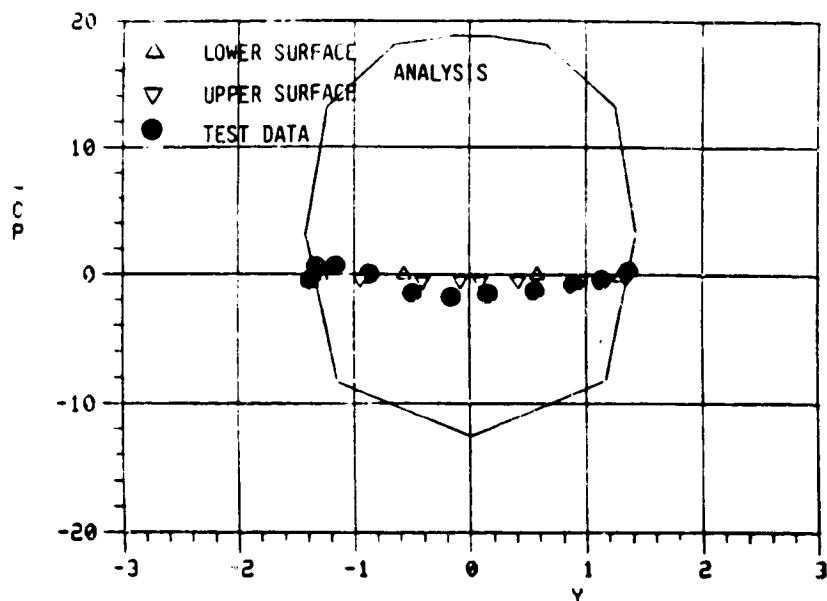


Figure 19(a). Front Fuselage--Typical Correlation with Test Data--0.05 Advance Ratio, Run/Point 22/139, Station 1.80 (0.09).

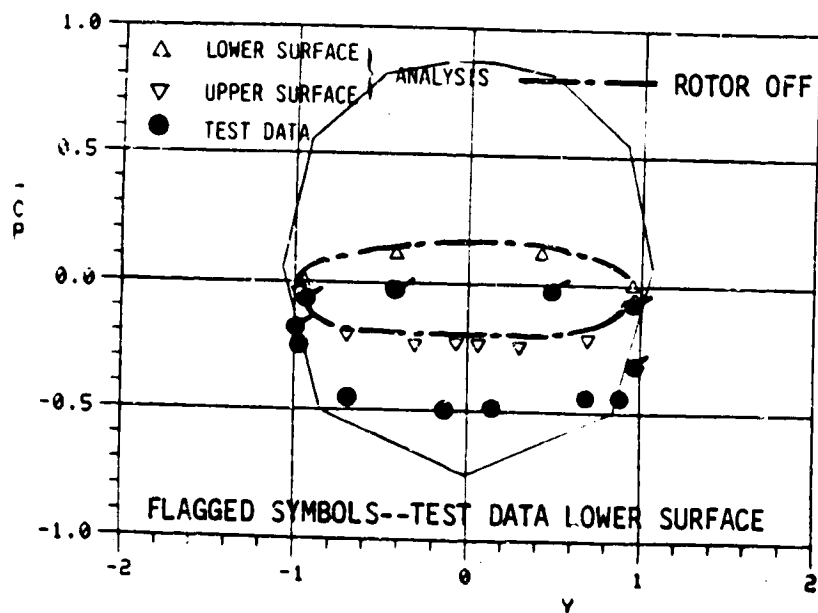


Figure 19(b). 0.15 Advance Ratio, Run/Point 25/148, Station 1.00 (0.05).

ORIGINAL PAGE IS  
OF POOR QUALITY

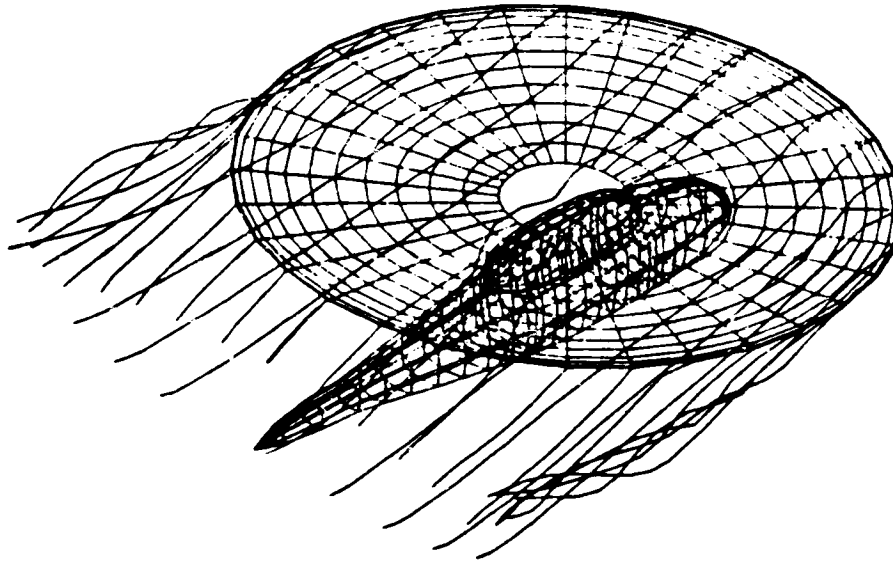


Figure 20. Calculated Distorted Wake--Low Advance Ratio.

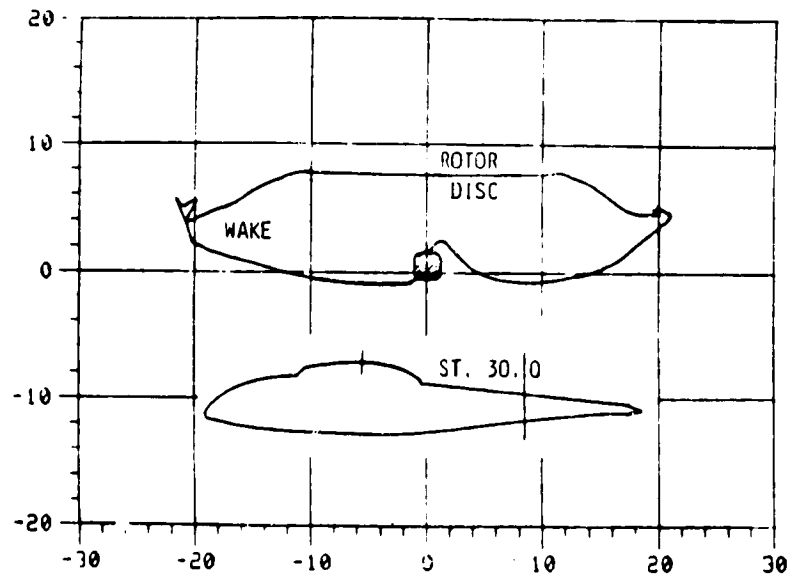


Figure 21. Cross Section through Typical Low Advance Ratio Wake (Station 30.0).

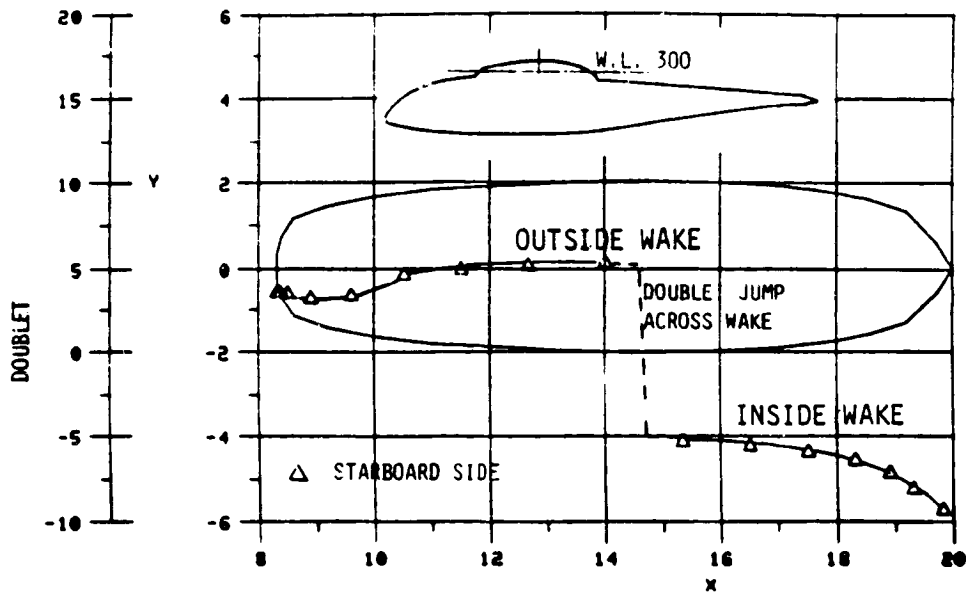
cross elements pass through the surface connecting to the adjacent streamwise filament. These carry with them, into the body solution, the jump in doublet strength which accounts for the change in flow conditions from outside to inside the wake.

The effectiveness of the procedure for handling the wake cutting problem is shown in Figure 22(a) where the doublet distribution along the pylon waterline cut is shown. The jump in strength across the wake edge is clear. In Figure 22(b), the velocity component in the streamwise direction shows no perturbation other than the changes in velocity associated with the changes in shape.

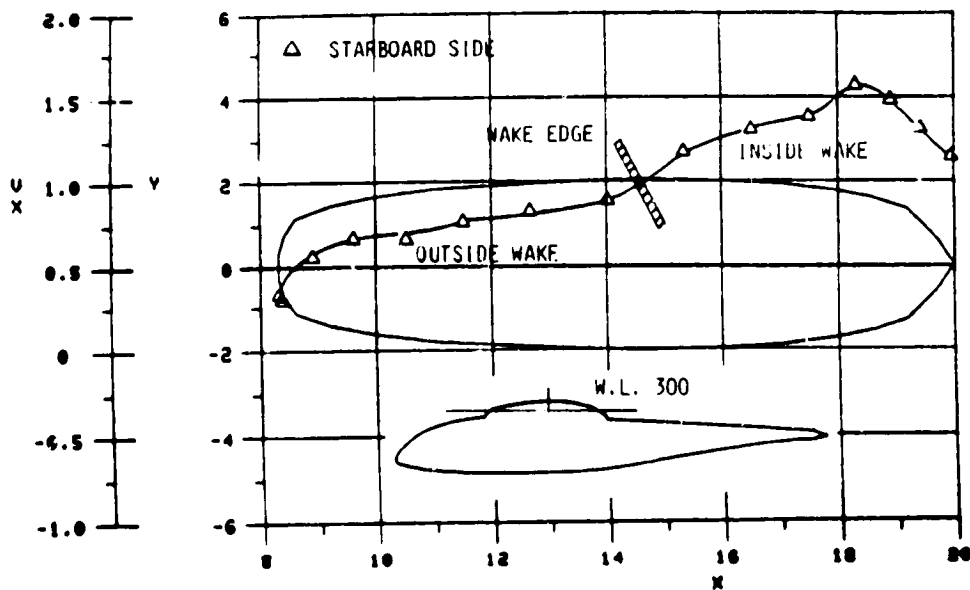
Based simply on the relative magnitude of the rotor inflow velocities, the effect of the rotor on the fuselage would be expected to decrease with increasing flight speed. This shows very clearly in Figure 23 where the vertical velocity component along a horizontal cut close to the model maximum is plotted for values of advance ratio of 0.05 and 0.15. In both cases the fuselage was set at the same angle of attack and the rotor was trimmed for level flight at 7,000 lb. GW and 12 ft.2 of drag with nominally zero pitching and rolling moment. At  $\mu = 0.15$ , the rotor-induced vertical velocity is very small and differences between right and left (advancing and retreating) sides are slight. At  $\mu = 0.05$ , however, where the rotor downwash is a substantial fraction of the forward flight speed, the side to side differences are quite marked with the more highly loaded, inboard, advancing side showing the stronger effect.

The trend of the influence of the fuselage on the rotor with speed is, of course, reversed as it is stronger at higher speeds. This is best illustrated by comparing the blade angle of attack distribution at an inboard and outboard station (0.4 and 0.9  $R/R_{TIP}$ ) for advance ratios of 0.05, 0.15 and 0.30 shown in Figures 24 and 25. As expected, the strong upwash over the nose and downwash over the aft fuselage are reflected in regions of increased and decreased angle of attack. At  $\mu = 0.05$ , the fuselage effect on the rotor is almost negligible; at  $\mu = 0.30$ , it dominates the picture. These dramatic changes in angle of attack result from the fuselage-induced flow field. Earlier analyses, the work of Landgrebe et al.<sup>2</sup> and Polzll,<sup>12</sup> are typical, failing to include coupling between fuselage and rotor flow fields, produce an inflow distribution that is symmetrical. The present approaches with full coupling shows a more nonuniform upwash, Figure 26, and one which certainly, in reflecting the lateral differences in rotor loading, is not symmetrical about the fuselage centerline.

ORIGINAL PAGE IS  
OF POOR QUALITY

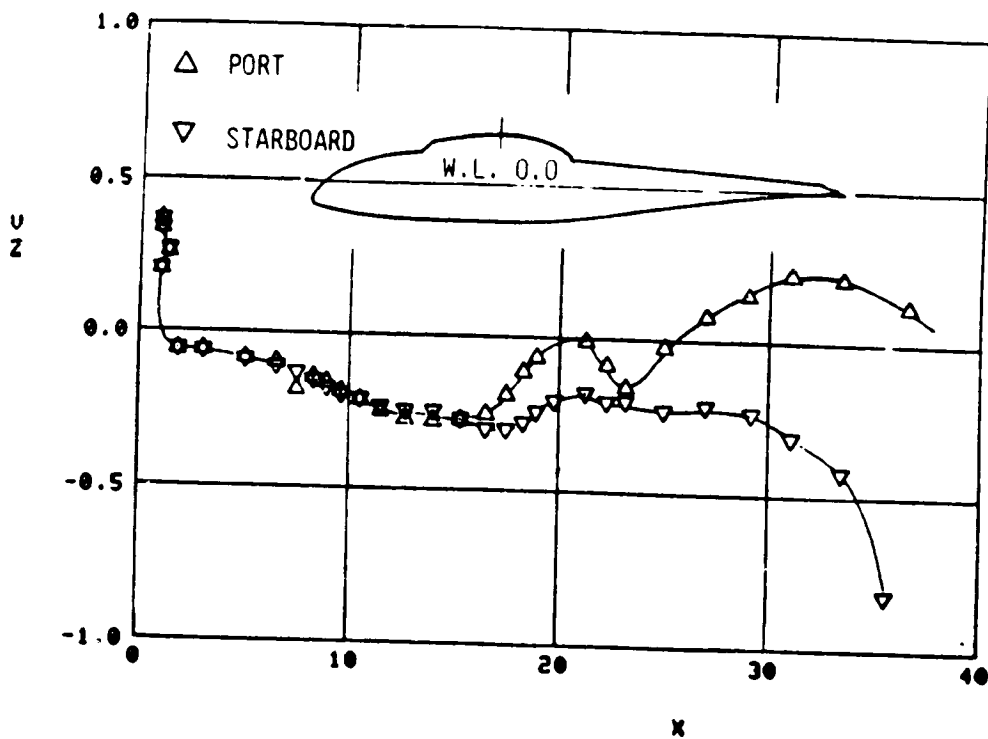


(a) Calculated Pylon Doublet Distribution--Low Advance Ratio (Waterline 3.00).

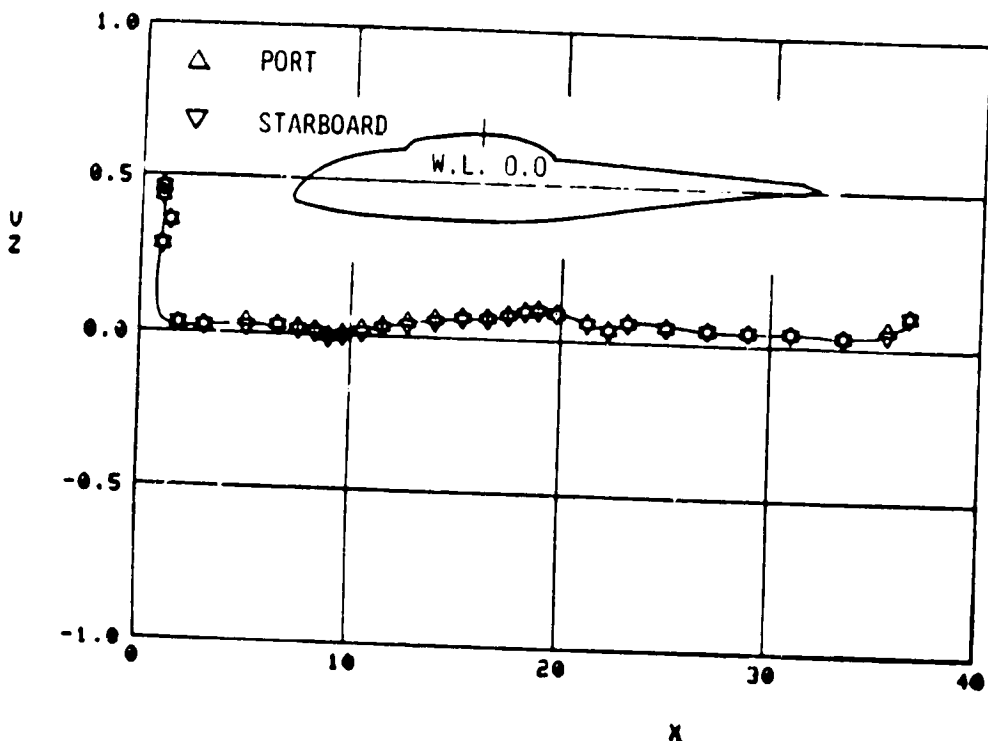


(b) Calculated Pylon Horizontal Velocity Ratio,  $V_X/V_{INF}$ -- Low Advance Ratio (Waterline 3.00).

Figure 22. Typical Effect of Rotor Wake/Pylon Intersection-- Body and Rotor Alone.



(a) Advance Ratio 0.05.



(b) Advance Ratio 0.15.

Figure 23. Calculated Vertical Velocity Ratio  $V_z/V_{\infty}$ ; Waterline 0.0; Body and Rotor Alone.

ORIGINAL PAGE IS  
OF POOR QUALITY.

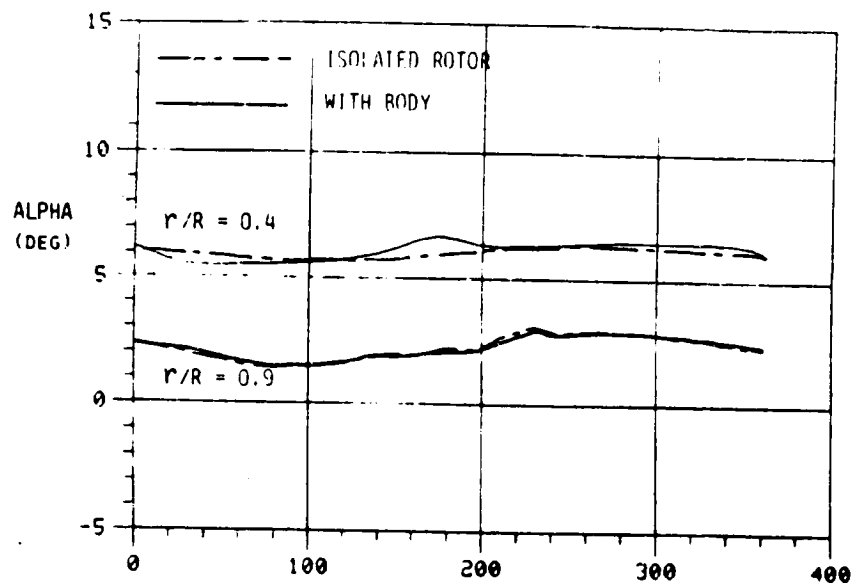


Figure 24. Calculated Effect of Body on Rotor Angle of Attack--  
0.05 Advance Ratio.

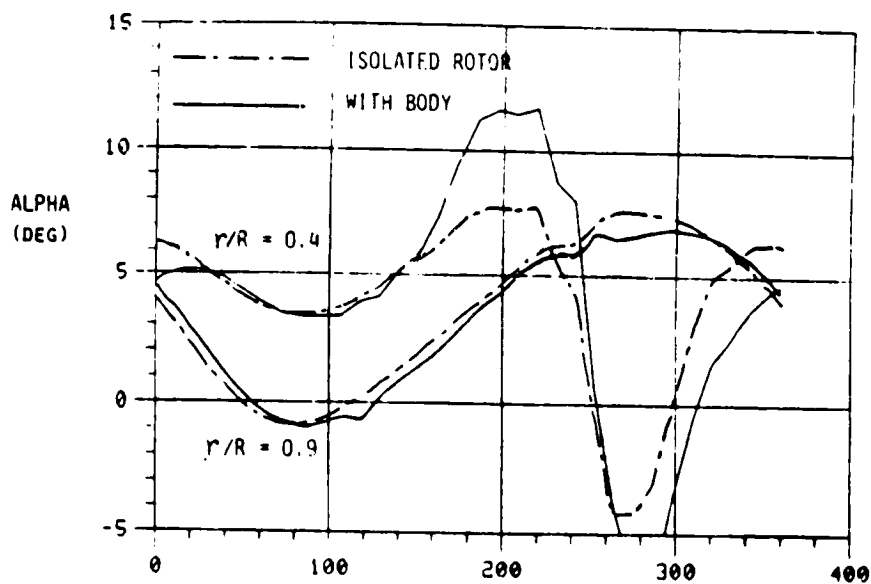


Figure 25. Calculated Effect of Body on Rotor Angle of Attack--  
0.30 Advance Ratio.

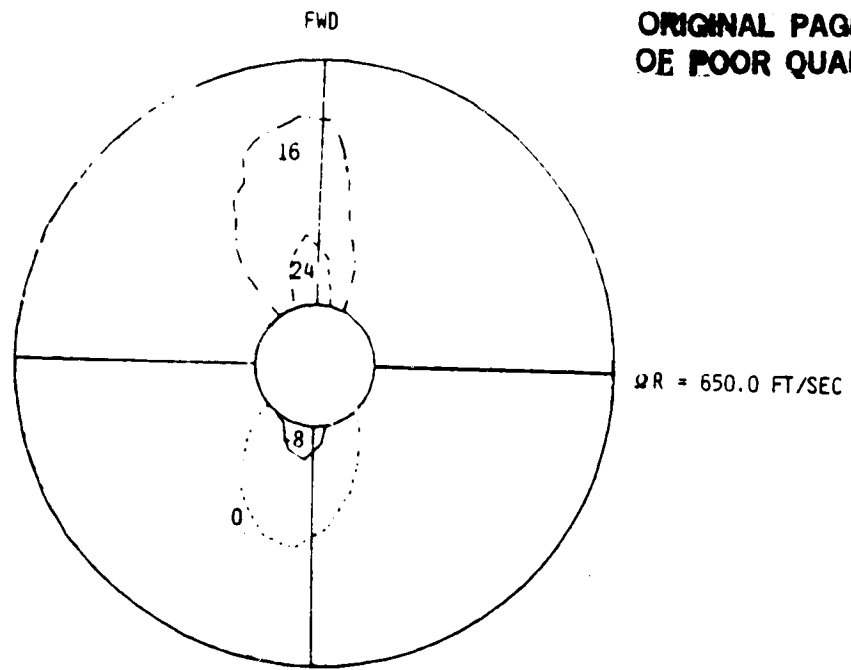


Figure 26. Calculated Contours of Upwash Velocity in Rotor Plane; Body and Rotor Alone; 0.30 Advance Ratio.

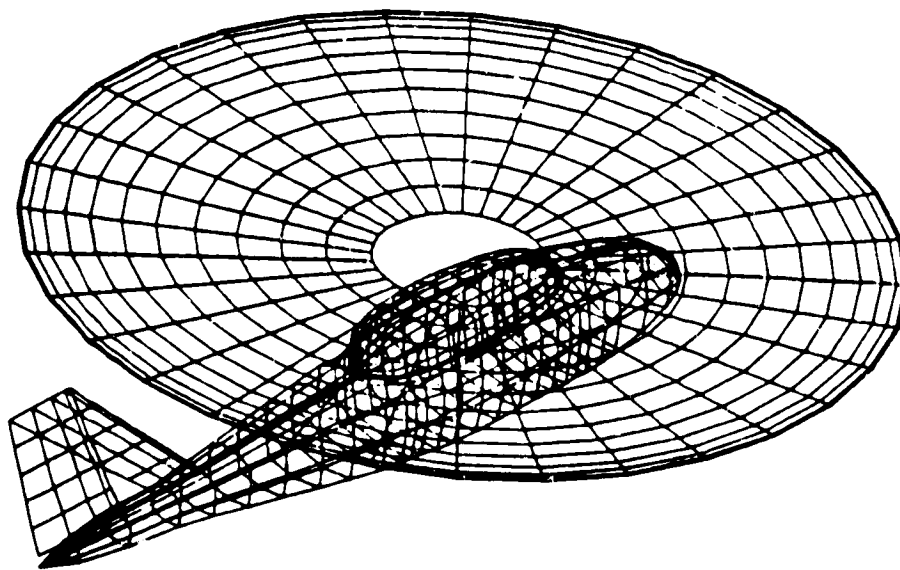


Figure 27. Body-Rotor Panel Model with Tail Assembly.

#### 4.3 The Effect of Configuration Elements on the Rotor/ Fuselage Flow Field

Adding representative horizontal and vertical stabiliser surfaces to the basic configuration has only a weak influence on the rotor flow field, but serves as a good example of the ability of the analysis to handle calculations where fuselage elements are embedded in and, in fact, pierce wake regions. For this configuration the tail surfaces, shown superimposed on the basic fuselage in Figure 27, were modelled using the "type 3" patch capability of program VSAERO.<sup>23</sup> This permits the use of simple lifting surface sections, modelled with a doublet lattice, to economically represent components in a situation where only lifting (as opposed to thickness) effects are important.

Figure 28 shows the chordwise and spanwise pressure distributions on the vertical stabiliser, with the lower portion immersed in the main rotor wake. The success of those portions of the program dealing with wake cutting can be measured by the smooth vertical development of pressures.

As might be expected the presence of the tail surfaces has only a small effect on the rotor loads, most of this coming from the slight retrimming required to compensate for the disturbance a loading on the rear of the disc caused by the small amount of circulation about the horizontal stabiliser. Figure 29 shows the comparison of blade angle of attack before and after adding the tail surfaces.

The further addition of nacelle units, Figure 30, however, has a substantial effect on the rotor flow field. Mounted on either side of the pylon they produce changes in the upwash field with an interesting indirect effect illustrated in Figure 31. This shows the angle of attack variations with azimuth at radial stations of 40% and 90% of the blade radius. Although mounted at 90° and 270° azimuth, their direct effect is seen all around the azimuth. However, the retreating blade change occurs in the relatively low energy region of the disc; for advance ratios higher than the 0.15 of the present example, it would be in the reverse flow region, and so the lateral rotor loading is put out of balance. The rotor must, therefore, be retrimmed and this is the indirect effect that is causing the observed changes at the outboard station.

Adding a mass in the center of the disc has an even more dramatic effect. The size of the blockage was chosen to represent the volume and frontal area of a rotor head with some kind of vibration adsorption equipment superimposed. The separated flow behind the rotor head was modelled and the wake transport and deformation was calculated in parallel with the deformation of the main rotor wake. Figure 32 shows an oblique view of the configuration and the calculated wake trajectories. The main rotor wake is present, but has been omitted from the picture for reasons of clarity. The calculated path aft and down matches the

ORIGINAL PAGE IS  
OF POOR QUALITY

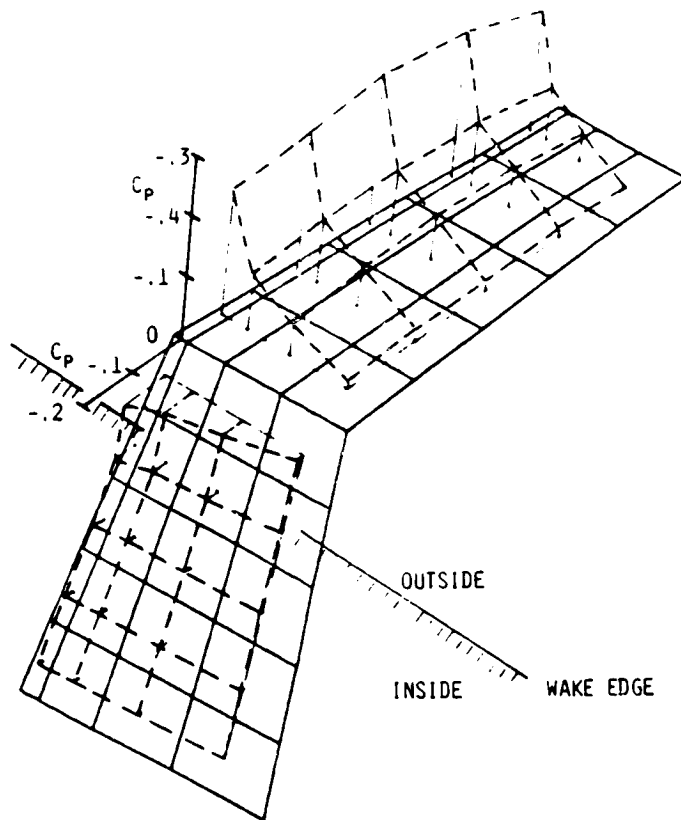


Figure 28. Pressure Distribution on Lifting-Surface Model of Tail Assembly-- 0.15 Advance Ratio.

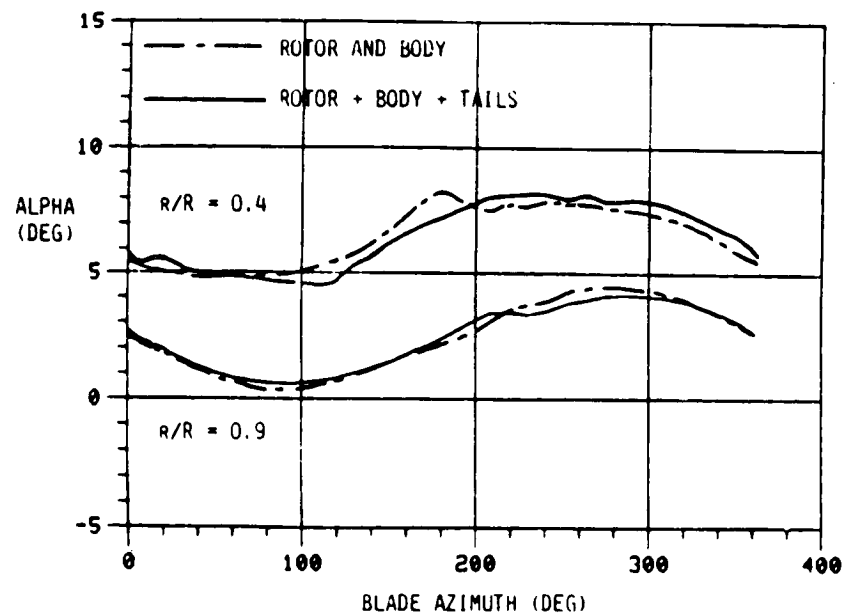


Figure 29. Effect of Tail Surfaces on Calculated Blade Angle of Attack; 0.15 Advance Ratio.

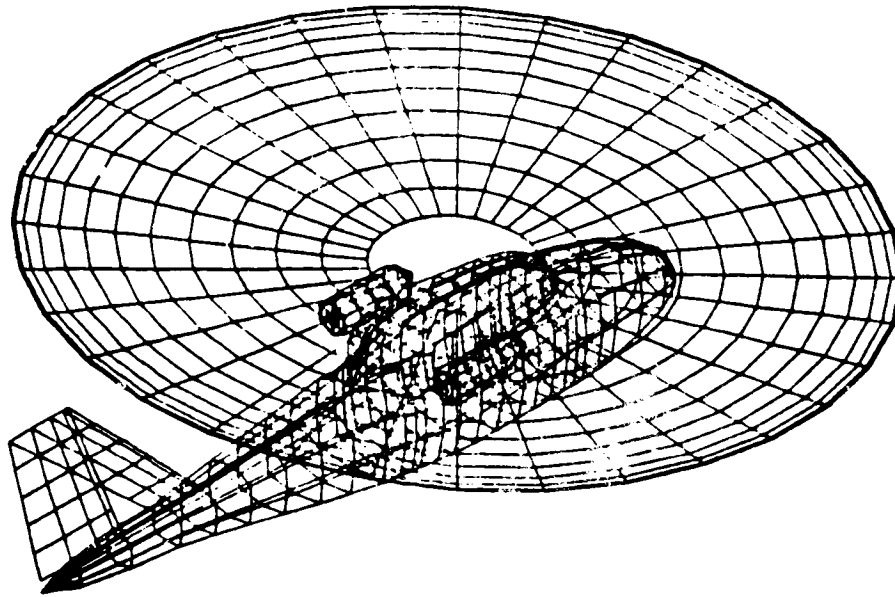


Figure 30. Basic Body Model with Nacelles and Tail Surfaces Added.

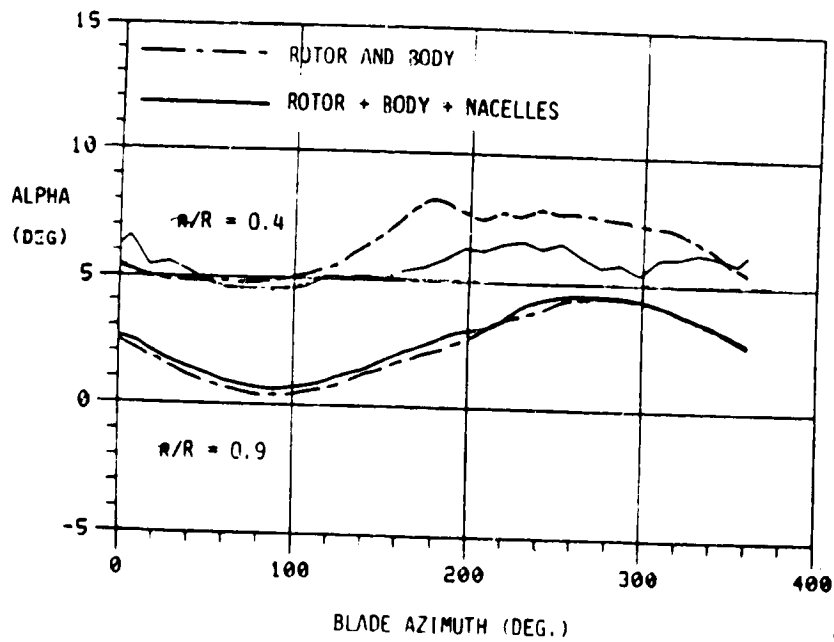


Figure 31. Effect of Nacelles on Calculated Blade Angle of Attack--0.15 Advance Ratio.

ORIGINAL PAGE IS  
OF POOR QUALITY

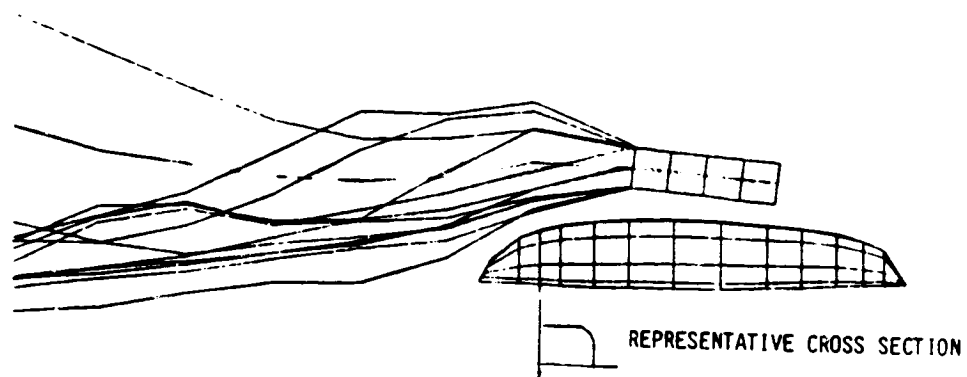


Figure 32. Calculated Rotor Head Model Wake Development--  
0.15 Advance Ratio.

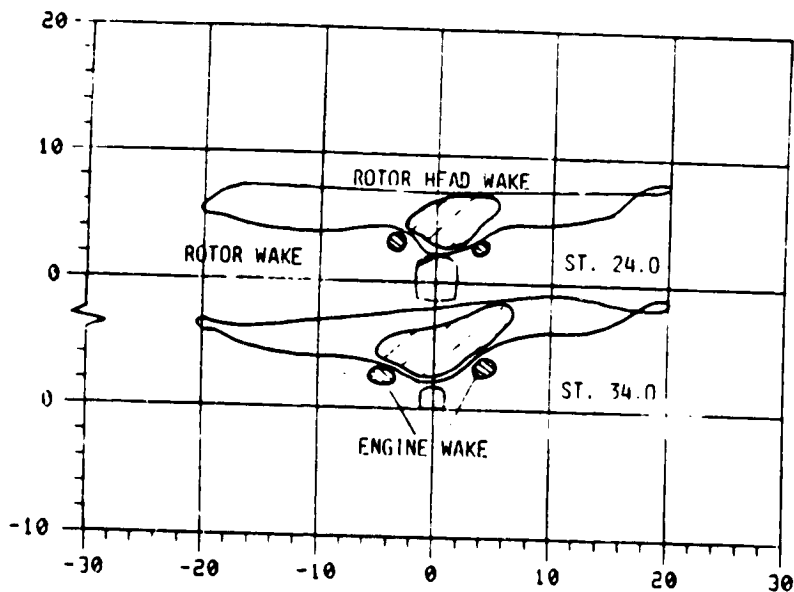


Figure 33. Rotor Head Wake Cross Sections--0.15 Advance Ratio.

observations of many authors. It should be pointed out here that no attempt was made to model the effects of hub rotation and, consequently, any lateral displacement is the result of asymmetry in the steady flow about the fuselage and through the rotor. Figure 33, showing cross sections through the aft fuselage and all the wake elements at the mid-span and tip of the downstream blade shows the wake convection more clearly.

The presence of the rotor head has a very strong effect on the blade behavior. Forced to accommodate not only the flow distortion associated with the presence of the rotor head mass itself, it must also pass through the "dead" region of the separated wake. The blade response to this perturbation dominates Figure 34 where the azimuthal variation of blade angle of attack at two stations is presented. Clearly, this will have a profound effect on the calculated aeroelastic response of the blade and could well be softened when elastic effects are included. The substantial changes in cyclic pitch required to retrim the rotor in the presence of the rotor head can be seen in the differences in local angle of attack at the outboard station also shown in Figure 34. It should be pointed out that this treatment of the rotor head as a simple bluff shape with no base ventilation is almost certainly exaggerating the effect. Further work is required in this area.

Several studies, Reference 24 is typical, have shown how the rotor head wake and regions of upper body separated flow can be controlled by the addition of a rotor head cap or "beanie" or by contouring of the aft pylon to provide an edge separation which rolls up and convects the separated flow out of the region of harm. Both these devices were studied using the analysis. Figure 35 shows the panel models of rotor head cap and the aft pylon modification and their wakes. The success of both devices in depressing the disturbed flow and the center of the main rotor wake is clearly seen in the wake cross sections at the trailing edge of the rotor disc shown in Figure 36. The strong roll-up of the wakes on the rotor cap and modified pylon shapes contrasts sharply with that noted on the basic rotor head. Again, although the main rotor wake was included in the calculation, it was omitted from the drawing for reasons of clarity.

The presence of the flow control devices was also felt in the blade aerodynamics. Figures 37(a) and (b) show the azimuthal variation of blade angle of attack both inboard and outboard and the softening effect of the flow control can be clearly seen in a comparison with the untreated, basic rotor head result in Figure 34. Plots of blade angle contours over the whole disc show again the softening effect of the flow control devices.

Again, it should be stressed that the rotor head effect in this study has been exaggerated to illustrate the analysis. A study of the actual flow field would require a more detailed and representative model especially regarding the base flow.

ORIGINAL PAGE IS  
OF POOR QUALITY

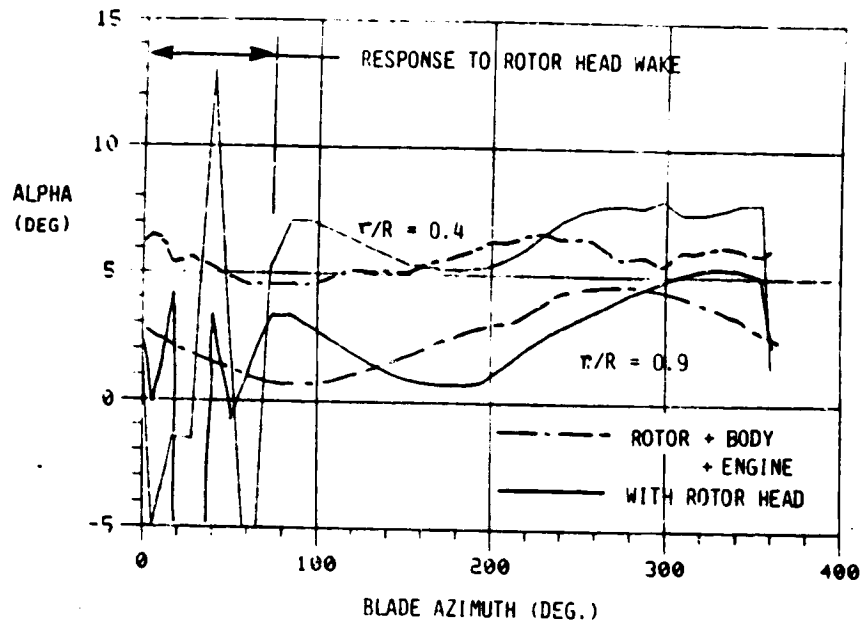


Figure 34. Effect of Rotor Head and Wake on Calculated Blade Angle of Attack--0.15 Advance Ratio.

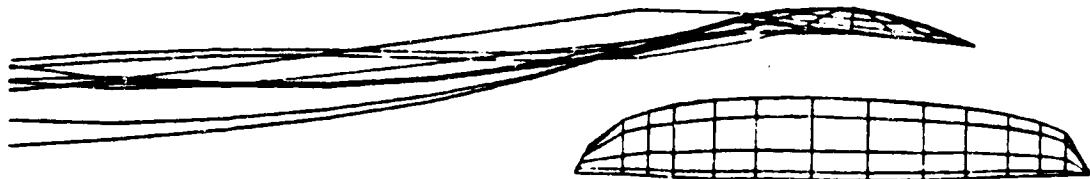


Figure 35(a). Calculated Rotor Head Cap Wake Development--0.15 Advance Ratio.

ORIGINAL PAGE IS  
OF POOR QUALITY

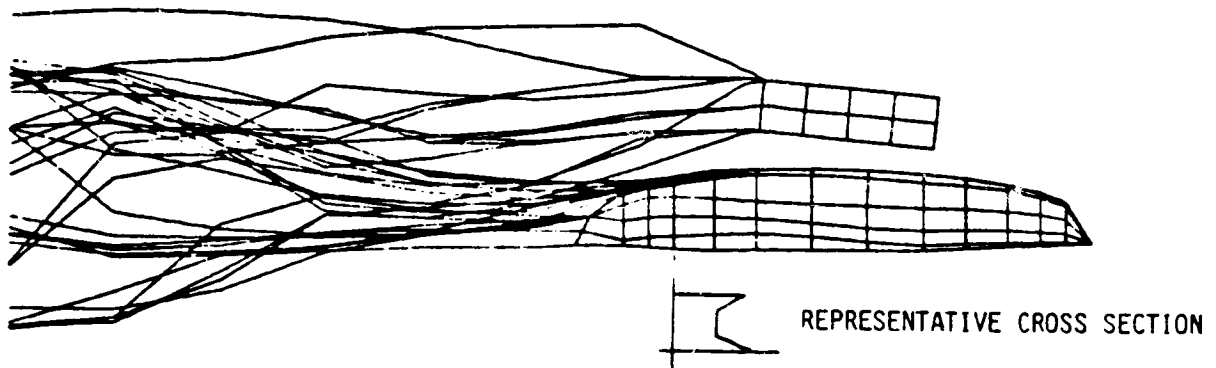


Figure 35(b). Calculated Rotor Head Wake Development with Modified Pylon--0.15 Advance Ratio.

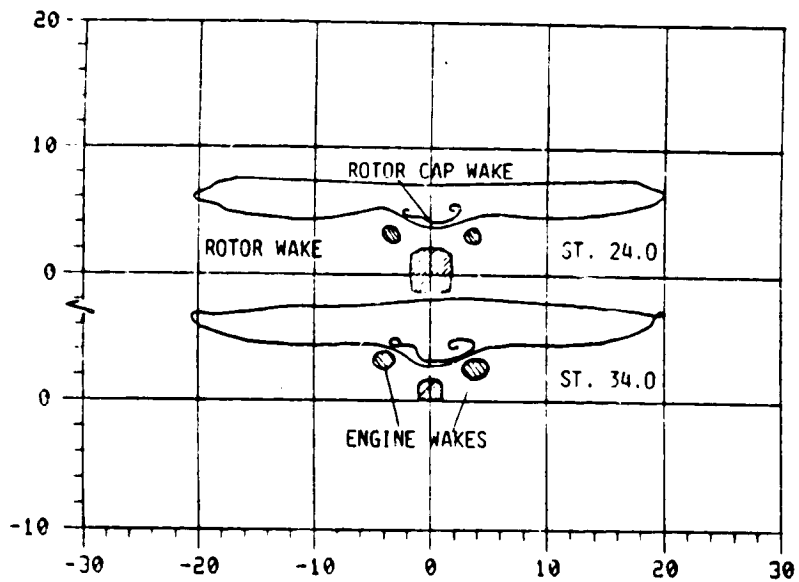


Figure 36(a). Calculated Wake Cross Section with Rotor Head Cap Wake--0.15 Advance Ratio.

ORIGINAL PAGE IS  
OF POOR QUALITY

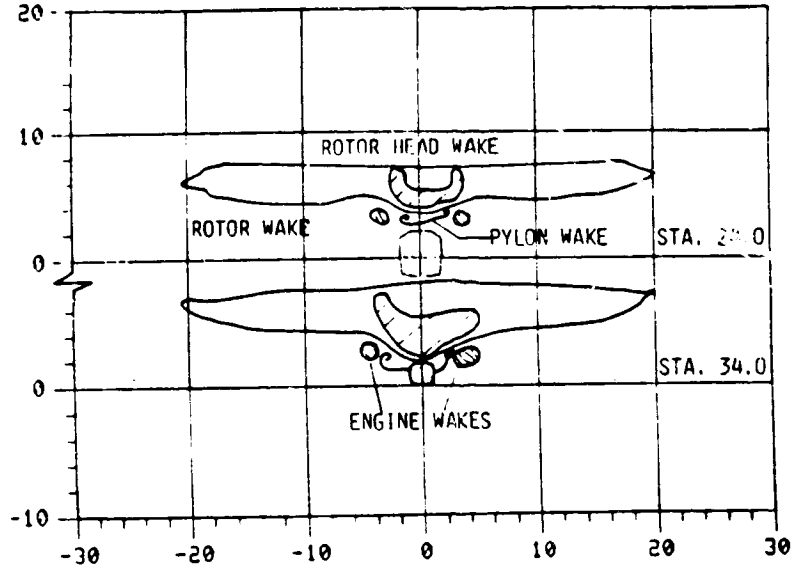


Figure 36(b). Calculated Wake Cross Section with  
Modified Pylon--0.15 Advance Ratio.

ORIGINAL PAGE IS  
OF POOR QUALITY

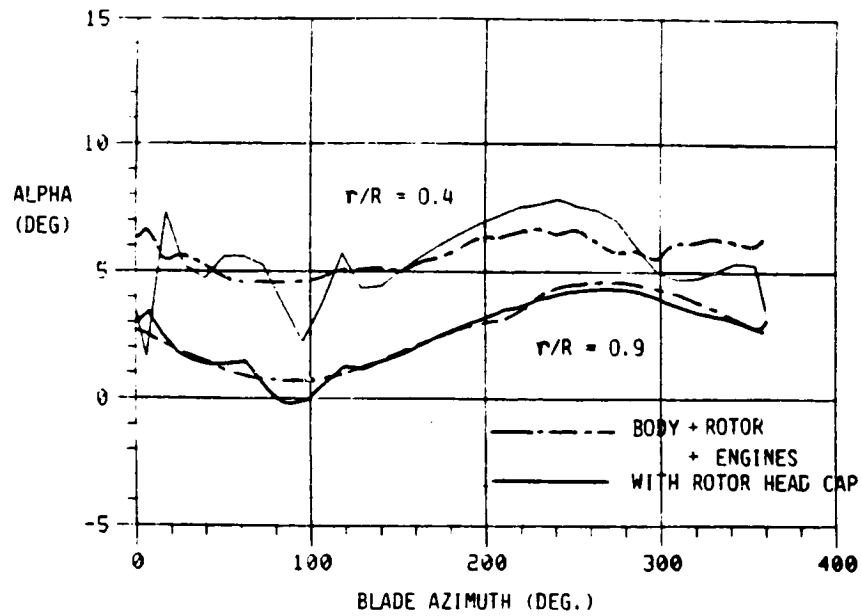


Figure 37(a). Effect of Rotor Head Cap on Calculated Blade Angle of Attack--0.15 Advance Ratio.

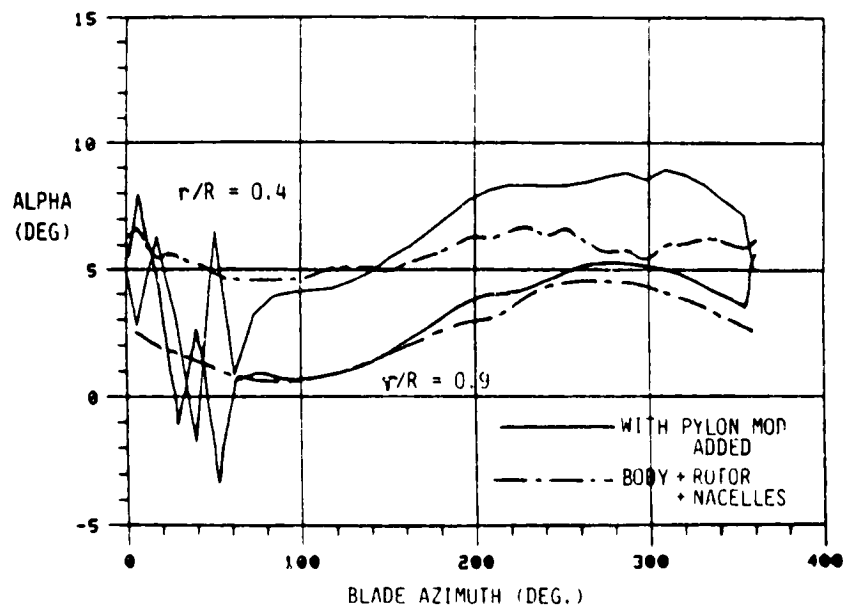


Figure 37(b). Effect of Pylon Modification on Calculated Blade Angle of Attack--0.15 Advance Ratio.

#### 4.4 The Potential to Study Full Configurations

The section above has shown how the analysis can be used to explore the influences of detailed configuration changes. If program capacity were increased from the current limit of 1000 panels, the analysis would have the capability to explore full vehicles, including multiple rotors. This is illustrated in Figure 38. Here, as an illustration, the full machine is modeled, fuselage, pylon, engine nacelles, horizontal and vertical stabiliser, rotor head cap and, finally, main and tail rotors. For the lifting components vortex sheath wakes, not shown in the drawing, are attached around the edges. The rotor head cap and the stabilisers are modelled, in the interest of economy, using a lifting surface rather than a full surface singularity model. If machine capacity had been available, a full panel model, including thickness effects, would have been used. Even with this simple model further stripped down to fit within the 1000-panel constraint by removing the nacelles, the effect of the tail rotor on the vertical stabiliser in the presence of the main wake can be demonstrated.

In Figure 39 the chordwise loading on the vertical fin in the presence of the main rotor with and without tail rotor is shown. The tail rotor is mounted and is operating such that the fin is on the inflow side. The graph shows the difference in pressure coefficient between the port and starboard surfaces of the vertical stabiliser. No attempt has been made to trim the lateral forces on the tail rotor/fin combination and the tail rotor is simply operating at a set fixed collective. As a consequence, the vertical stabiliser is operating in an inflow field which tends to generate side force counter to that of the tail rotor. This is, of course, unproductive and in practice the two would be adjusted to complement rather than fight each other.

At the 0.15 advance ratio of the calculation, the influence of the tail rotor on the main rotor was almost negligible (less than 0.1% of the total). This could be caused by a direct tail rotor on main rotor effect; by a second-order tail rotor on tail surface and then main rotor effect; or it may be the result of the cycle to cycle imprecision in the iterative process.

ORIGINAL PAGE IS  
OF POOR QUALITY

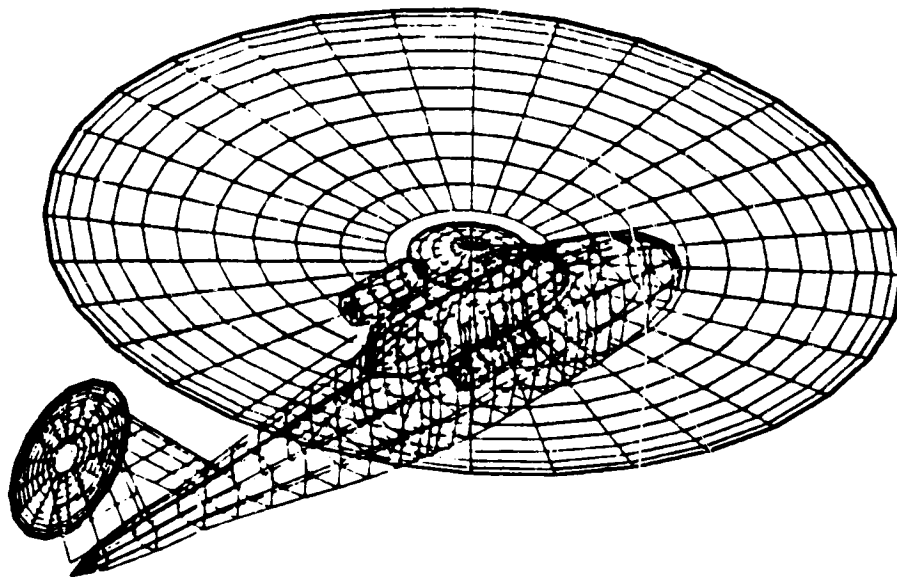


Figure 38. Mock-up of Full Configuration with Rotor Head Cap.  
(Actual Run Exceeds Present Program Panel Capacity)

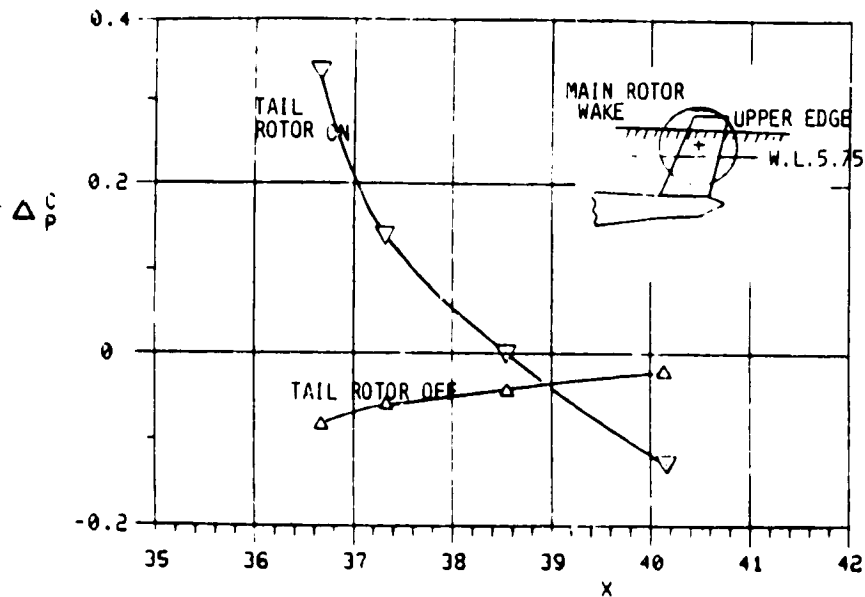


Figure 39. Effect of Tail Rotor on Vertical Stabiliser  
Loads at Waterline 5.75 (Main Rotor Present--  
0.15 Advance Ratio).

## 5.0 CONCLUSIONS AND RECOMMENDATIONS

An analysis has been developed which permits a fully coupled solution of the rotor and airframe behavior of realistic helicopters. The effect of the rotor/body coupling on the rotor inflow has been illustrated and the significance of the effect of configuration elements, particularly the rotor head and rotor head cap devices, demonstrated. The role of the rotor head cap and pylon flow control devices in moving the separated wake and the center of the main rotor wake was shown for a typical helicopter configuration.

Several additional steps must be taken to verify the usefulness of the analysis beyond the performance and handling qualities applications of the present study. In order to be useful to the dynamicist, the higher harmonics of loading associated with discrete blade vortex encounters must be added (how this can be achieved was discussed in the earlier report on this work by the present author<sup>18</sup>), and the resulting blade loadings coupled to an aeroelastic analysis. This would be further facilitated if the program capacity were expanded beyond the current 1000-panel version. If this were done, much greater detail in rotor disc modelling would be possible than is possible with the present, relatively crude, 32 azimuthal steps in the rotor solution.

Despite the relative crudity of the model, the author feels that with this analysis it is now possible to explore the highly interactive flow field around the helicopter and that other configurations previously analysed with relatively empirical approaches can now be studied in detail with a representative model. The most likely candidate in this category is the tilt-rotor concept, where now, with the demonstrated wake cutting capability of the present program, a full analysis of the dual rotor, wing, fuselage flow field becomes possible.

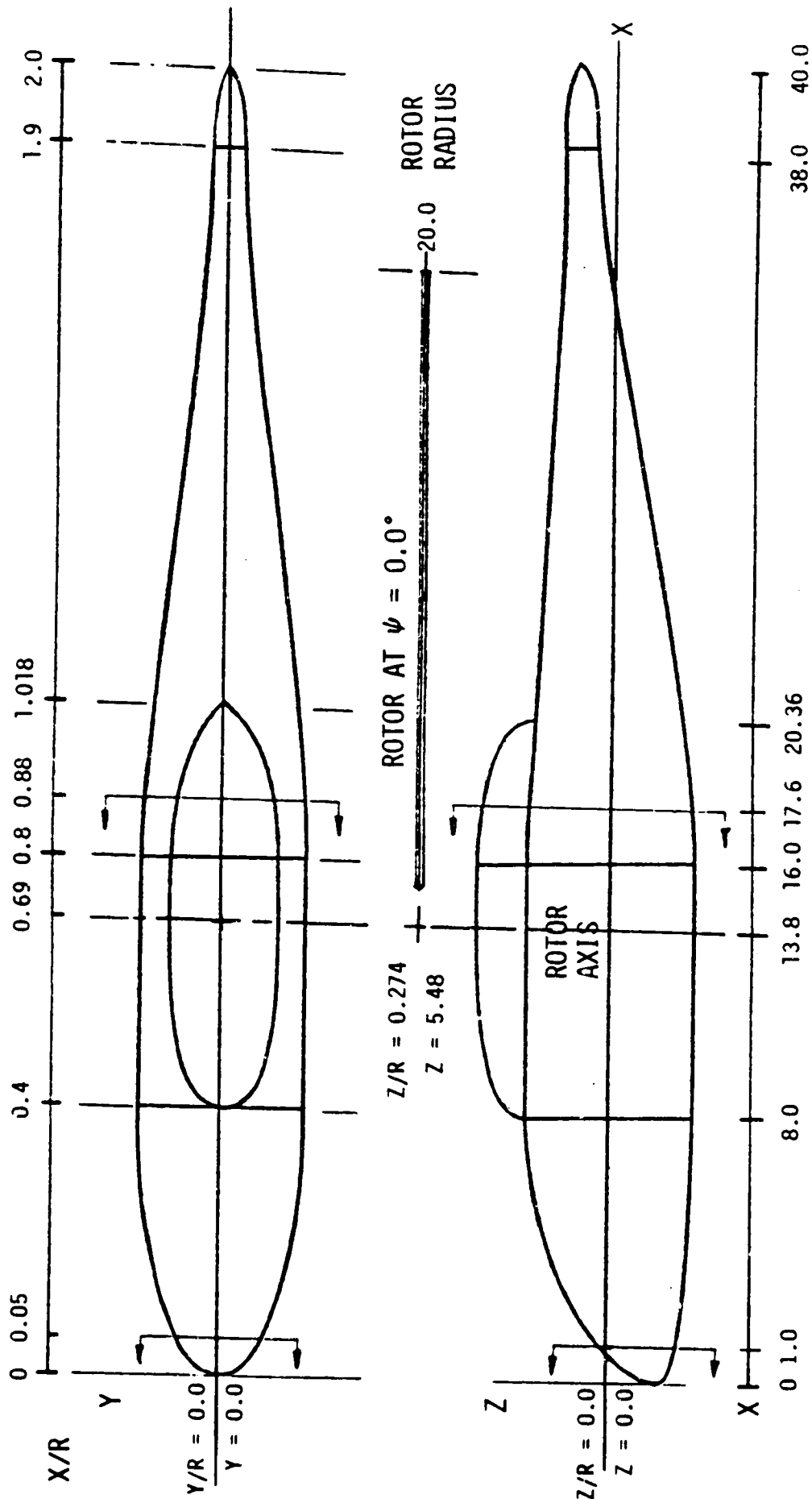
Although the initial results of the study are encouraging, one area of weakness has been identified. In the discussion of the correlation it was noted, particularly at low advance ratio, that the wake skew angle did not follow the expected values beyond the rotor near field. This has been identified a consequence of the way in which the type-4 (higher-energy) wake is modelled in the basic VSAERO program. In this report the wakes were modelled using a piecewise constant doublet segment between each wake grid plane. Relative to the way in which the wake behaves in the real world, the stepwise constant model de-emphasises the far-wake effects. Modifications to the wake model which would correct the problem have been identified and should be incorporated if work is continued on the body/rotor program.

## 6.0 REFERENCES

1. Sheridan, P.F. and Smith, R.P., "Interactional Aerodynamics: A New Challenge to Helicopter Technology", Presented at the 35th Annual Forum of the AHS, 1979.
2. Landgrebe, A.J., Moffit, R.C. and Clark, D.R., "Aerodynamic Technology for Advanced Rotorcraft", Paper Presented at the AHS Symposium, Essington, PA, 1976.
3. Wilson, J.C. and Mineck, R.E., "Wind Tunnel Investigation of Helicopter-Rotor Wake Effects on Three Helicopter Fuselage Models", NASA TMX-3185, 1975.
4. Freeman, C.E. and Mineck, R.E., "Fuselage Surface Pressure Measurements of a Helicopter Wind Tunnel Model with a 3.15-Meter Diameter Single Rotor", NASA TM-80051, 1979.
5. Freeman, C.E. and Wilson, J.C., "Rotor-Body Interference (ROBIN) Analysis and Test", Paper Presented at the 36th Annual National Forum, AHS, Washington, D.C., May 1980.
6. Betzina, M.D. and Shinoda, P., "Aerodynamic Interaction between a 1/6-Scale Helicopter Rotor and a Body of Revolution", NASA TM-84247, Ames Research Center, Moffett Field, CA, June 1982.
7. Arcidiano, P.J. and Sopher, R., "A Review of Rotor Loads Prediction Methods", AGARD Conference Preprint AGARD-CP-334-14, Fluid Dynamics Specialists Meeting, London, May 1982.
8. Smith, R.V., "Some Effects of Wake Distortion due to a Fuselage Flowfield on Rotor Thrust Limits", Paper Presented at ARO Workshop on Rotor Wake Technology, Raleigh, N.C., 1979.
9. Young, C., "Development of the Vortex Ring Model and its Influence on the Prediction of Rotor Loads", AGARD Conference Preprint, AGARD-CPP-334-11, Fluid Dynamics Specialists Meeting, London, May 1982.
10. Jepson, D., Moffitt, R., Hilzinger, K. and Bissell, J., "Analysis and Correlation of Test Data from an Advanced Technology Rotor System", NASA CR-152366, July 1980.
11. Huber, H. and Polz, G., "Studies of Blade to Blade and Rotor-Fuselage-Tail Interferences", AGARD Conference Reprint, May 1982.
12. Stricker, R. and Polz, G., "Calculation of the Viscous Flow around Helicopter Bodies", Paper Presented at the 3rd European Rotorcraft and Powered Lift Forum, Aix-en-Provence, France, September 1977.

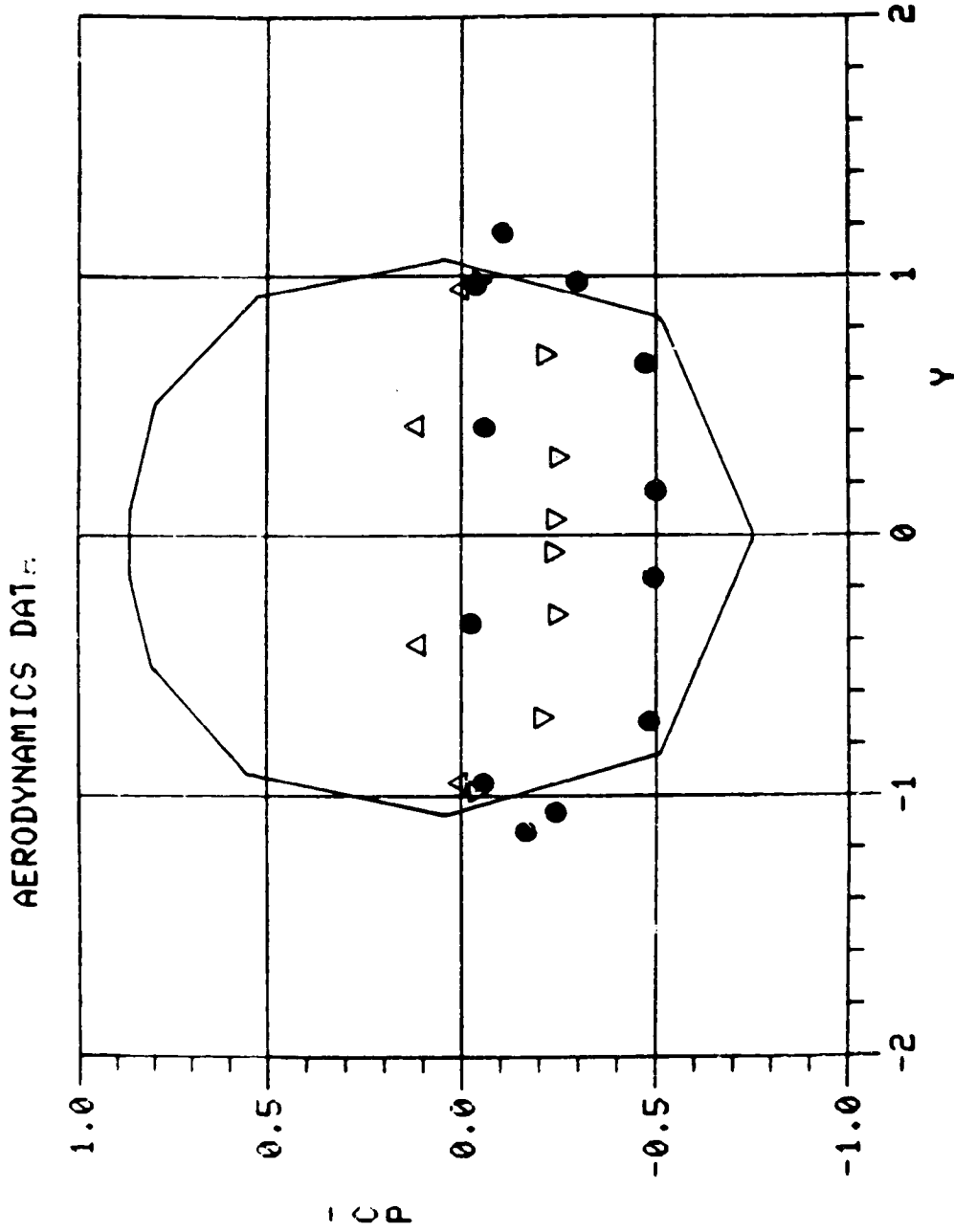
13. Clark, D.R., Dvorak, F.A. et al., "Helicopter Flow Field Analysis", Final Report for Period April 1977 - September 1978, USARTL-RT-79-4, Ft. Eustis, VA 1979.
14. Clark, D.R., "A Study of the Effect of Aft Fuselage Shape on Helicopter Drag", Paper Presented at the 6th European Rotorcraft and Powered Lift Aircraft Forum, Bristol, England, September 1980.
15. Freeman, C.E., "Development and Validation of a Combined Rotor-Fuselage Induced Flowfield Computational Method", NASA TP-1656, 1980.
16. Heyson, H.H. and Katzoff, S., "Induced Velocities near a Lifting Rotor with Nonuniform Disk Loading", NACA Report 1319, 1957.
17. Clark, D.R., "An Outline of a Method for Predicting Fully Coupled Body/Rotor Interference", Paper Presented at the ARO Workshop on Rotor Wake Technology", Raleigh, N.C., 1979.
18. Clark, D.R. and Maskew, B., "An Analysis of Airframe/Rotor Interference in Forward Flight", Paper Presented to the 7th European Rotorcraft Powered Lift Aircraft Forum, Garmisch-Partenkirchen, FRG, September 1981.
19. Maskew, B. and Dvorak, F.A., "Analysis of Vortex/Surface Interactions using Panel Methods", Paper Presented at the 1981 U.S. Air Force - FRG DEA Meeting, Gottingen, West Germany, April 1981.
20. Maskew, B., "Prediction of Subsonic Aerodynamic Characteristics--A Case for Low-Order Panel Methods", AIAA J. Aircraft, Vol. 19, No. 2, February 1982.
21. Landgrebe, A.J. and Cheyney M.C., Jr., "Rotor Wakes--Key to Performance Prediction", AGARD Conference Proceedings No. 111, Marseilles, France, September 1972.
22. Clark, D.R., "Use of Analytic Tools in the Design and Development of Rotorcraft", Paper No. 1, Presented at the 4th European Rotorcraft and Powered Lift Aircraft Forum, Stresa, Italy, September 1978.
23. Maskew, B., "Program VSAERO, A Computer Program for Calculating the Nonlinear Aerodynamic Characteristics of Arbitrary Configurations. User's Manual", Prepared for NASA Ames Research Center, Moffett Field, CA, under Contract NAS2-8788, April 1982.
24. Roesch, P. and Vuillet, A., "New Designs for Improved Aerodynamic Stability on Recent Aerospatiale Helicopters", Paper Presented at the 37th Annual Forum of the AHS, New Orleans, LA, 1981.





Test Model Schematic (After Freeman and Mineck, Ref. 4)  
 Correlation Presented in Calculation (X) Axis System -R = 20 ft.

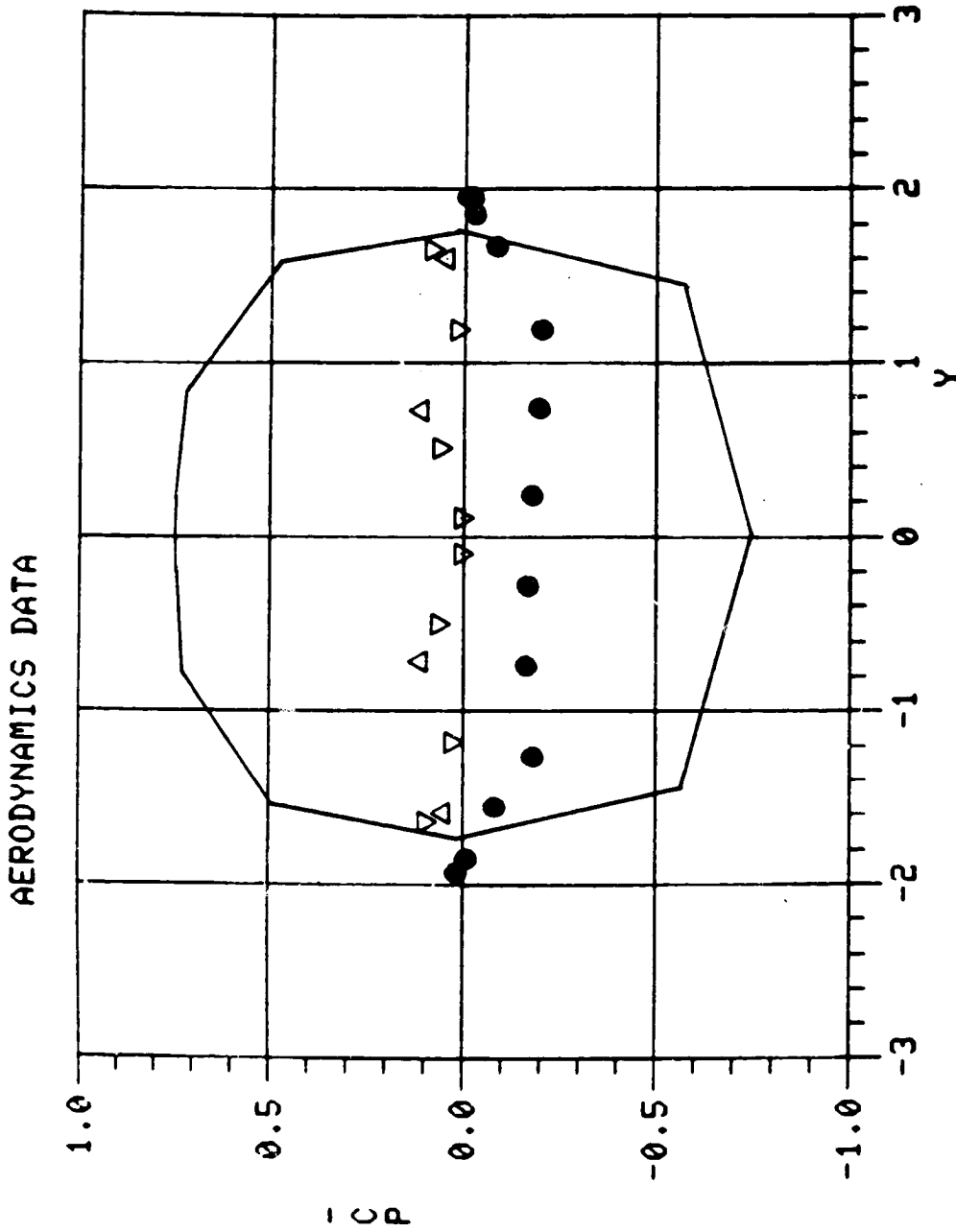
ORIGINAL PAGE IS  
OF POOR QUALITY



BODY, ROTOR 0.15 ADVANCE RATIO  
STATION CUT X = 1.00

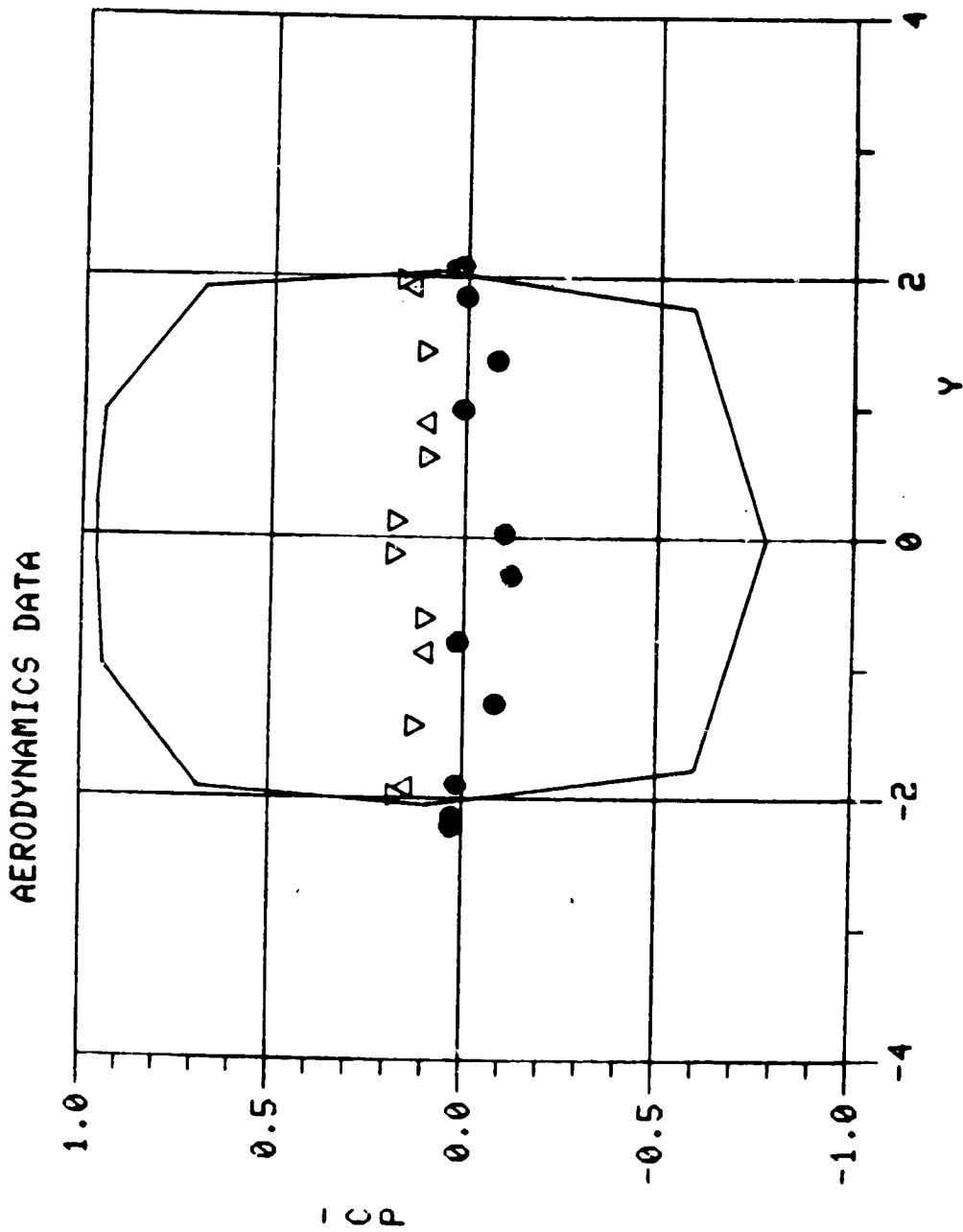


ORIGINAL PAGE IS  
OF POOR QUALITY



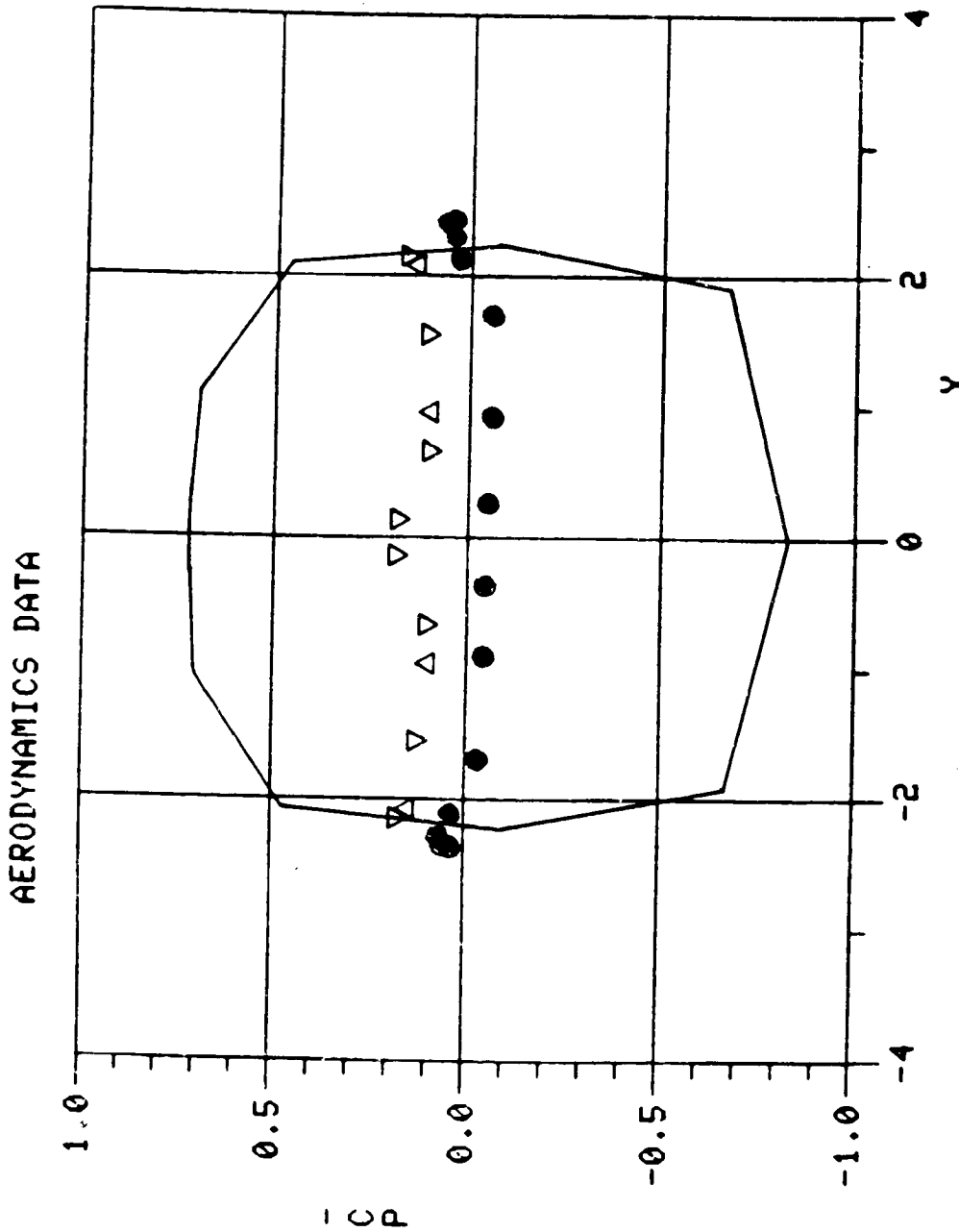
BODY, ROTOR 0.15 ADVANCE RATIO  
STATION CUT X - 2.80

ORIGINAL PAGE IS  
OF POOR QUALITY



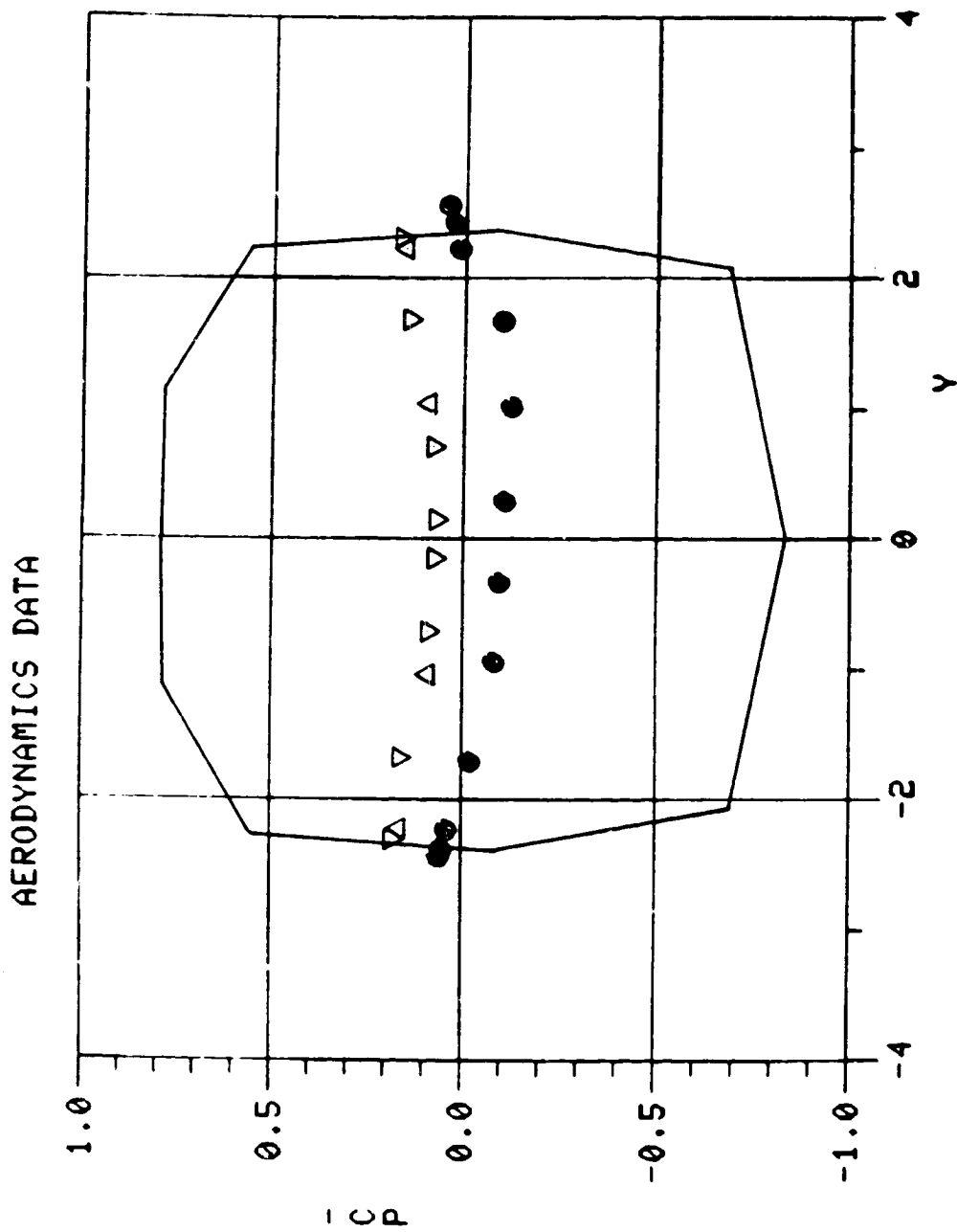
BODY, ROTOR 0.15 ADVANCE RATIO  
STATION CUT X = 4.00

ORIGINAL PAGE IS  
OF POOR QUALITY



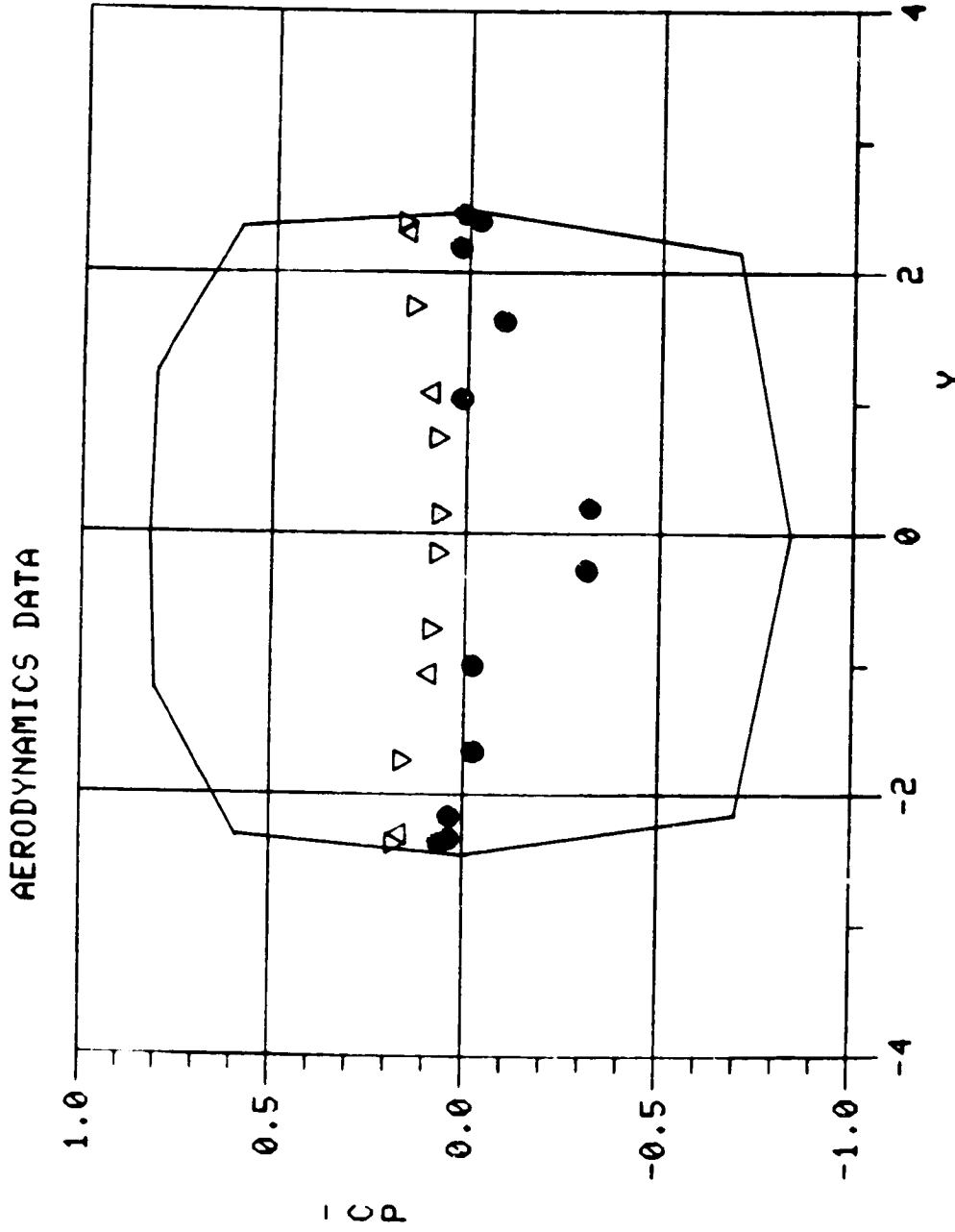
BODY, ROTOR 0.15 ADVANCE RATIO  
STATION CUT X - 5.00

ORIGINAL PAGE IS  
OF POOR QUALITY



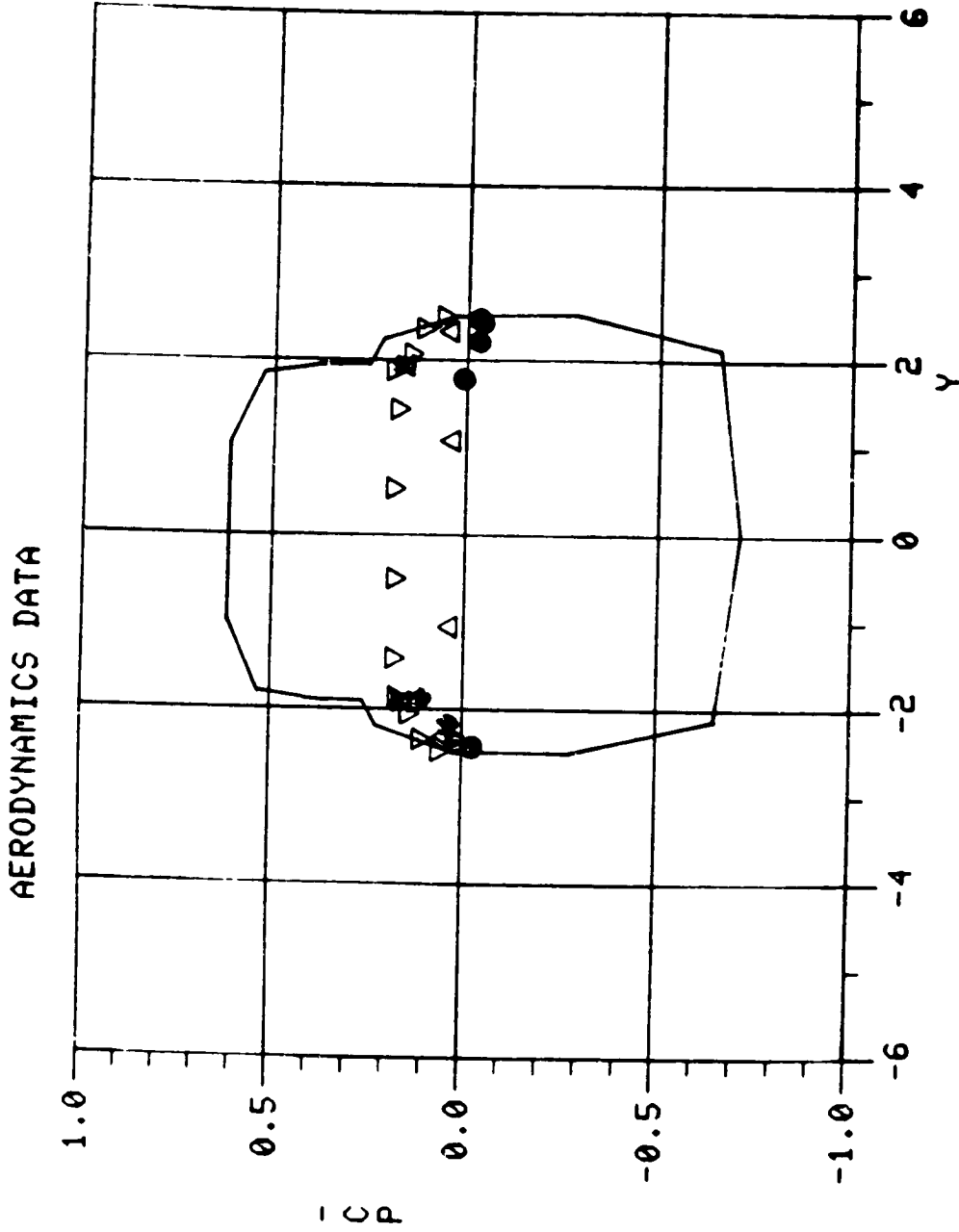
BODY, ROTOR 0.15 ADVANCE RATIO  
STATION CUT X • 6.00

ORIGINAL PAGE IS  
OF POOR QUALITY



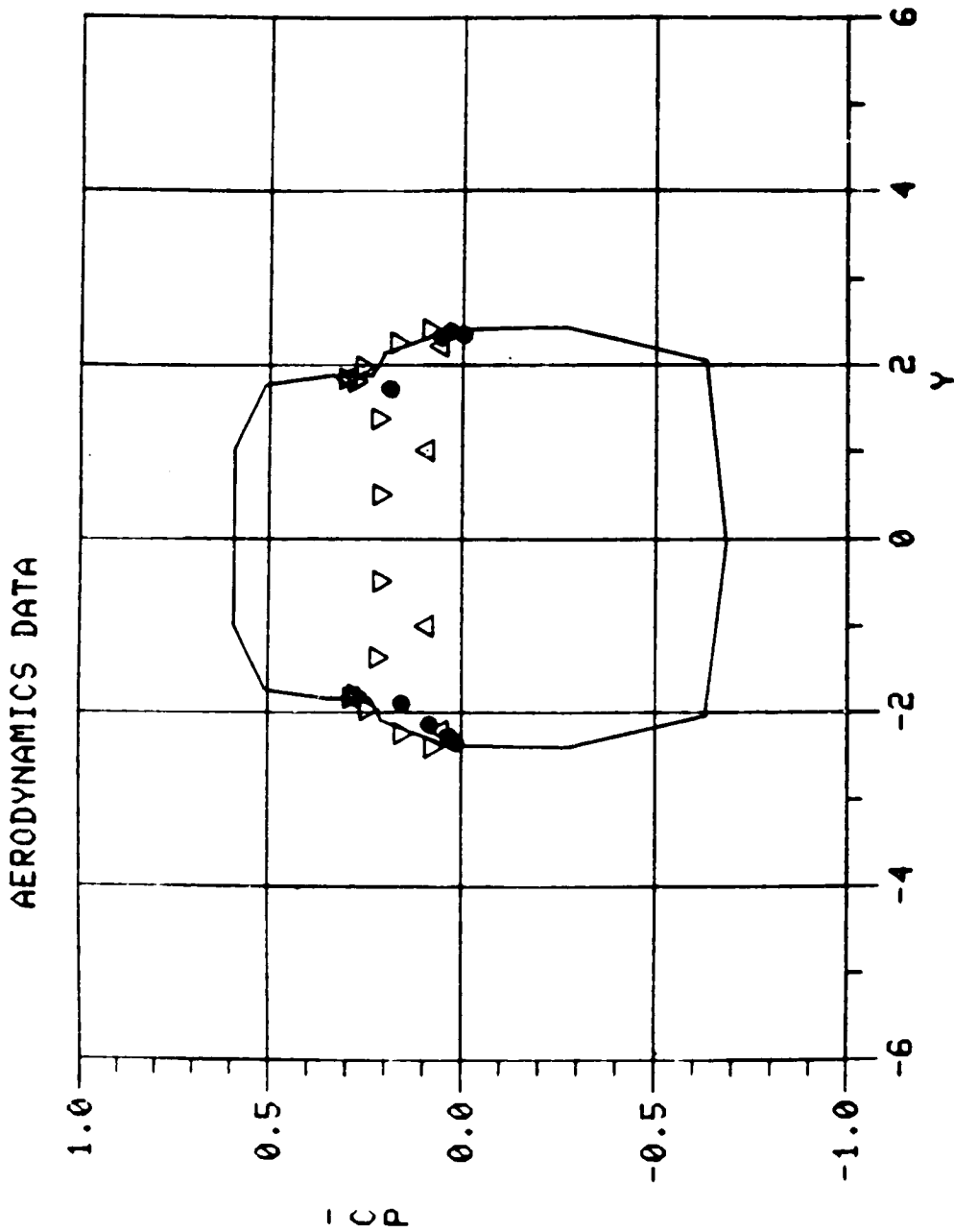
BODY, ROTOR 0.15 ADVANCE RATIO  
STATION CUT X = 6.80

ORIGINAL PAGE IS  
OF POOR QUALITY



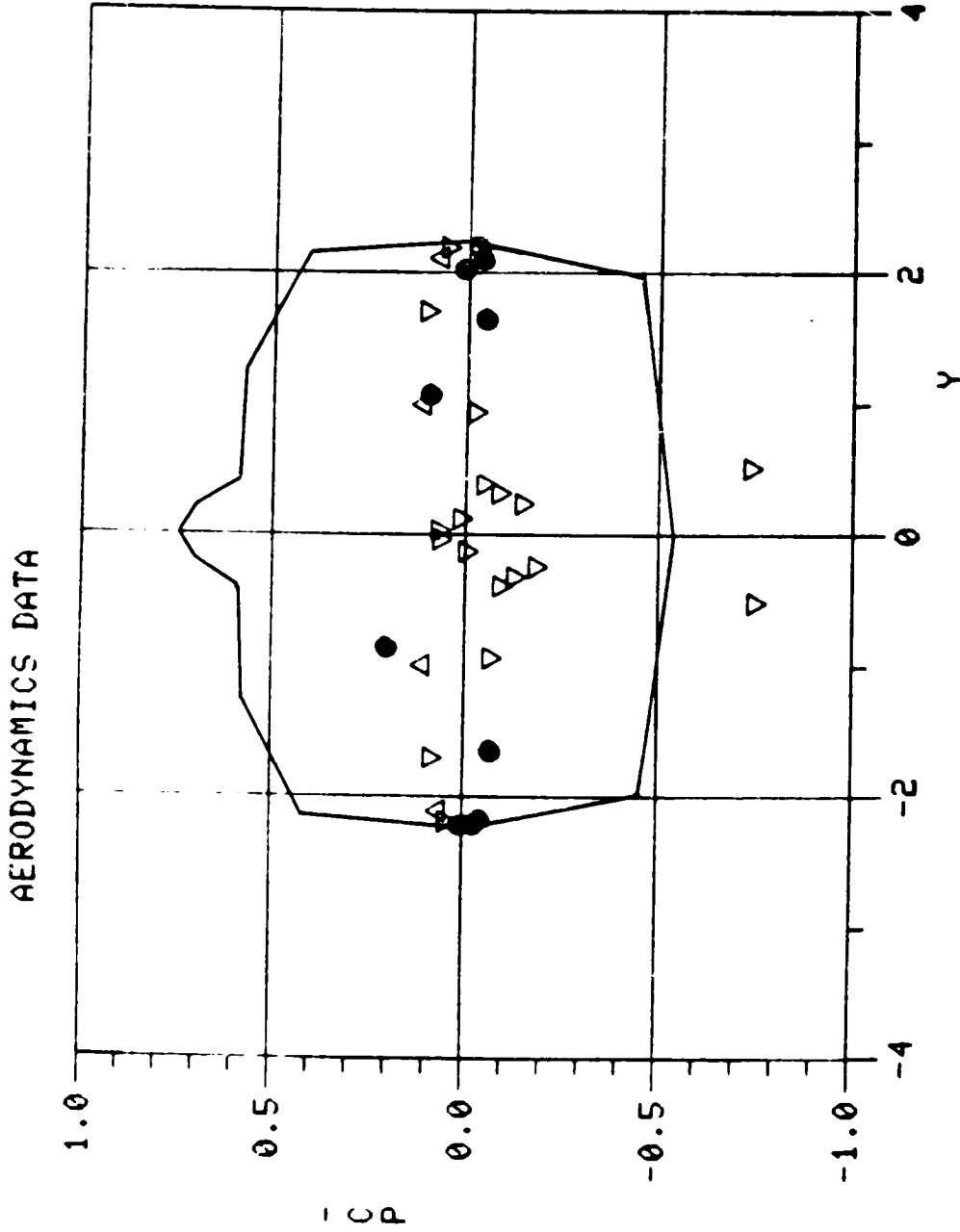
BODY, ROTOR 0.15 ADVANCE RATIO  
STATION CUT X • 12.00

ORIGINAL PAGE IS  
OF POOR QUALITY



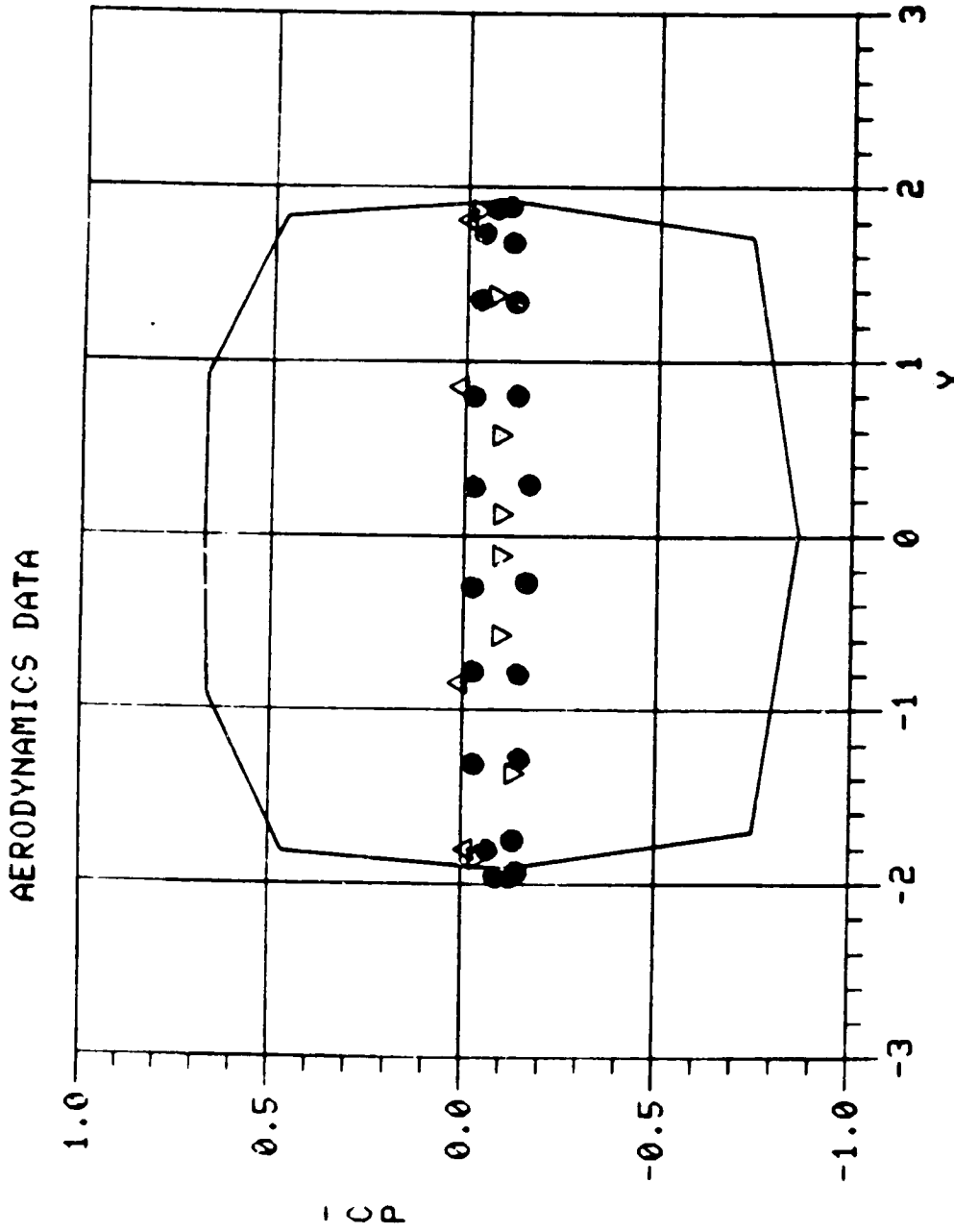
BODY, ROTOR 0.15 ADVANCE RATIO  
STATION CUT X • 17.60

ORIGINAL PAGE IS  
OF POOR QUALITY



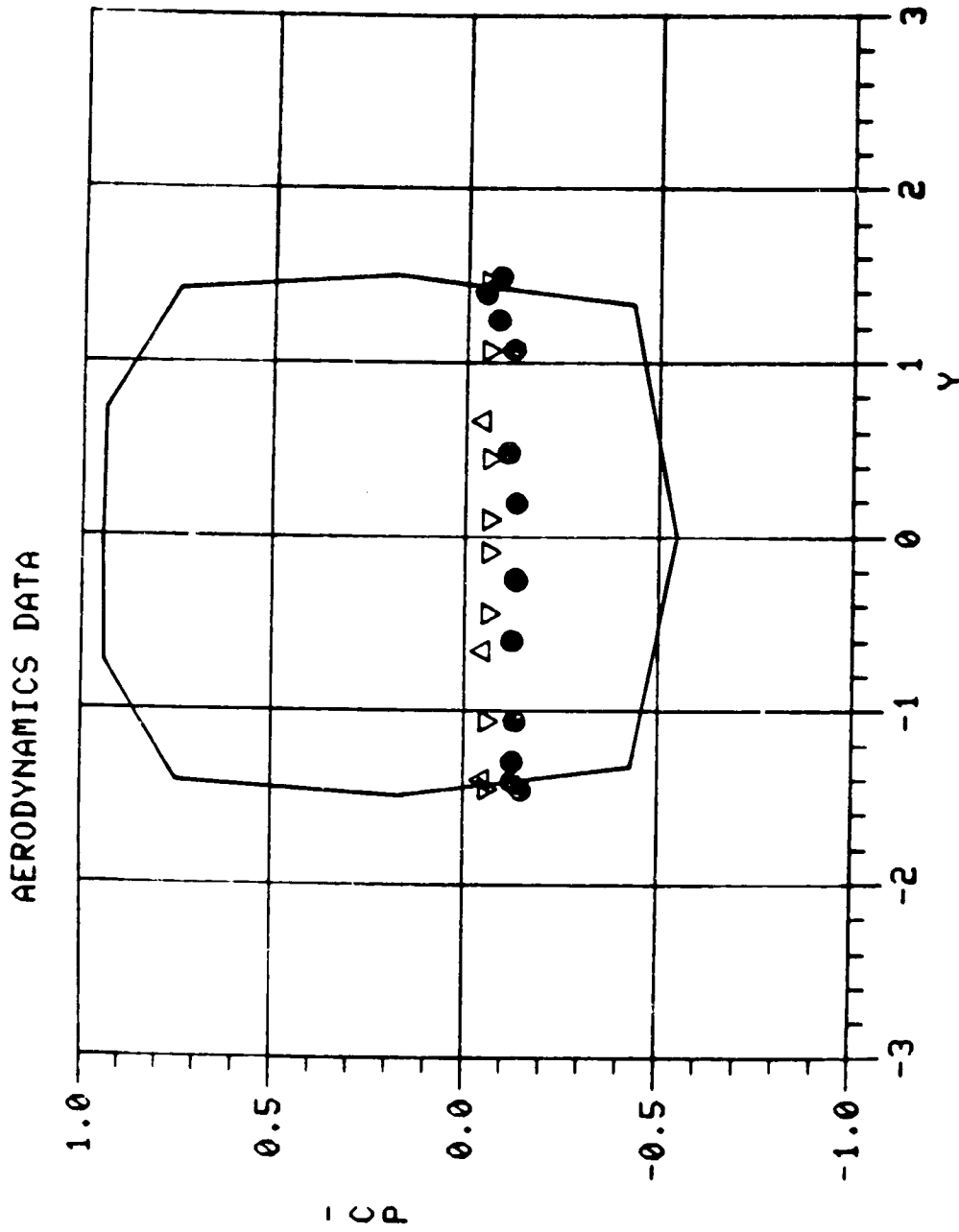
BODY, ROTOR 0.15 ADVANCE RATIO  
STATION CUT X - 20.00

ORIGINAL PAGE IS  
OF POOR QUALITY



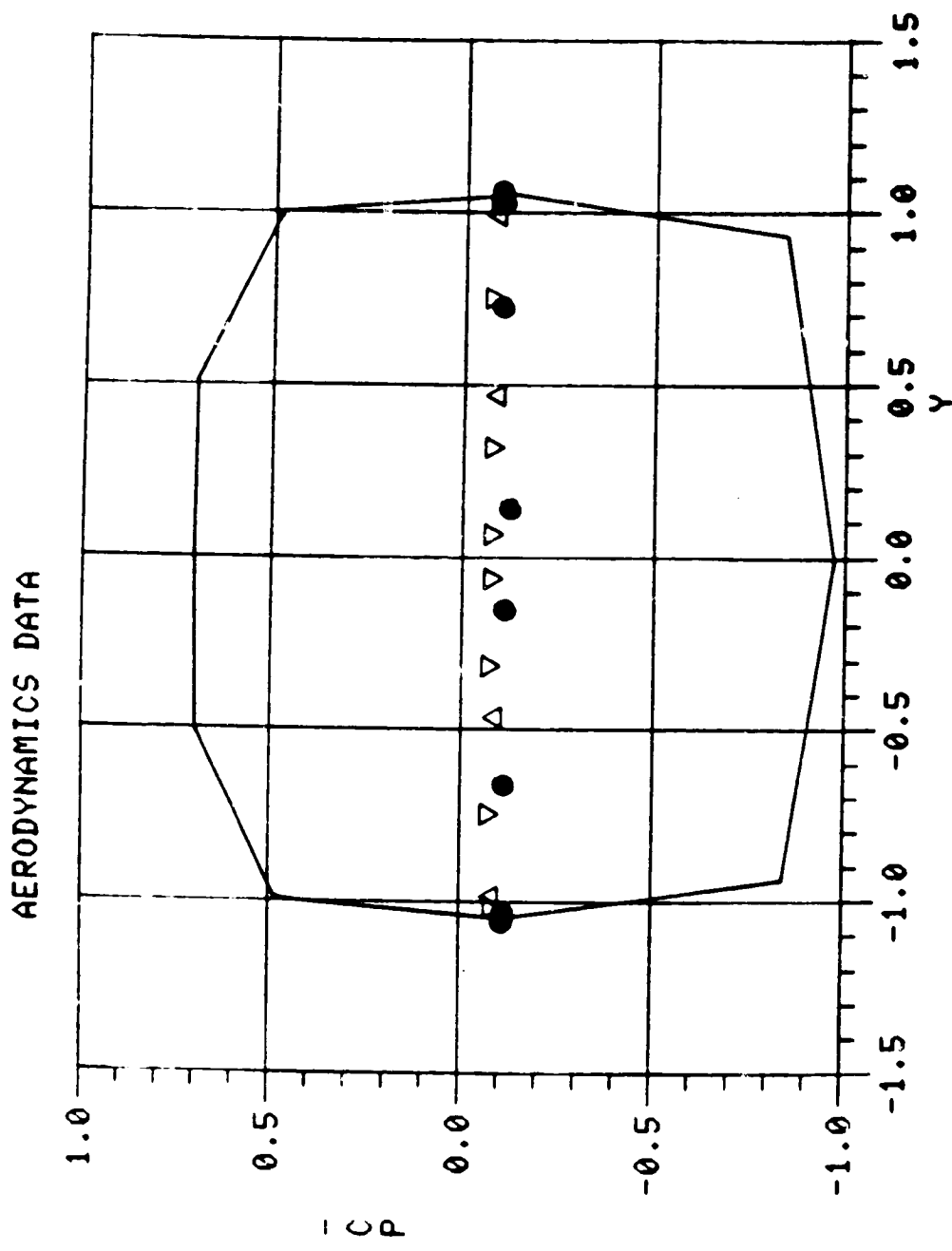
BODY, ROTOR 0.15 ADVANCE RATIO  
STATION CUT X • 23.20

ORIGINAL PAGE IS  
OF POOR QUALITY



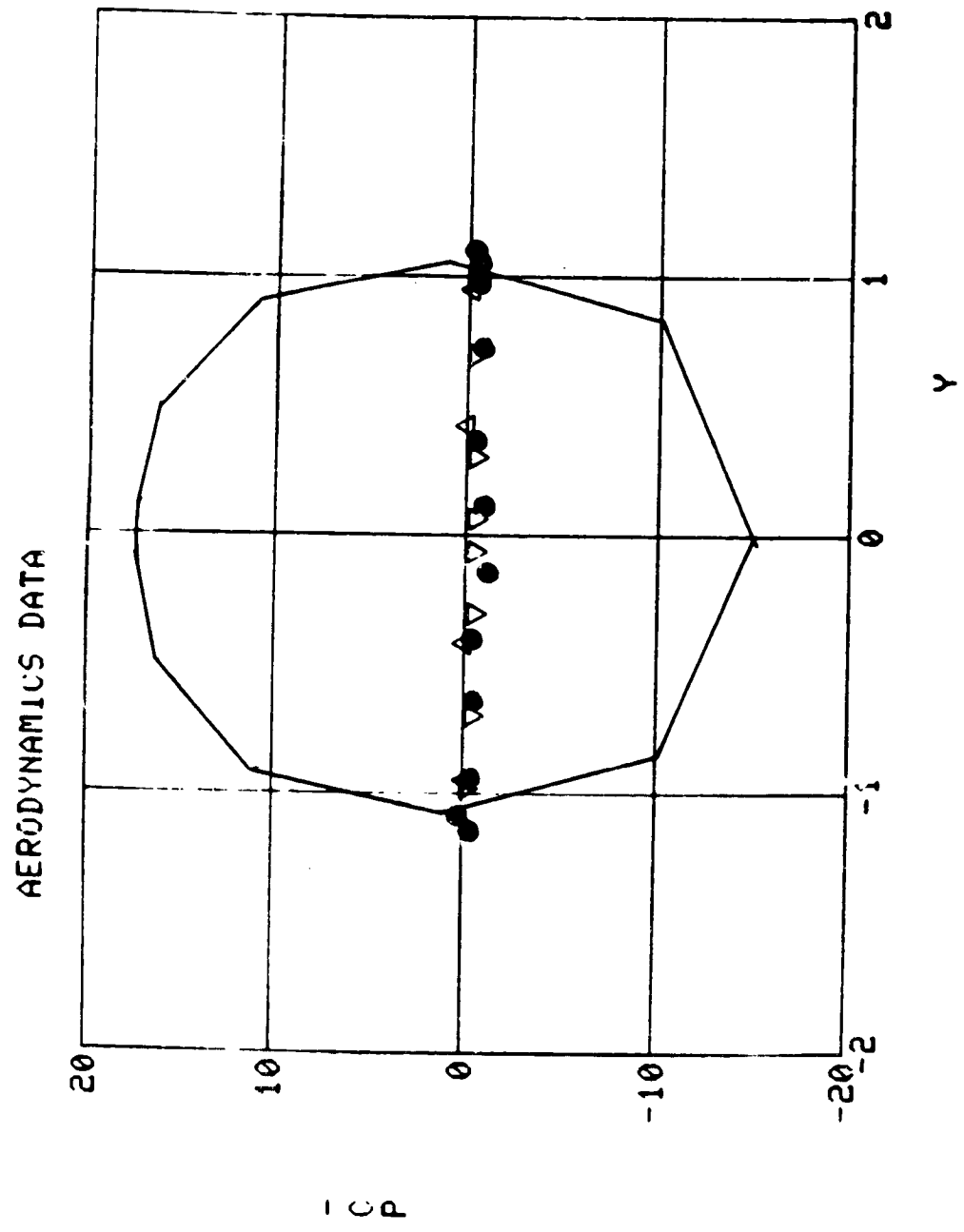
BODY, ROTOR 0.15 ADVANCE RATIO  
STATION CUT X • 26.80

ORIGINAL PAGE IS  
OF POOR QUALITY



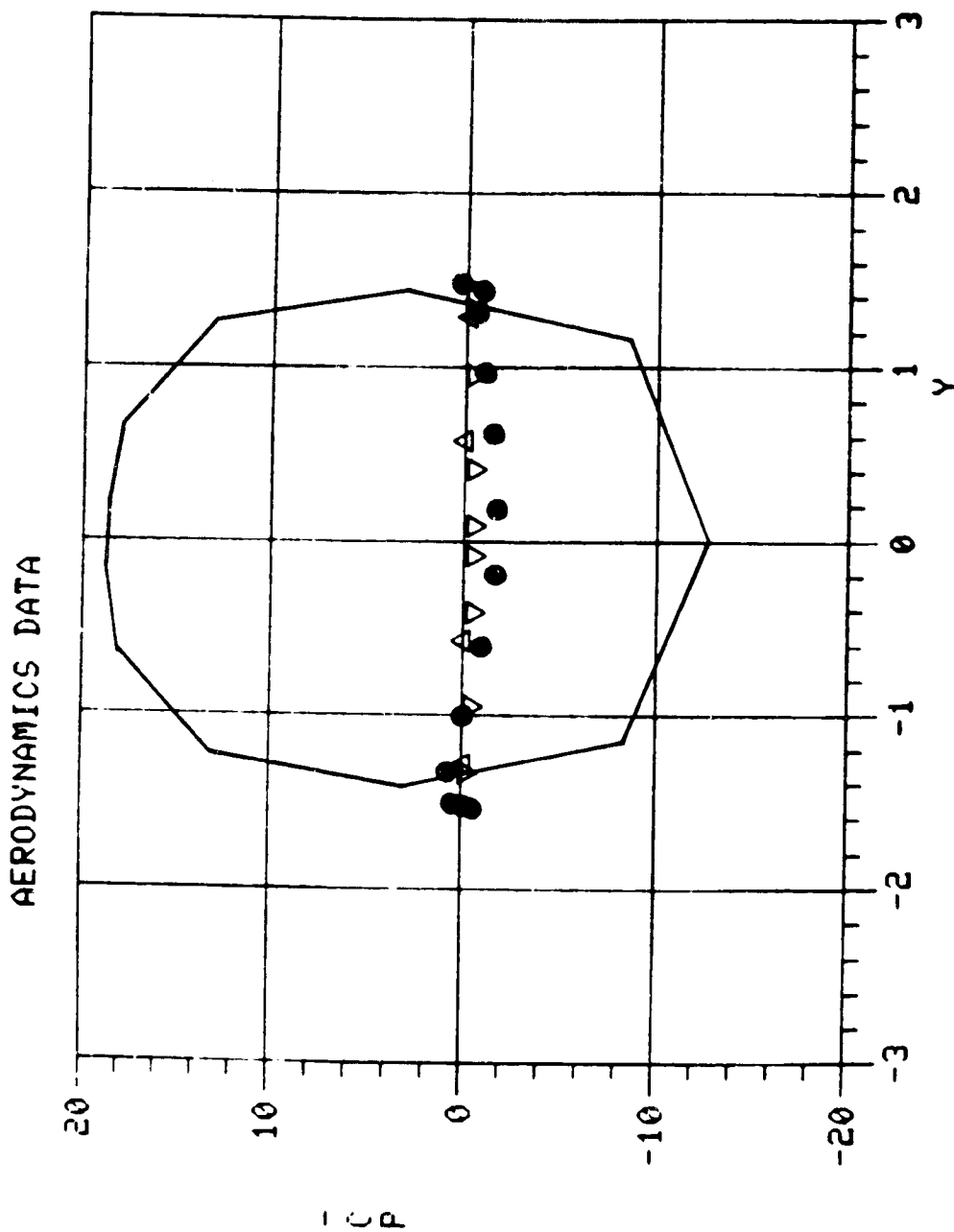
BODY, ROTOR 0.15 ADVANCE RATIO  
STATION CUT X = 30.60

ORIGINAL PAGE IS  
OF POOR QUALITY



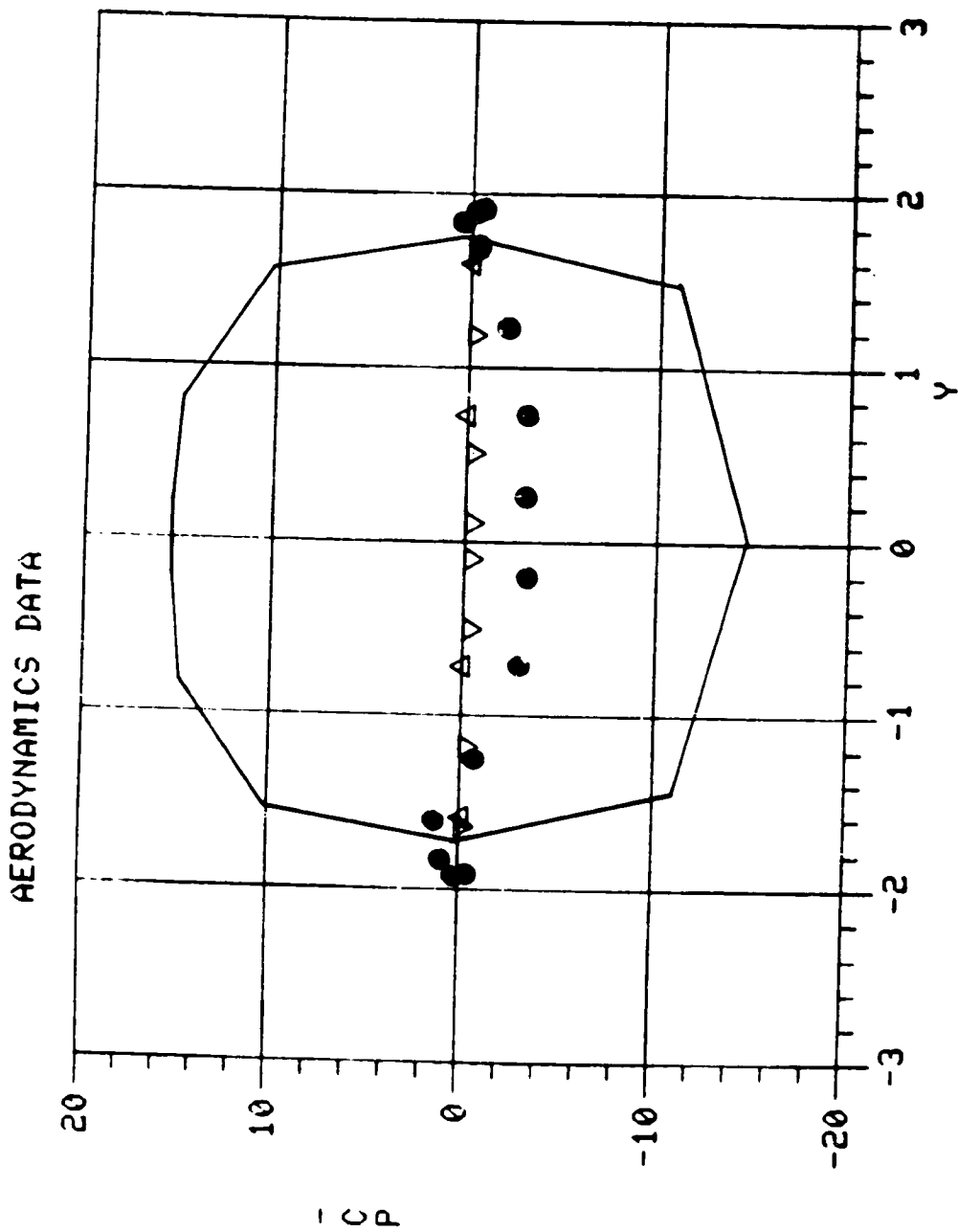
BODY, ROTOR 0.05 ADVANCE RATIO  
STATION CUT X = 1.00

ORIGINAL PAGE IS  
OF POOR QUALITY



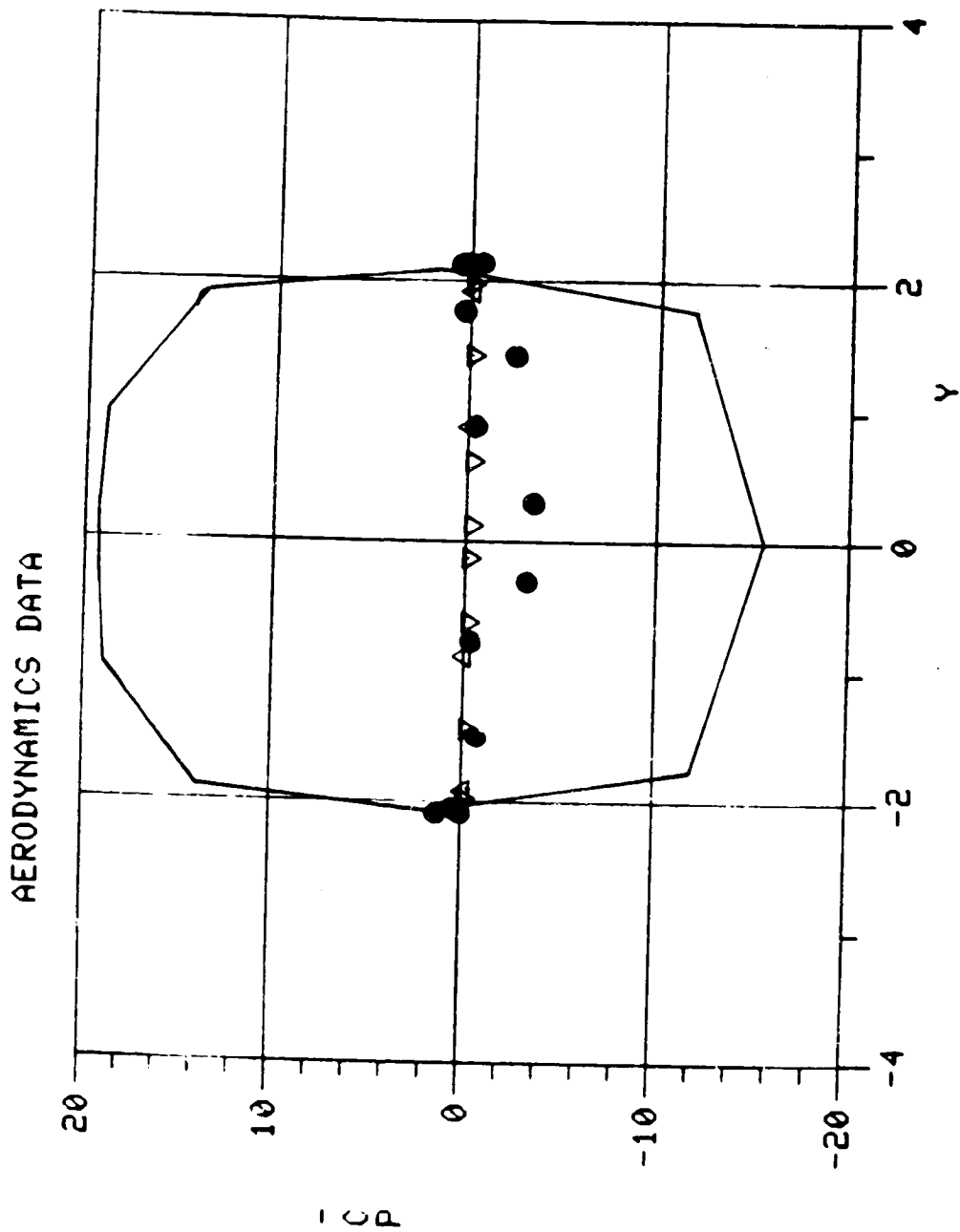
BODY, ROTOR 0.05 ADVANCE RATIO  
STATION CUT X - 1.80

ORIGINAL PAGE IS  
OF POOR QUALITY.



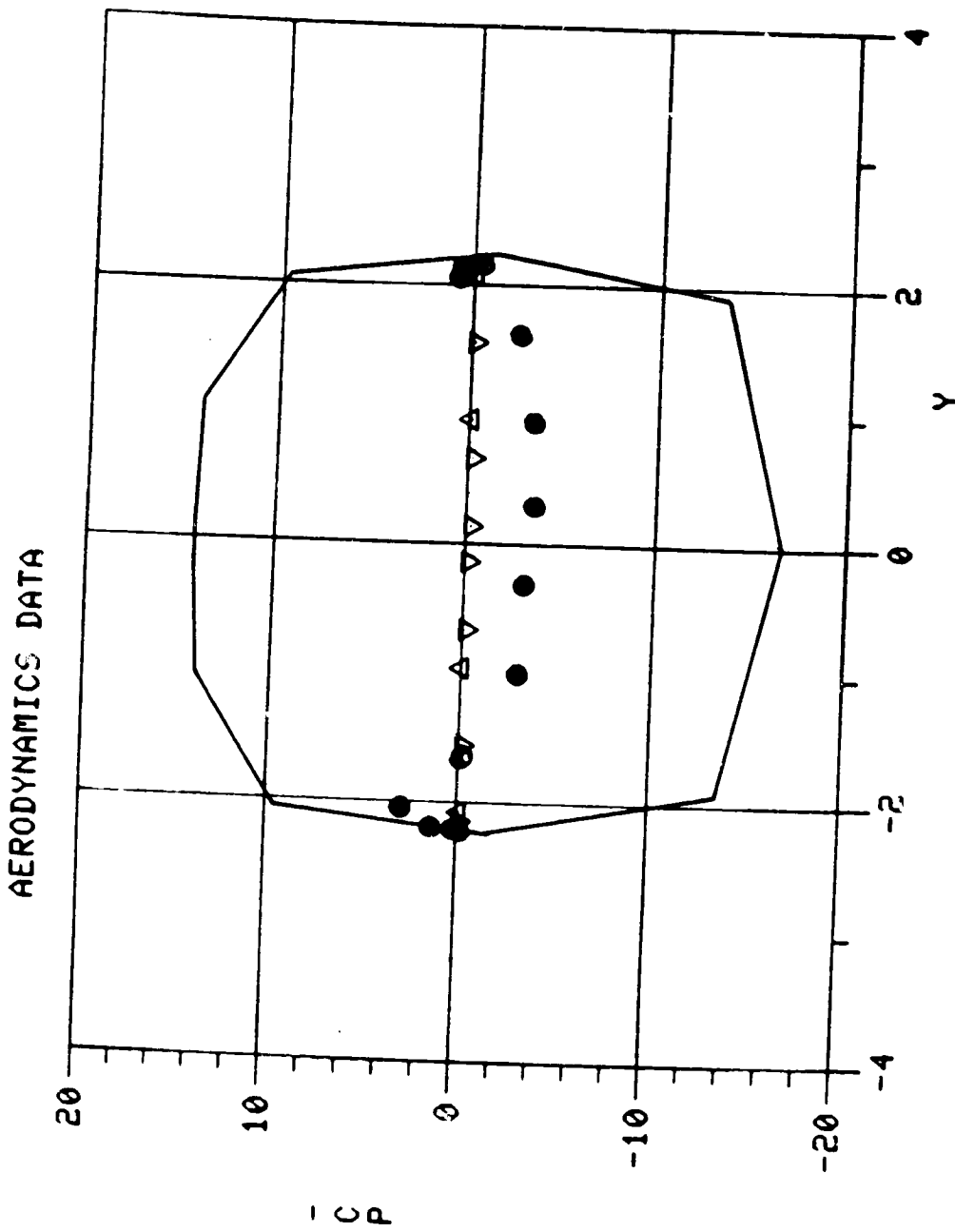
BODY, ROTOR 0.05 ADVANCE RATIO  
STATION CUT X - 2.80

ORIGINAL PAGE IS  
OF POOR QUALITY



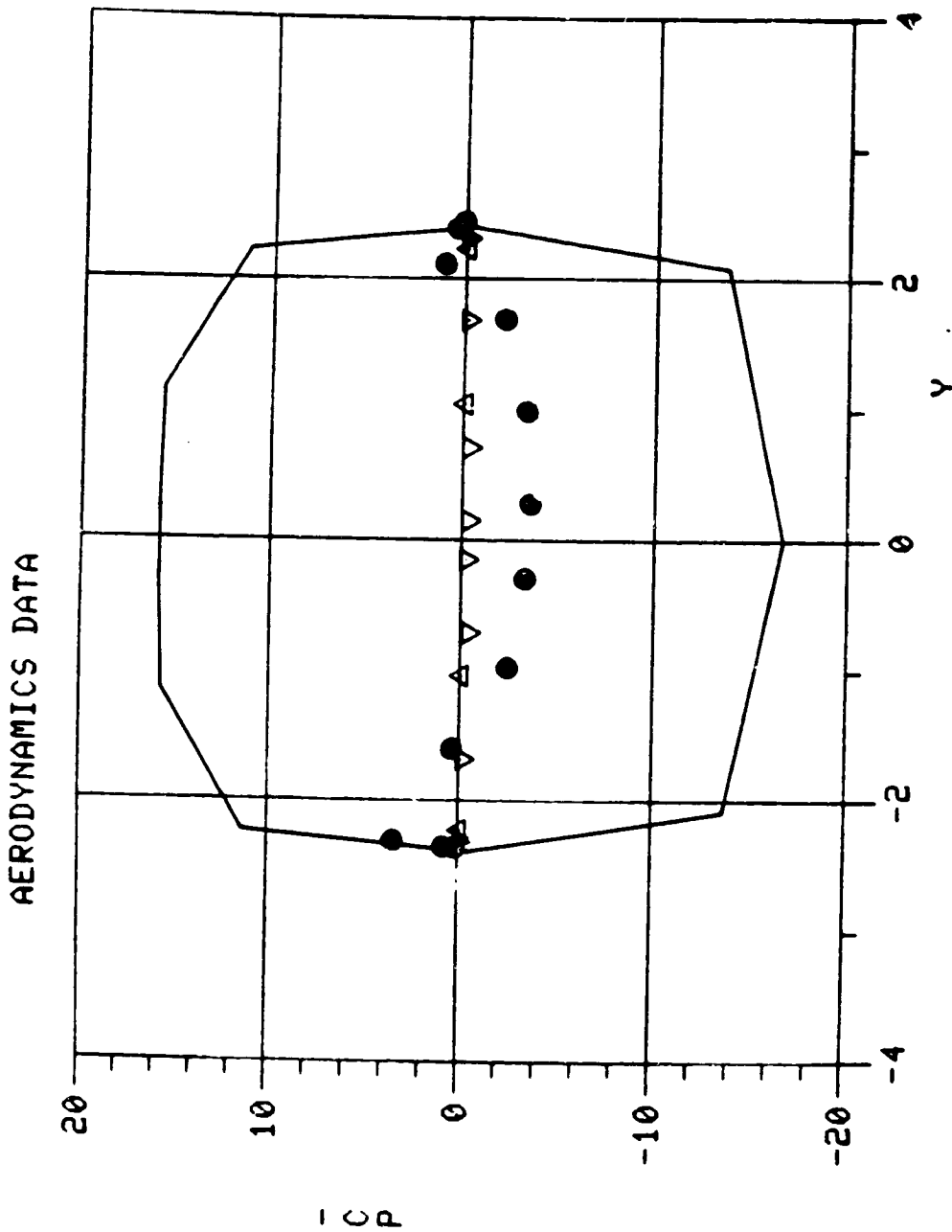
BODY, ROTOR 0.05 ADVANCE RATIO  
STATION CUT X . 4.00

ORIGINAL PAGE IS  
OF POOR QUALITY



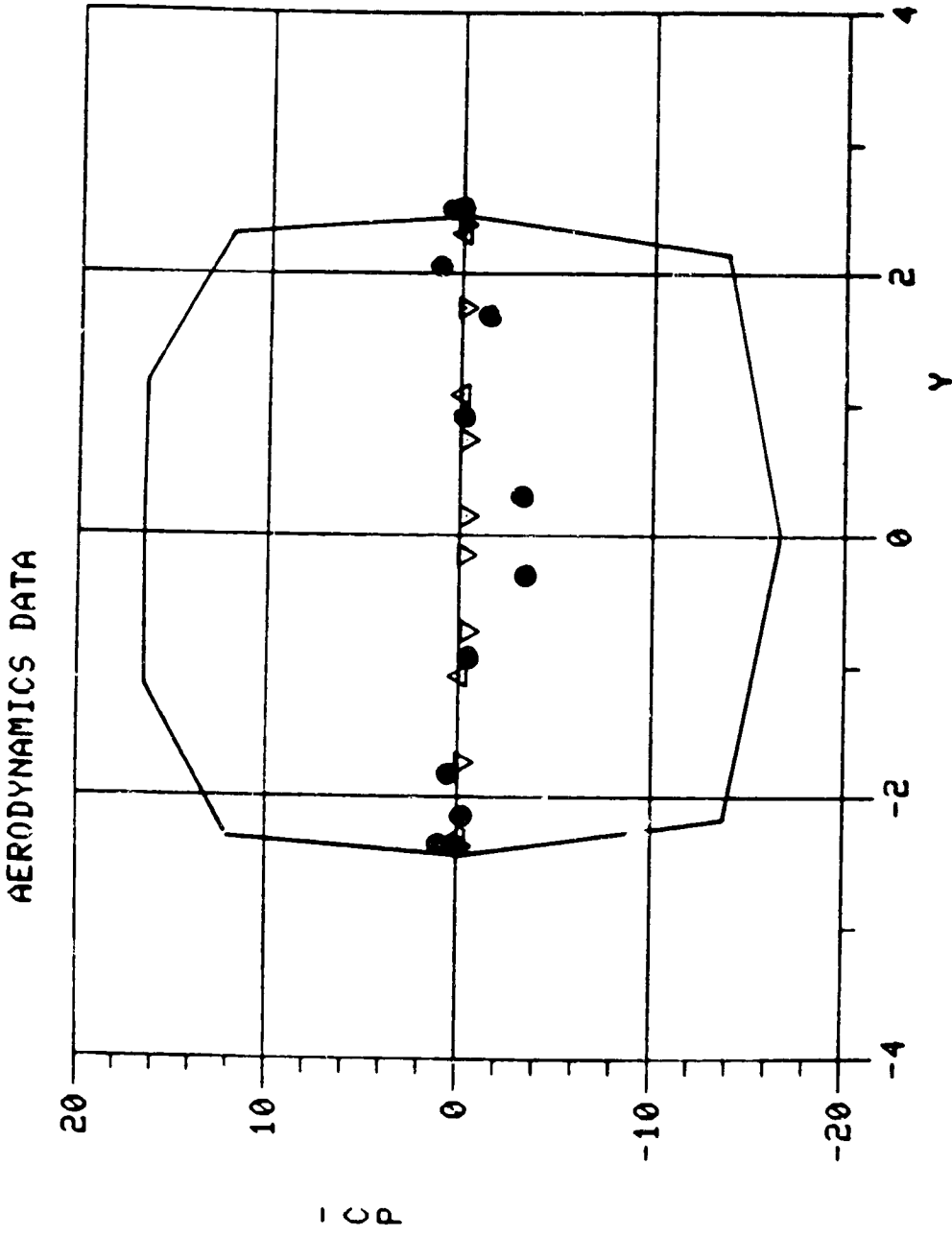
BODY, ROTOR 0.05 ADVANCE RATIO  
STATION CUT X . 5.00

ORIGINAL PAGE IS  
OF POOR QUALITY



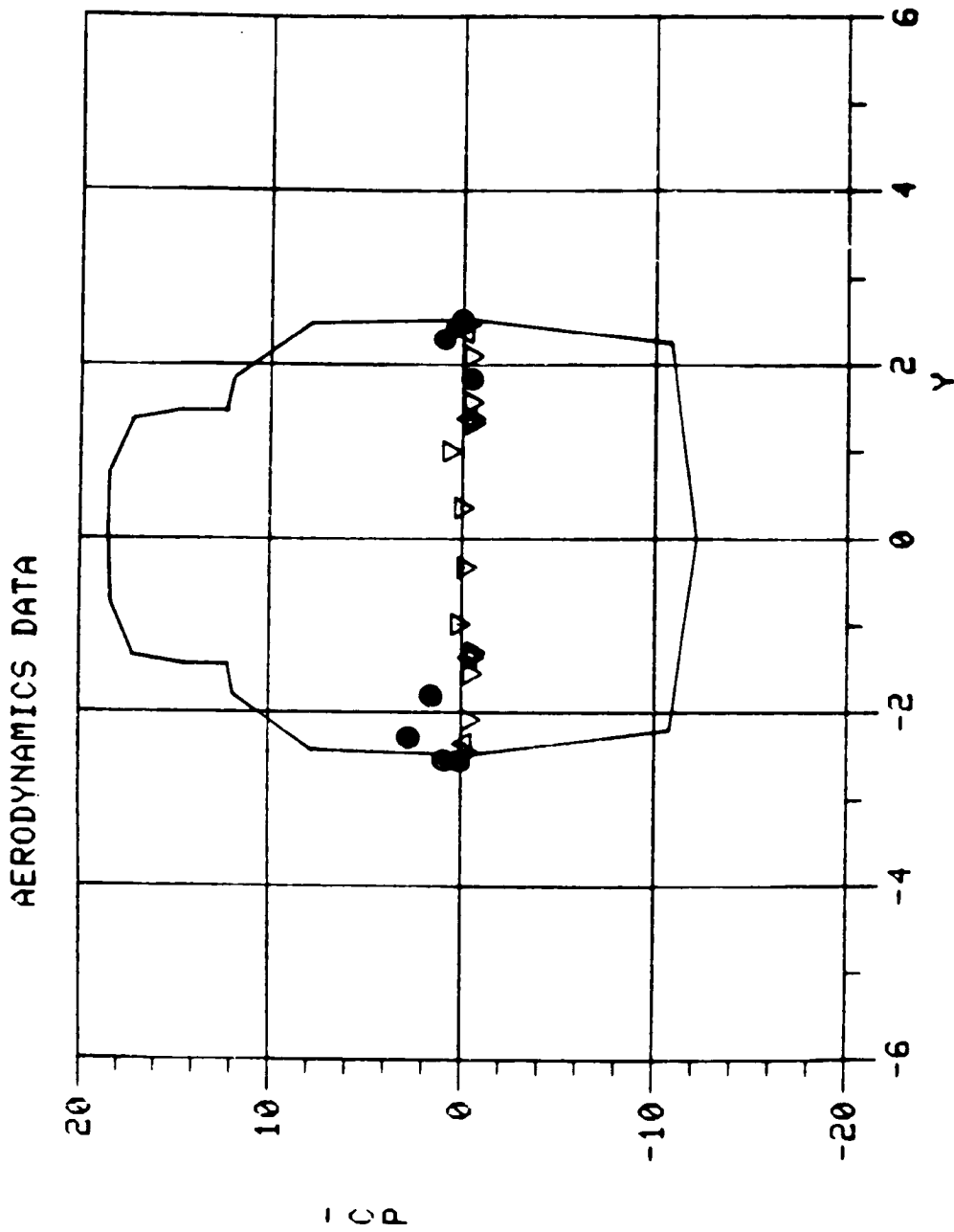
BODY, ROTOR 0.05 ADVANCE RATIO  
STATION CUT X • 6.00

ORIGINAL PAGE IS  
OF POOR QUALITY



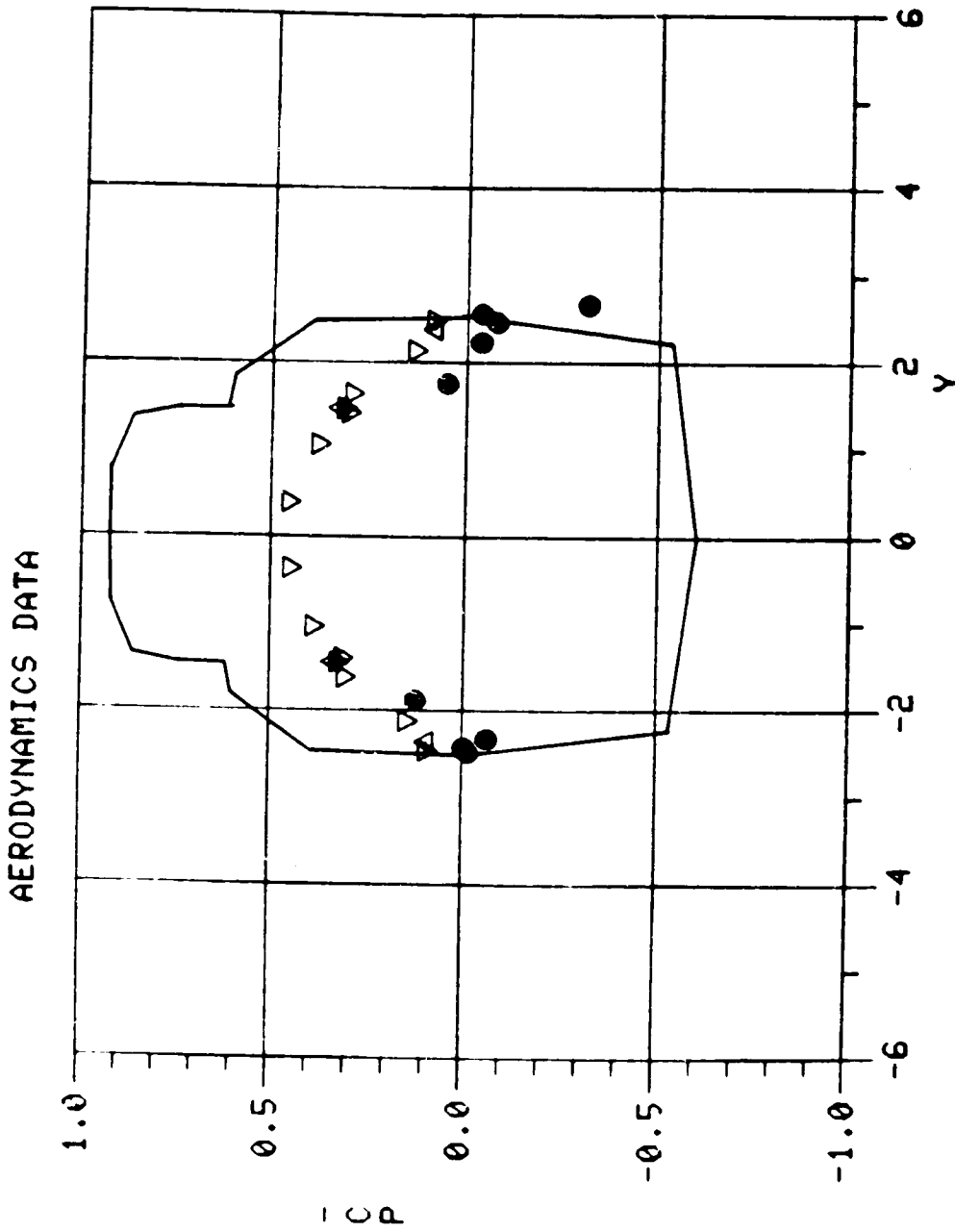
BODY, ROTOR 0.05 ADVANCE RATIO  
STATION CUT X - 6.80

ORIGINAL PAGE IS  
OF POOR QUALITY



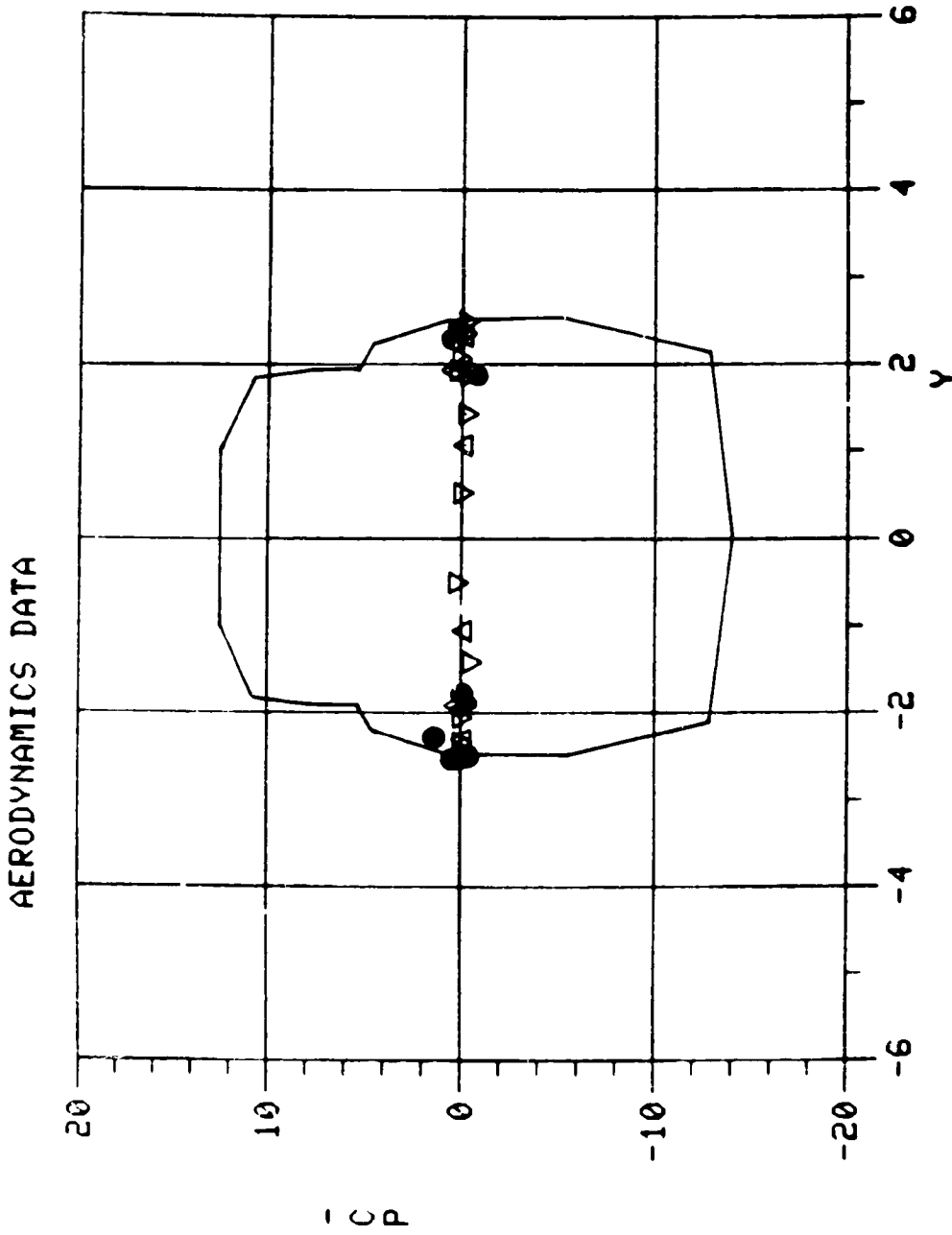
BODY, ROTOR 0.05 ADVANCE RATIO  
STATION CUT X • 9.02

ORIGINAL PAGE IS  
OF POOR QUALITY



BODY, ROTOR 0.15 ADVANCE RATIO  
STATION CUT X • 9.20

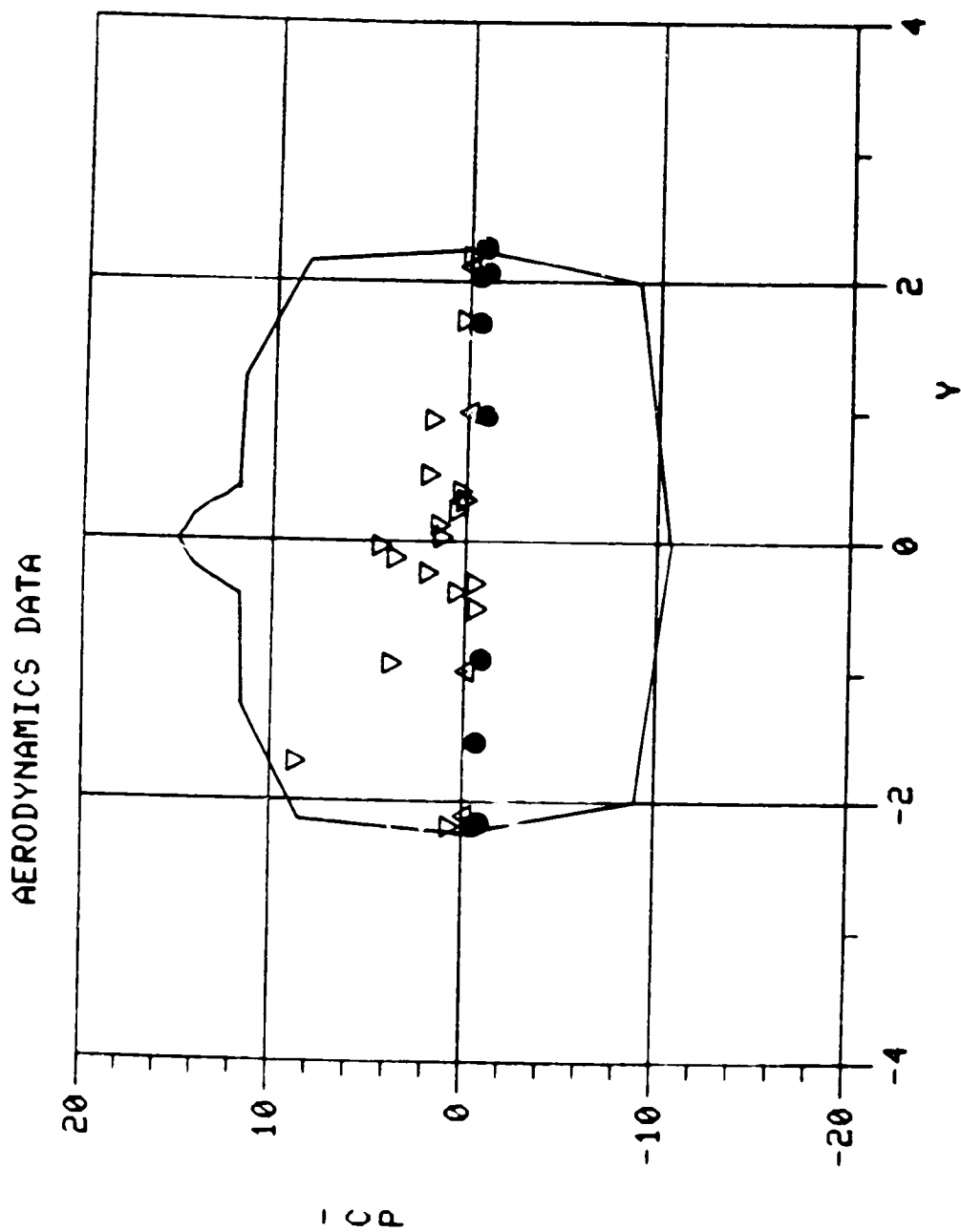
ORIGINAL PAGE IS  
OF POOR QUALITY



BODY, ROTOR 0.05 ADVANCE RATIO  
STATION CUT X • 12.00

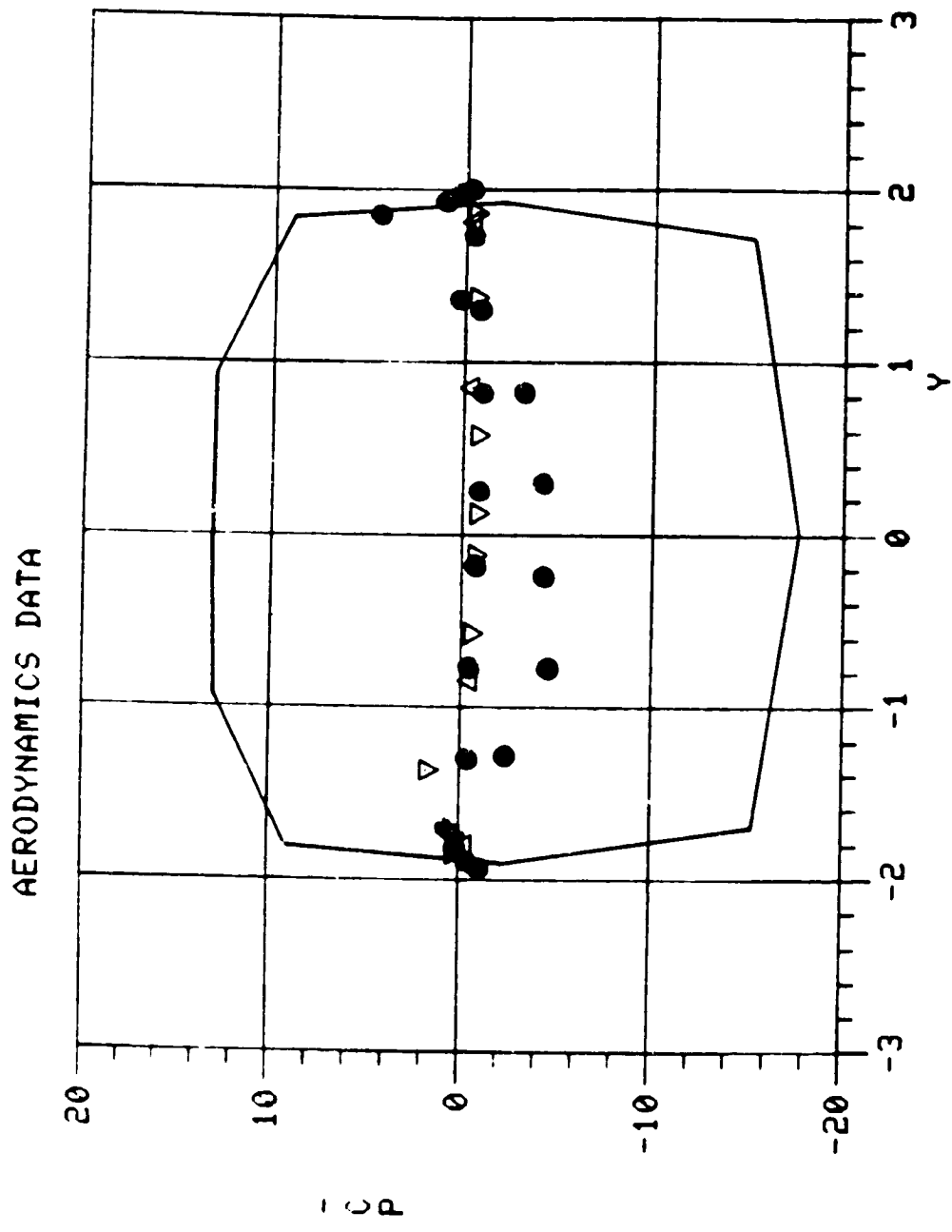


ORIGINAL PAGE IS  
OF POOR QUALITY



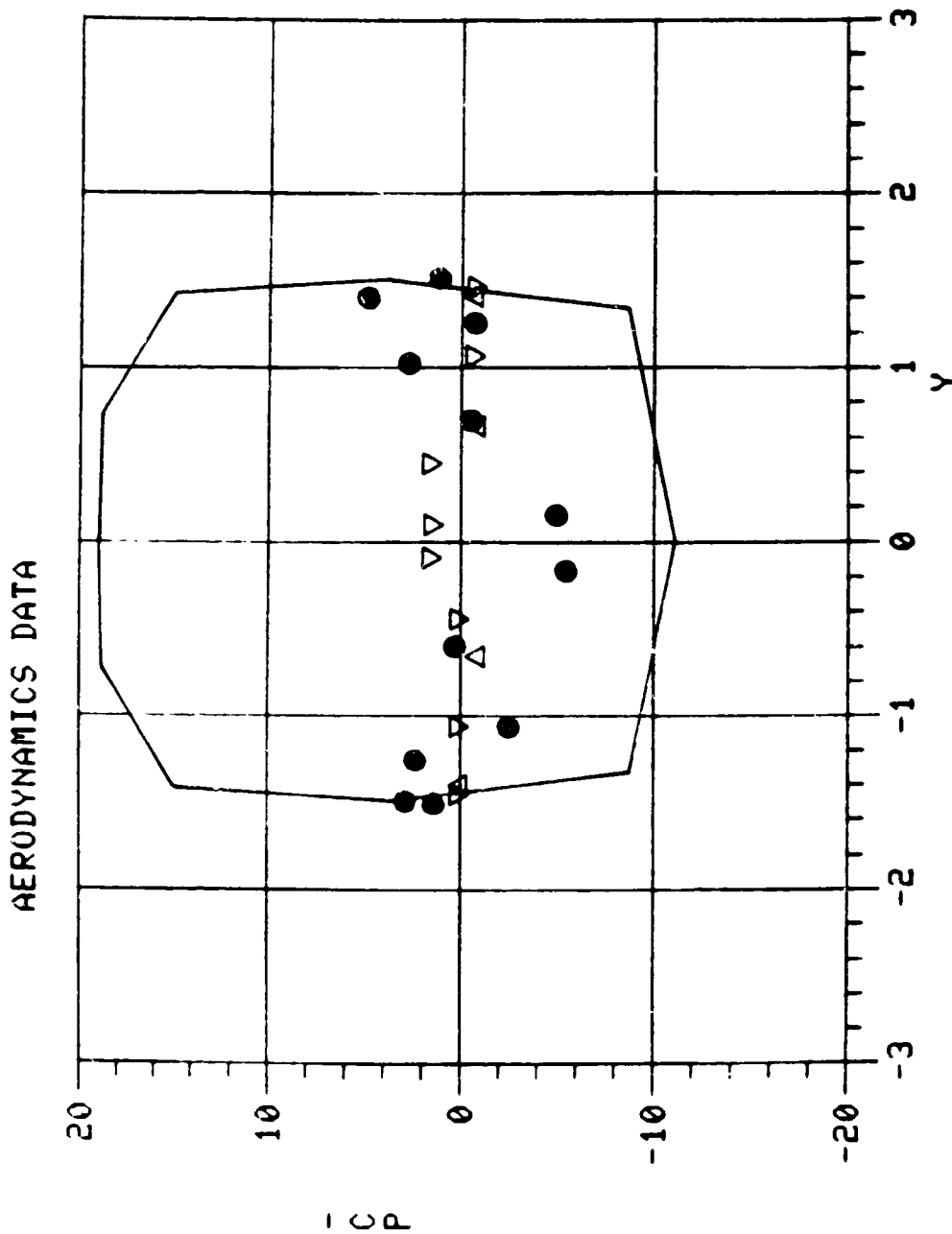
BODY, ROTOR 0.05 ADVANCE RATIO  
STATION CUT X - 20.00

ORIGINAL PAGE IS  
OF POOR QUALITY.



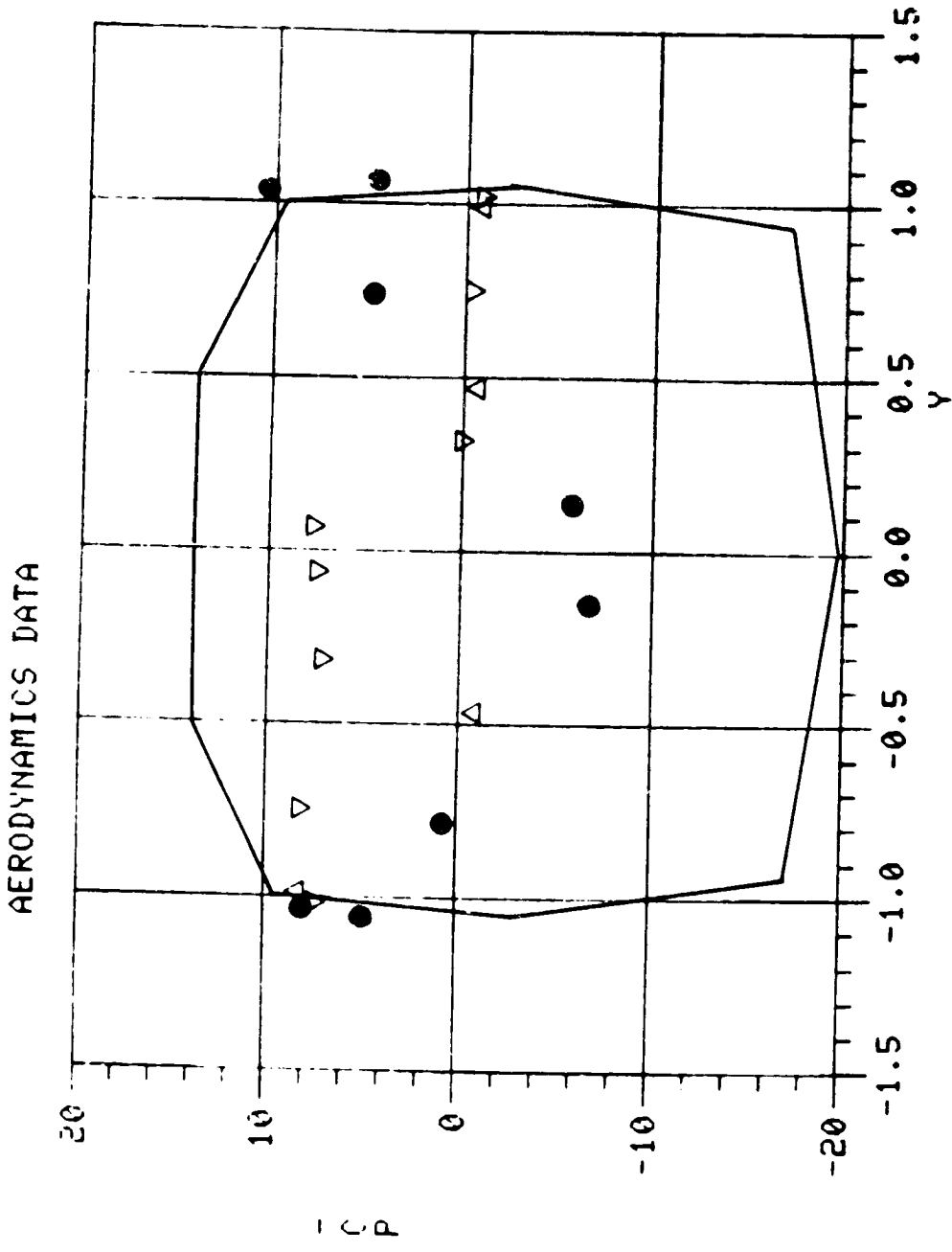
BODY, ROTOR 0.05 ADVANCE RATIO  
STATION CUT X - 23.20

ORIGINAL PAGE IS  
OF POOR QUALITY



BODY, ROTOR 0.05 ADVANCE RATIO  
STATION CUT X • 26.80

ORIGINAL PAGE IS  
OF POOR QUALITY



BODY, ROTOR 0.05 ADVANCE RATIO  
STATION CUT X • 30.60

1. Report No. CR- 177340	2. Government Accession No.	3. Recipient's Catalog No.	
4. Title and Subtitle Study for Prediction of Rotor/Wake/Fuselage Interference Part I: Technical Report		5. Report Date March 1985	
		6. Performing Organization Code	
7. Author(s) D. R. Clark B. Maskev		8. Performing Organization Report No. 8304-I	
		10. Work Unit No.	
9. Performing Organization Name and Address Analytical Methods, Inc. 2047 - 152nd Avenue, N.E. Redmond, WA 98052		11. Contract or Grant No. NAS2-10620	
		13. Type of Report and Period Covered Final, 6/1/80-11/1/83	
12. Sponsoring Agency Name and Address NASA Ames Research Center Moffett Field, CA 94035		14. Sponsoring Agency Code 505-42-11	
		15. Supplementary Notes Point of Contact: Technical Monitor, Charles A. Smith M/S 247-1, NASA Ames Research Center Moffett Field, CA 94035 (415)694-6714	
16. Abstract A method has been developed which allows the fully coupled calculation of fuselage and rotor airloads for typical helicopter configurations in forward flight. To do this, an iterative solution is carried out based on a conventional panel representation of the fuselage and a blade element representation of the rotor where fuselage and rotor singularity strengths are determined simultaneously at each step and the rotor wake is allowed to relax (deform) in response to changes in rotor wake loading and fuselage presence. On completion of the iteration, rotor loading and inflow, fuselage singularity strength (and, hence, pressure and velocity distributions) and rotor wake are all consistent.  The results of a fully coupled calculation of the flow around representative helicopter configurations are presented. The effect of fuselage components on the rotor flow field and the overall wake structure is detailed and the aerodynamic interference between the different parts of the aircraft is discussed. In particular, the flow field developed by the rotor head is followed and the effect of a rotor head cap and pylon modifications in redirecting the rotor head flow are illustrated. Good correlation between measured and calculated fuselage airloads in low-speed flight is achieved and correspondence with observed flow field behavior is demonstrated.			
17. Key Words (Suggested by Author(s)) Rotor Air Loads Fuselage Rotor Loads Helicopter Aerodynamic Interference		18. Distribution Statement  Unlimited  Subject category 01	
19. Security Classif. (of this report) UNCLASSIFIED	20. Security Classif. (of this page) UNCLASSIFIED	21. No. of Pages 82	22. Price*